Alma Mater Studiorum – Università di Bologna

DOTTORATO DI RICERCA IN

CHIMICA

Ciclo XXVII

Settore Concorsuale di afferenza: **03/B1**

Settore Scientifico disciplinare: **CHIM/03**

PHOTOACTIVE NANODEVICES FOR POTENTIAL BIOLOGICAL APPLICATIONS

Presentata da: **Valentina Carboni**

Coordinatore Dottorato **Relatore**

Prof. Aldo Roda **Prof. Alberto Credi**

Esame finale anno 2015

CONTENTS

To my mother,
who taught me
how important
is determination
in everyday life.

List of abbreviations

AcOH	Acetic Acid
ATP	Adenosine Triphosphate
BPO	Benzoyl Peroxide
CAC	Critical Aggregation Concentratiom
CB7	Cucurbit[7]uril
CD	Circular Dichroism
CF^{3-}	5(6)-carboxyfluorescein
CV	Cyclic voltammetry
DLS	Dynamic Light Scattering
DNA	Deoxyribonucleic Acid
DOPC	1,2-dioleoyl-*sn*-glycero-3-phosphocholine
DPV	Differential Pulse Voltammetry
DRV	Dried-Rehydrated Vesicle
EYPC	Egg Yolk Phosphatidylcholine
FATMLV	Frozen and Thawed Multilamellar Large Vesicles
FRET	Förster Resonance Energy Transfer
GUV	Giant Unilamellar Vesicles
ICD	Induced Circular Dichroism
LUV	Large Unilamellar Vesicle
MDMO-PPV	poly[2-methoxy-5-(3′,7′-dimethyloctyloxy)-1,4-phenylenevinylene]
MLV	Multilamellar Large Vesicles
MLV-REV	Multilamellar Large Vesicles prepared by Reverse-Phase Evaporation Method
MUV	Medium sized Unilamellar Vesicles
MVV	Multivesicular Vesicles
NAT	N-2-aryl-triazoles
NBS	*N*-bromosuccinimide
OLED	Organic Light Emitting Diode
OLV	Oligolamellar Vesicles
P3HT	Poly-3-hexylthiophene

PBS	Phosphate Buffer Saline
PCBM	1-[3-methoxycarbonyl)propyl]-1-phenyl-[6,6]C_{61}
PDI	Polydispesity Index
PEDOT-PSS	Poly(3,4-ethylendioxythiohene)-polystyrene-para-sulphonic acid
PEG	Polyethylene glycol
PMMA	Poly(methylmethacrilate)
POPC	1-palmitoyl-2-oleoyl-*sn*-glycero-3-phosphocholine
PPV	Poly(*p*-phenylenevinylene)
PTB7	Poly{4,8-bis[(2-ethylhexyl)oxy]benzo[1,2-b:4,5-b']dithiophene-2,6-diyl-alt-3-fluoro-2-[(2-ethylhexyl) carbonyl]thieno[3,4-b]thiophene-4,6-diyl}
REV	Reverse-phase Evaporation prepared Vesicle
RGD	Arginylglycylaspartic Acid
RNA	Ribonucleic Acid
SAM	Self-Assembled Monolayer
SCE	Satured Calomel Electrode
SPLV	Stable Plurilamellar Vesicle
SUV	Small Unilamellar Vesicle
$TBAPF_6$	Tetrabutylammonium Hexafluorophosphate
TEA	Triethylamine
$TEAPF_6$	Tetraetylammonium Hexafluorophosphate
TFA	Trifluoroacetic Acid
TPD	*N,N′*-Bis(3-methylphenyl)-*N,N′*-diphenylbenzidine
UV	Unilamellar Vesicle
VET	Vesicles made by Extrusion Technique

Abstract

Biological systems are complex and highly organized architectures governed by noncovalent interactions, which are responsible for molecular recognition, self-assembly, self-organization, adaptation and evolution processes. These systems provided the inspiration for the development of supramolecular chemistry, that aimed at the design of artificial multicomponent molecular assemblies, properly designed to perform different operations: each constituting unit performs a single act, whereas the entire supramolecular system is able to execute a more complex function, resulting from the cooperation of the constituting components. Supramolecular chemistry deals with the development of molecular systems able to mimic naturally occurring events, for example complexation and self-assembly through the establishment of noncovalent interactions. Moreover, the application of external stimuli, such as light, allows to perform these operations in a time- and space-controlled manner. These systems can interact with biological systems and, thus, can be applied for bioimaging, therapeutic and drug delivery purposes. In this work the study of biocompatible supramolecular species able to interact with light is presented. The first part deals with the photophysical, photochemical and electrochemical characterization of water-soluble blue emitting triazoloquinolinium and triazolopyridinium salts. Moreover, their interaction with DNA has been explored, in the perspective of developing water-soluble systems for bioimaging applications. In the second part, the effect exerted by the presence of azobenzene-bearing supramolecular species in liposomes, inserted both in the phospholipid bilayer and in the in the aqueous

core of vesicles has been studied, in order to develop systems able to deliver small molecules and ions in a photocontrolled manner. Moreover, the versatility of azobenzene and its broad range of applications have been highlighted, since conjugated oligoazobenzene derivatives proved not to be adequate to be inserted in the phospholipid bilayer of liposomes, but their electrochemical properties made them interesting candidates as electron acceptor materials for photovoltaic applications.

Keywords: blue emitters, bioimaging, DNA, liposomes, azobenzene, drug delivery, ion transport, photovoltaic applications.

Chapter 1
Introduction

1.1 Complexity of biological systems

From a chemical point of view biological systems are complex and highly organized multicomponent molecular architectures able to perform different and essential operations.

The basis of their activity lies in the interplay between parts that constitute them, enabling them to perform operations that do not merely correspond to the sum of the abilities of single constituent parts. Communication represents the direct consequence of the interaction between the external environment and biological systems and it occurs in a highly specific manner, following the "lock and key" principle postulated by Hermann Emil Fischer in 1894[1].

Biological systems are able to self-assemble, leading to complex nano- and micrometric architectures able to store and transduce informations. The best example of self-assembly is represented by DNA double helix. It is the strongest paradigm of how important are noncovalent interactions, since in this case self-assembly of nucleotides allows storage of the whole genetic information, that represents the basis of life.

Other important features of biological systems are their ability to adapt themselves to external conditions, their self-repairing and regulation capability. For example, proteins have a three-dimensional structure that is the result of the

folding process and it allows them to perform their activity. For example, haemoglobin is an allosteric transport protein for oxygen and it experiences a conformational change when oxygen binds on its prostetic *heme* group, in order to best accommodate oxygen molecules in a cooperative manner (*Figure 1.1*).

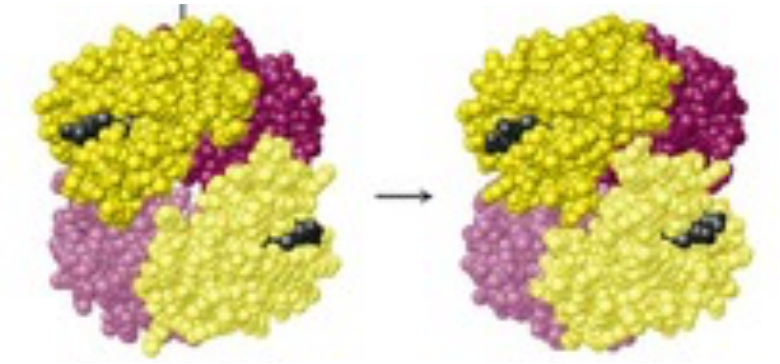

***Figure 1.1*- 3D structure of deoxy (left) and oxyhaemoglobin (right).**

Moreover, since it possesses an allosteric site, it is able to regulate its transport activity on the basis of external conditions: in fact, formation of a complex with 2,3- biphosphoglycerate (2,3-BPG) allows the regulation of haemoglobin affinity for oxygen and, consequently, regulates oxygen pressure in lungs on the basis of external oxygen concentration.

It is interesting to notice that all these essential operations occur in a highly compartmentalized and microscopic environment, that contains all the necessary for its survival. The fundamental building block for biological systems is the cell, which stores the genetic information and contains all the useful tools that enable the communication between the external environment and the cell itself as well as the energetic supply required in order to work autonomously and properly.

1.2 Supramolecular chemistry: at the boundary between chemistry and biology

It is undeniable that biological systems offered a great starting point for the development of artificial systems exhibiting similar features. Inspired by this high sophistication and efficiency, traditional chemistry shifted its attention towards noncovalent interactions, which constitute the basis that governs

biological systems. By learning from biological systems, a different approach arises and this new perspective contributed to the development of supramolecular chemistry, that is defined as "the chemistry of the entities generated by intermolecular noncovalent interactions".[2]

Jean-Marie Lehn, who in 1987 was awarded the Nobel Prize together with D.J. Cram and C.J. Pedersen for "their development and use of molecules with structure-specific interactions of high selectivity",[3] wrote that "beyond the molecule, supramolecular chemistry aims at developing highly complex chemical systems from components interacting by noncovalent intermolecular forces" and that "supramolecular chemistry has paved the way toward apprehending chemistry as an information science through the implementation of the concept of molecular information with the aim of gaining progressive control over the spatial (structural) and temporal (dynamic) features of matter and over its complexification through self-organization, the drive to life".[2]

Mimicry of naturally occurring molecular interactions aimed at developing new tools in chemistry, moving the attention from covalent interactions towards noncovalent ones, which constitute the humus for growth of supramolecular chemistry. This novel approach concerns the design of artificial supramolecular systems displaying the efficiency and selectivity present in Nature, keeping in mind that "the chemist may find inspiration in the ingenuity of biological events and encouragement in the demonstration that such high efficiencies, selectivities [...] can indeed be attained" and, moreover, he has to keep in mind that "chemistry is not limited to systems similar to those found in biology, but it is free to create novel species". These words, written in 1988[2] by J.M. Lehn summarize the principles that constitute the basis for the design and development of supramolecular systems.

In fact, supramolecular systems are novel molecular species that resemble living systems, since they rely on molecular recognition, self-assembly, self-organization, adaptation and evolution. Like biological systems, supramolecular ones are not able to perform their operations if they their components do not assemble together and do not interact: in a supramolecular system every constituting subunit is able to exist independently from the others, but interaction between them is essential to perform their activity.

The best example among biological systems that describes properly concepts mentioned above is represented by enzymes.[4] Enzymes are protein systems composed of many subunits adopting a three-dimensional structure in order to catalyse chemical reactions that are essential for cell survival. There is a deep relation between their structure and function, since the conformation they adopt is the most suitable in order to carry out their activity and interaction between every subunit is essential in order to achieve the enzymatic activity. More specifically, if denaturation or dissociation occurs, the enzyme looses its catalytic activity. Moreover, it is essential that their active site interacts with the substrate in a highly specific and complementary fashion: in fact, the formation of the active complex is found to be essential for catalysis. The active complex can be defined as a supramolecular complex since there is no covalent bond between the active site of the enzyme and the substrate. This is one of the myriads of examples of host-guest complexes provided by Nature and supramolecular chemistry deals with the development of systems able to mimic them. A host-guest complex represents the simplest example of a supramolecular system: it is made up by a host molecule that contains binding sites able to interact with a guest in a highly specific and complementary manner. As for biological systems, noncovalent interactions are the basis for molecular recognition and self-assembly: the resulting supramolecular complex is thus able to perform operations that host and guest do not possess when they are separated. Therefore, supramolecular systems can be defined as multicomponent molecular assemblies properly designed to perform different operations: each constituting unit performs a single act, whereas the entire supramolecular system is able to execute a more complex function, resulting from the cooperation of the constituting components. Every component is chosen in order to be able to carry out its function after the application of orthogonal external stimuli, such as pH variations, redox and light inputs. In the last decades, incorporation of the azobenzene photochromic unit made possible the development of artificial supramolecular systems able to perform different operations as a consequence of the interaction with light. These systems resemble systems belonging to the macroscopic world, such as logic gates, memories, devices and machines, but their dimensions are in the nanometric scale.[5]

1.3 Biological membranes

Amphiphilic compounds are able to self-assemble in water when they have a concentration that is above the critical aggregation concentration (CAC), due to the hydrophobic effect and this process is responsible for the appearance of different three-dimensional structures. Phospholipids are amphiphilic compounds, consisting of a polar phosphate headgroup and a hydrophobic region made of hydrocarbon chains and they are able to self-assemble in water affording different structures (*Figure 1.2*), that are predicted by the *packing parameter (p)*.

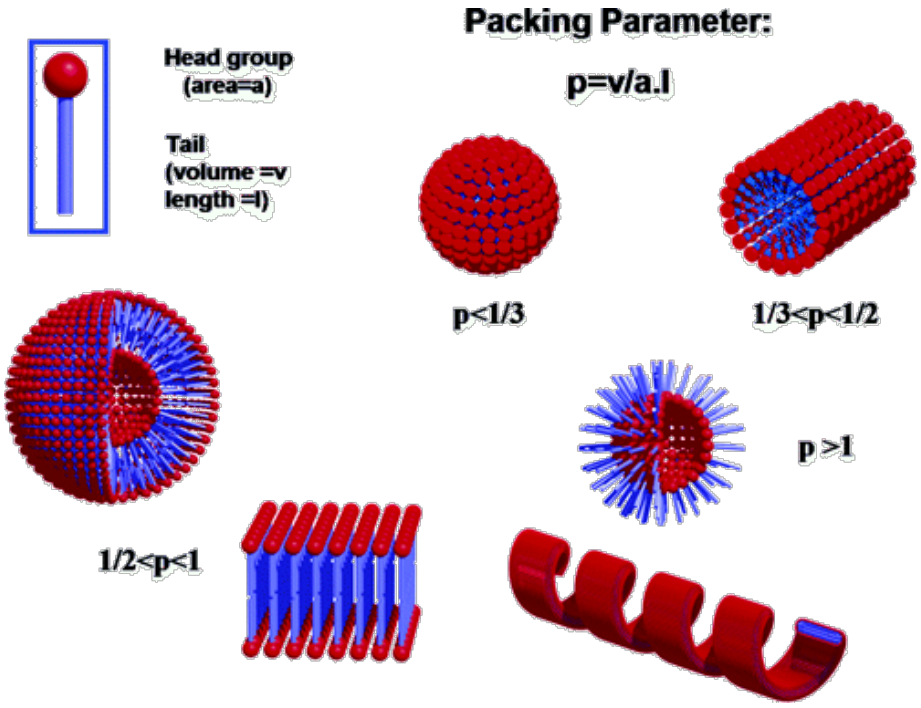

***Figure 1.2*- Different aggregate morphologies of phospholipids predicted by the packing parameter. Reproduced with permission from *Chem. Rev* 2005, 105, 4, 1445-1490. © 2005 American Chemical Society.**

This parameter was first introduced by Israelachvili[6] and it is defined as

$$p = \frac{v}{l * a}$$

where a represents the surface area of the phosphate headgroup v and l denote the volume and the length of the alkyl chains. When $0.5 < p < 1$, phospholipids

self-assemble in double layers, that represent the structural motif found in vesicles and biological membranes.

Biological membranes constitute the barrier that separates the cytosolic cellular content from the external world, protecting organelles and the genetic information from external damaging. Moreover, membranes define cellular borders and regulate molecular trafficking from the aqueous cytosolic compartment to the external medium and vice versa. They are robust and flexible at the same time, allowing the cell to undergo modifications in its shape during its growth, replication or fusion. Another important function of biological membrane consists in their ability to keep some organic compounds and ions in the cytosolic environment, since they act as selective permeable barriers. In fact, biological membranes are complex architectures composed not only of phospholipids (*Figure 1.3*) and they are not passive barriers: in fact, in addition to phospholipids, carbohydrates and different classes of proteins are present and the relative amount of proteins and lipids are essential in order to determine the function of the resulting membrane. Intramembranous proteins span the bilayer thickness of biological membranes and possess specific functions: for example, the transport of some organic compounds and inorganic ions occurs against a concentration gradient by means of protein pumps; receptors located on the surface of the plasmatic membrane are involved in signal transduction, since they receive extracellular signals and convert them in modifications inside the cell environment.

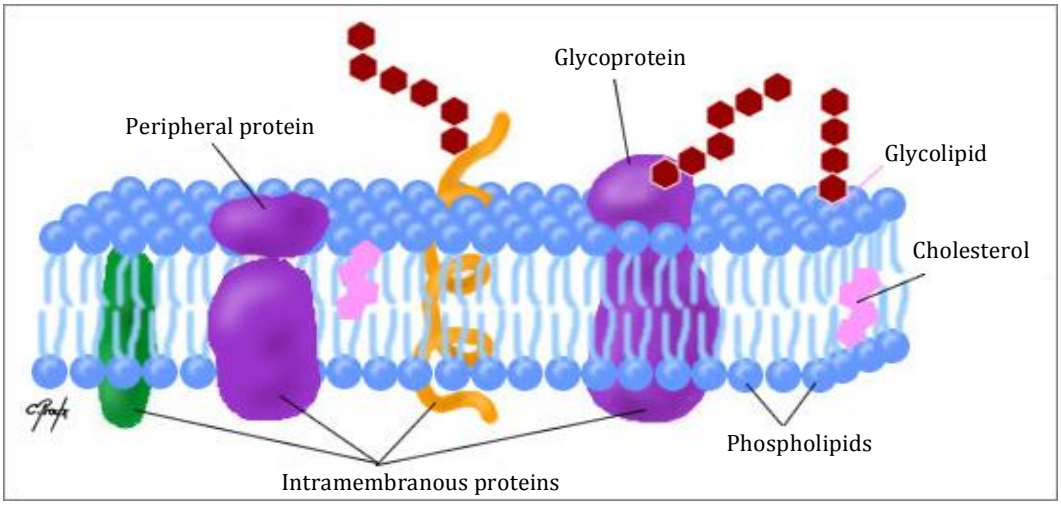

***Figure 1.3*- Structure of cell membrane. Reproduced from http://www.cours-pharmacie.com/biologie-cellulaire/les-membranes- cellulaires.html**

In addition to the aforementioned components, cholesterol has been observed in cellular membranes and its presence affects physicochemical properties[7] of the membrane in which it is inserted. More specifically, it orients pointing the OH group towards the polar head group of phospholipids and its apolar steroid ring interacting with lipid hydrocarbon chains. Cholesterol is found to decrease the fluidity of membranes above the gel-liquid phase transition temperature (T_m),[8] thus reducing their permeability[9] and mobility of phospholipids hydrocarbon chains by introducing a high degree of order.[9a,10] In fact, the model that best describes the supramolecular structure of biological membranes is the *fluid mosaic model* developed by Singer and Nicholson in 1972,[11] introducing the double layer arrangement of phospholipids and sterols in aqueous environment, with their polar groups pointing towards the aqueous external environment and to the aqueous internal core; in contrast, their apolar region is shielded form the polar external environment and is located within the bilayer, as evidenced by many different instrumental techniques including NMR and neutron diffraction.[12] This constitutes the basilar structural motif for biological membranes and transmembrane proteins are inserted in membrane bilayer in an asymmetric manner, allowing to discriminate between the two resulting portions of the membrane. Due to noncovalent interactions that govern lipids and proteins arrangement in membranes, there is a high degree of mobility within phospholipid bilayer and proteins and lipids are able to move laterally in the plane of the membrane.

1.4 Liposomes

Liposomes are artificial vesicles that were discovered in 1964 by Bangham[13] and since then they have been extensively studied since their similarity with biological membranes, biocompatibility and easy preparation. They are spherical objects suspended in water, possessing a double layer of phospholipids that surrounds an internal aqueous core. Due to the amphiphilic nature of phospholipids, the insertion of compounds occurs according to their lipophilicity: hydrophilic guests are encapsulated in the aqueous liposomal core,

whereas lipophilic ones are inserted in their bilayer and guests having intermediate lipophilicity are partitioned both in the liposomal core and bilayer.[14]

Liposomes are assembled from cholesterol and naturally occurring phospholipids, whose structure and composition resemble that of biological membranes: in fact, in both cases the double layer of phospholipids represents the structural motif. Since they are artificially prepared systems, it possible to modulate superficial properties and performance by properly choosing bilayer constituents. In fact, it is reported that unsaturation, charge, nature of headgroup species and hydrocarbon length affect T_m, which represents an important parameter that, indirectly, refers to permeability and stability of liposomal suspensions. For example, long-chain phospholipids have a higher T_m respect to those bearing shorter ones[15] and the presence of double bonds increases the entropic disorder, lowering T_m. An issue associated to the presence of acyl chains bearing double bonds, is linked to the easy oxidation[16] experienced by these moieties and this results in lowering of liposomal stability. In this sense, liposomes constitute a flexible platform for biological applications, namely gene and drug delivery, since their mechanical and surface properties can be tuned by a proper choice of constituent phospholipids.

1.4.1 Classification

The most general definition of liposomes outlines them as spherical vesicles having dimensions ranging from 30 nm to several micrometers (usually 2.5). They consist of one or more phospholipid bilayers around an aqueous compartment and they can be classified according to their dimensions, composition, application and preparation procedure adopted.

Vesicle size is an important parameter, since it determines the stability and circulation half-life of vesicles in the blood stream of living organisms. Dimensions allow to distinguish different categories of liposomes:[17]

- *Multilamellar large vesicles* (MLV), diameter > 500 nm;
- *Oligolamellar vesicles* (OLV), diameter100 nm-1μm;
- *Unilamellar vesicles* (UV), all size range;

- *Small unilamellar vesicles* (SUV), diameter 20-100 nm;
- *Medium sized unilamellar vesicles* (MUV);
- *Large unilamellar vesicles* (LUV), diameter> 100 nm;
- *Giant unilamellar vesicles* (GUV), diameter> 1 μm;
- *Multivesicular vesicles* (MVV), diameter> 1 μm.

Liposomes are also classified on the basis of their composition and four classes are identified (*Figure 1.4*):

- *Conventional liposomes,* that are composed only of phospholipids and cholesterol. They are mainly used for macrophage targeting and vaccines administration, but the main drawback associated with them relies in their relatively short blood circulation time.
- *Long-circulating liposomes*, that are also called "stealth" or "sterically stabilized" liposomes since their external surface is decorated by covalently linking polyethyleneglycol, thus allowing selective targeting of pathological areas;
- *Immunoliposomes*, that bear specific antibodies or antibody ligands on their surface in order to achieve more specific targeting;
- *Cationic liposomes*, that are composed of cationic lipids and are used for gene delivery.

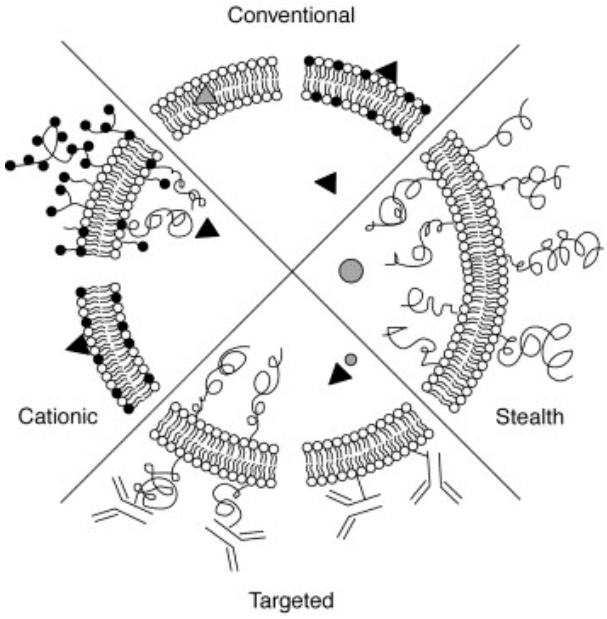

***Figure 1.4*- Schematic representation of four major liposomes type, according to the composition of their liposomal membranes. Reproduced with permission from *Pharm. Sci. & Tech. Today,* 1998, 1, 1, 19-31. © 1998 Elsevier Ltd.**

Finally, liposomes are classified on the basis of the preparation method chosen.[17] This allows to distinguish between six different categories:

- REV: single or oligolamellar vesicles prepared employing the reverse-phase evaporation method;
- MLV-REV: multilamellar vesicles prepared employing the reverse-phase evaporation method;
- SPLV: stable plurilamellar vesicles;
- FATMLV: MLV prepared by freeze-thaw cycles;
- VET: vesicles made by extrusion methods;
- DRV: vesicles prepared by dehydration-rehydration method.

1.4.2 Preparation

Several different strategies for liposomes preparation are reported and their common denominator relies in the following four stages:

1. Drying lipids solubilized in an organic solvent, in order to form the so-called *lipid film*;
2. Rehydration of the homogeneous phospholipid film;
3. Purification, in order to remove extravesicular impurities;
4. Analysis.

Liposomes have been extensively employed as biocompatible nanocarriers for drug delivery and for this purpose, loading of hydrophilic drugs can be carried out by passive (i.e. during liposomes formation) or active loading (i.e. encapsulation in preformed vesicles) techniques. Moreover, rehydration of the homogeneous phospholipid film can be performed either with only water or with a solution containing a hydrophilic drug and in this latter case, it allows to load the hydrophilic drug by means of passive loading. The passive loading technique comprises three different methods:

1. Mechanical dispersion methods;
2. Solvent dispersion methods;
3. Detergent removal method for the removal of non-encapsulated material.

1.4.2.1 Mechanical dispersion methods

Mechanical dispersion techniques allow the hydration of the homogeneous phospholipid film and comprise different types of methods:

- *Sonication*, that consists in sonication (either probe or bath sonication) of MLV in order to get SUVs;
- *Extrusion*, that involves the extrusion of small volumes of MLVs solution through a small orifice;
- *Freeze-thaw cycles*, in which SUVs are quickly frozen and thawed slowly and the formation of unilamellar vesicles results from SUV fusion during the freezing and thawing processes;
- *Lipid film hydration by hand shaking*;
- *Lipid film hydration by non hand shaking*;
- *Lipid film hydration by freeze drying*;
- *Micro-emulsification*;
- *Membrane extrusion*.

1.4.2.2 Solvent dispersion method

This methodology comprises:

- *Solvent vaporization*, in which a solution of phospholipid in ether or ether-methanol is gradually added to an aqueous solution of the material to be encapsulated at 55°/65° C or under reduced pressure. In this way, removal of the organic solvent allows the formation of liposomes, even if the resultant populations are non homogeneous;
- *Reverse phase evaporation method*, which is based on the creation of inverted micelles, that are dispersed in mixture of a buffered aqueous phase (containing the molecules to be loaded) and an organic phase and subjected to sonication. Evaporation of the organic solvent leads to gel state, that collapses and then to bilayer formation.

Usually, removal of nonencapsulated material is performed by employing different methods, including dialysis, gel-permeation chromatography and by using detergent absorbers.

Insertion of apolar guests in the phospholipid bilayer is obtained in two different ways:

1. Addition of an appropriate amount of the lipophilic guest to a phospholipid solution and solvent removal. The obtained *lipid cake* is then hydrated with a proper volume of buffer;
2. Addition of an adequate amount of guest dissolved in THF or methanol to preformed liposomes and solvent evaporation.

1.4.3 Applications

Liposomes have been extensively used as carriers in many different fields, from pharmaceutical and cosmetic industry to food and farming ones.

Due to the amphiphilic nature of phospholipids, liposomes are able to trap both hydrophilic and hydrophobic compounds, avoiding their decomposition once entrapped and their release at the designed site of action by application of different external stimuli. As mentioned before, it is possible to modulate the insertion of compounds according to their lipophilicity: hydrophilic guests are encapsulated in the aqueous liposomal core, whereas lipophilic ones are inserted in their bilayer and guests having intermediate logP are partitioned both in the liposomal core and bilayer.[14]

Because of their biocompatibility, low toxicity and to the mentioned dualism, they have been extensively used in pharmaceutical industry for drug and gene delivery and bioimaging by embedding fluorescent probes, such as QDs in their bilayer[18] and nowadays many liposomal formulations are commercially available (*Table 1.1*).[19-31]

***Table 1.1*- List of liposomes/lipid based drug approved products in market. Reproduced with permission from *J. Contr. Rel.*, 2014, 193, 122-138. © 2014 Elsevier Ltd.**

No	Product name	Therapy	Drug	Particle diameter (Zavg)	Type	Lipid composition	Drug form	Purpose
Liposome – Nano sized products								
1	Ambisome	Fungal	Amphotericin B	< 100 nm	LUV	HSPC/Cholesterol/DSPG, D/L wt ratio = 0.16	Lyophilized powder	To improve stability and reduce nephrotoxicity
2	DaunoXome	Cancer	Daunorubicin	~45 nm	SUV	DSPC/Cholesterol D/L wt ratio = 0.054	Suspension	To reduce toxicity
3	Doxil	Cancer	Doxorubicin	~100 nm	LUV	HSPC/Cholesterol/DSPEmPEG 2000 D/L wt ratio = 0.125	Suspension	To increase blood circulation/control release/ drug targeting
4	Lipo-Dox	Cancer	Doxorubicin	~180 nm	LUV	DSPC/Cholesterol/DSPEmPEG 2000	Suspension	To increase blood circulation/control release/ drug targeting
5	Myocet	Cancer	Doxorubicin	~190 nm	LUV	EggPC/Cholesterol D/L wt ratio = 0.25	Lyophilized powder	To improve stability due to non-pegylation
6	Visudyne	Ocular	Verteporfin	< 100 nm	LUV	EggPG/DMPC D/L wt ratio = 0.13	Lyophilized powder	To increase solubilization and stability
7	Epaxal	Vaccine	Inactivated hepatitis A virus (strain RG-SB)	~150 nm	LUV (Virosomes)	DOPC/DOPE	Suspension	To induce immunity to variety of antigens without adverse effects associated with other adjuvants
8	Inflexal V	Influenza	Inactivated hemaglutinine of influenza virus strains A and B	~150 nm	LUV (Virosomes)	DOPC/DOPE	Suspension	To induce immunity to variety of antigens without adverse effects associated with other adjuvants
Liposome – Micron sized products								
9	Depocyt	Neoplastic and lymphomatous meningitis	Cytarabine	10–20 μm	MVL (DepoFoam)	DOPC/DPPG/Cholesterol/Triolein, D/L wt ratio = 0.813	Suspension	To control release
10	DepoDur	Pain management	Morphine sulfate	10–20 μm	MVL (DepoFoam)	DOPC/DPPG/Cholesterol/Triolein/ Tricalrylin, D/L wt ratio = 1.13	Suspension	To control release
Lipid complex – Nano and Micron sized products								
11	Abelcet	Fungal	Amphotericin B	< 5 μm	Disc like	DMPC/DMPG, D/L wt ratio = 1.02	Suspension	To improve drug loading
12	Amphotec	Fungal	Amphotericin B	~130 nm	Ribbon like	Cholesteryl sulfate, D/L wt ratio = 1.89	Lyophilized powder	To improve drug loading and stability

Many advantages are associated to the employment of liposomes as biocompatible nanocarriers, including

- Loading of therapeutically active agents;
- Prolonged and sustained drug release;
- Drug accumulation at the targeted site;
- Improved bioavailability of the encapsulated drug.

However, the use of conventional liposomes is limited by their fast elimination from the blood stream and their capture by the cells of rethiculo-endothelial system, especially those located in the liver. To overcome these issues and develop more selective and efficient drug delivery systems, a number of improvements[32] were made, especially to achieve the sustained release of encapsulated drugs.

In the last decade, a real evolution in the stabilization, drug encapsulation[33] and decoration of the liposomal surface took place, affording more sophisticated and selective nanocarriers (*Figure 1.5*).

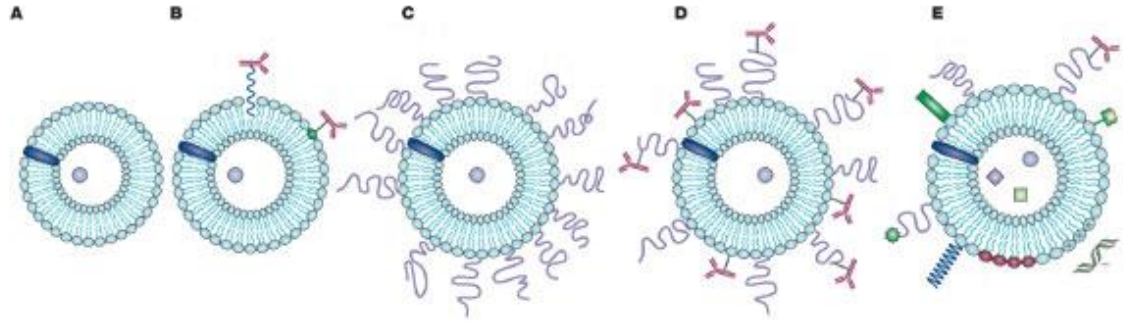

***Figure 1.5*- Evolution of liposomes: conventional liposomes (A), immunoliposomes (B), long-circulating liposomes (C), long-circulating immunoliposomes (D), new generation liposomes (E). Reproduced with permission from *Nature Rev. Drug Disc.* 2005, 4, 145-160. © 2005 Macmillan Publishers Ltd.**

First, liposomal surface was decorated with ligands able to recognize and bind targeted cells, affording *immunoliposomes.*[34] Since the majority of liposomes accumulated in the liver because of insufficient time for the interaction with the target, their surface was coated with biocompatible polymers such as poly(ethylenglycole) (PEG), which forms a protective cover and reduces liposome recognition by cells of the rethiculo-endothelial systems. In this way, *long-circulating liposomes* demonstrated longer bioavailability of the encapsulated drug.[35] For these reasons, the have been extensively and successfully employed in cancer chemotherapy.[22-24, 36]

Long-circulating immunoliposomes combine the properties of immunoliposomes and PEG-ylated liposomes, by coating the liposomal surface with ligands bearing a spacer PEG. This approach paved the way for the decoration of liposomal surface with different kind of ligands, including antibodies,[37] folate receptors,[38] transferrin,[39] vitamin and grow factor receptors,[40] allowing to improve selectivity and cytotoxicity.

1.5 Biomimetic membrane systems

Since liposomes are obtained by self-assembly of naturally occurring phospholipids and liposomal membranes evoke biological membranes, these biomimetic systems have been extensively studied to investigate cellular organization[41] and transport phenomena.[42] In eukaryotic cells, transport of substrates that are essential for their survival is ensured by transmembrane

channels, proteins, transporters and pumps. They allow the passage of specific ions and polar species such as carbohydrates and aminoacids by means of passive or active transport (*Figure 1.6*).

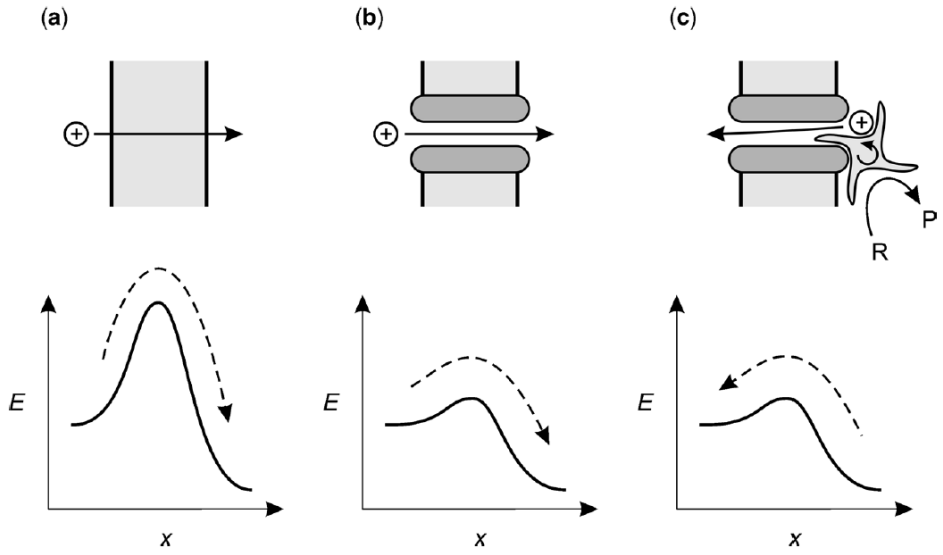

***Figure 1.6*- Transport mechanisms of ions across lipid bilayers: passive transport (diffusion mechanism) (a), passive transport mediated by an ion channel (b), active transport (c). Reproduced with permission from *Molecular Devices and Machines—Concepts and Perspectives for the Nanoworld*, Wiley-VCH, 2008. © 2008 Wiley VCH Verlag.**

Passive transport occurs without any external energy supply and is a thermodynamically favoured process. It refers to the movement of ions and polar species by means of a concentration gradient established between the exterior and the interior of the cell. The movement of species across the membrane is usually described as a movement "down a concentration gradient", since species diffuse from an area possessing a high concentration of species to another one of lower concentration.

Active transport of species across biological membranes is not thermodynamically favoured, but it occurs when coupled with other exergonic ones, such as light absorption or ATP hydrolysis, that furnish the required energetic supply and allows the passage of species "against the concentration gradient".

Mimicry of these naturally occurring devices allows the development of artificial systems able to release their cargo after the application of an external stimulus: this is possible by inserting properly designed compounds in the phospholipid

bilayer or interior of liposomes. Switchable passive transport of liposomal content can be achieved by applying different external stimuli, such as variation of pH, heat and light:[43] interaction between the applied trigger and the inserted guest results in a structural change of the guest, allowing the release of encapsulated material.

Among the mentioned external triggers, light exhibits many advantages related to its application, referring to the possibility to control its spatial and temporal delivery. Moreover, a large variety of light sources are available, including tunable laser sources able to produce femtoseconds pulses or continuous illumination, and these light sources proved to be safe and relatively cheap. Following these considerations, a tremendous research effort has been made in the last 30 years, in order to develop biocompatible light-operating drug delivery prototypes able to release their cargos exhibiting a high spatial and temporal delivery precision.

1.5.1 Transport of ions

Transport of ions across biomembranes is essential for the balance of electrochemical potential of cells, their volume and osmotic balance and are involved in cellular signalling. It has been reported that defects in transmembrane transport of anions (more specifically Cl^-) are involved in the appearance of various 'channelopathies'[44], such as Dent's disease, osteoporosis and cystic fibrosis.[45]

As mentioned before, transport proteins, pumps and channels mediate passive and active transport of ions across biomembranes. Moreover, ion channel-mediated transport of anions through membranes can take place following three different mechanisms, accordingly to the transport stoichiometry and direction (*Figure 1.7*).[46]

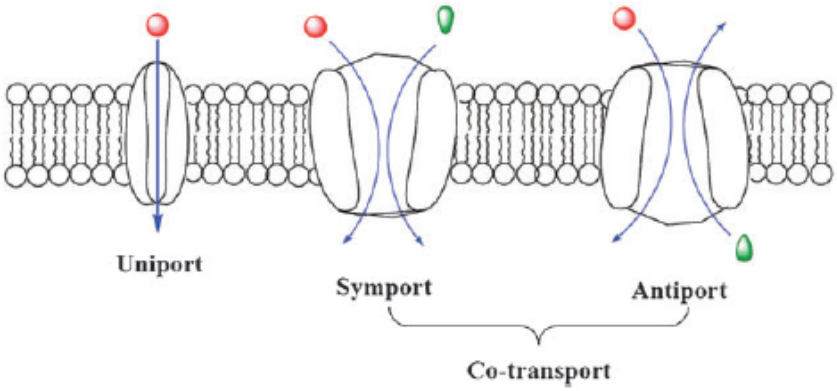

***Figure 1.7*- Classification of transport based on stoichiometry and direction of transport. Reproduced with permission from *Chem. Soc. Rev.* 2010, 39, 3843-3862. © 2010 Royal Society of Chemistry.**

A *uniport process* occurs when a single ion is transported across membrane, whereas when two different ions are transported simultaneously, the ion channel acts as a *co-transporter*. Co-transport can be *symport* or *antiport*, depending on whether the transported species follow the same direction or not.

Naturally occurring proteins ensure the passage of ions by establishing selective, multiple and non-covalent interactions, namely electrostatic hydrogen bond interactions.[46]

Many naturally occurring ionophores are reported and among them few examples of compounds exhibiting anionophoric activity are present, including prodigiosins,[47]ceramide[48] and some acylglycerols.[49]

Following these examples, artificial examples of systems able to establish anion recognition and transport processes across liposomal membranes have appeared in literature.[46,50]

The first attempt to mimic the activity of the mentioned natural systems refers to the use of synthetic prodigiosin analogues[51] and alkaloids derivatives.[52]

Other synthetic systems were found to exhibit good anion transport activity, including steroid-based receptors (namely cholapods[53] and cholaphanes[54]) and macrocyclic compounds, such as functionalized calixarenes,[65] calixpyrroles[56] and azobenzene-bearing cyclodextrins,[57] allowing the pH[57a]- or light[57b,c]-triggered anion transport across membranes. Moreover, calixpyrroles proved to exhibit enhanced cytotoxic activity, inducing cell apoptosis by disrupting cellular ion homeostasis.[58]

Another important family of anion transporters is represented by those exploiting π-anion interactions:[59] these systems consist of oligo-naphtalenediimide and oligo-perylenediimide rods able to span the membrane thickness and to establish π-anion interactions with Cl^- anion. Recently, insertion of 4-ehynylbenzylimidazolium salts able to form rigid channels in liposomal membranes resulted in efficient Cl^- transport, by means of both electrostatic and π-anion interactions.[60]

Transport of cations constitutes the basis for the biological activity of many antibiotics, such as the polypeptidic one gramicidin, that is able to form channels having suitable dimensions for the selective passage of Na^+ and K^+ ions.[61]

Insertion of photoactive compounds, bearing known photochromic organic moieties such as spyropyran, retinoyl, stilbene and azobenzene, allows to achieve the phototriggered permeation of membranes.

For example, gramicidins covalently linked with a photoactive azobenzene spacer[62] allowed to observe photomodulation of the conductance of the transmembrane channel and introduced the concept of photoregulation of electrochemical potential of vesicles, by means of photoinduced cation transport across membranes.

Light-triggered permeabilization of liposomal membranes towards K^+ ions was achieved by incorporation of azobenzene derivatives[63] in liposomal membranes, able to afford ion permeation through the formation of transient pores. Moreover, this model explains the efflux of small molecules from vesicles and laid the groundwork for the design and development of drug delivery liposomal systems.

1.5.2 Transport of small molecules

The passage of small molecules across biomembranes occurs as a consequence of creation of concentration gradients between the intracellular and extracellular environment because of the selective permeable behaviour of biomembranes, but is usually facilitated by specific transmembrane proteins. For example, transport of carbohydrates is accelerated by specific transmembrane proteins, that allow to keep a constant concentration of glucose.

Release of solutes from liposomal aqueous core is the main challenge in the development of drug delivery systems and it is due to formation of defects and pores[64] in the membrane. This can occur spontaneously or in the presence of specific organic compounds inserted liposomal bilayers able to recognize the occurrence of an osmotic stress[65] or able to release liposomal content after the application of external stimuli, such as pH,[43,66] heat[67] and light.[68]

Light-triggered release of liposomal content implies the destabilization of lipid membrane as a consequence of a photoreaction,[68, 69] e.g. photisomerization, photocleavage or photopolymerization (*Figure 1.8*).

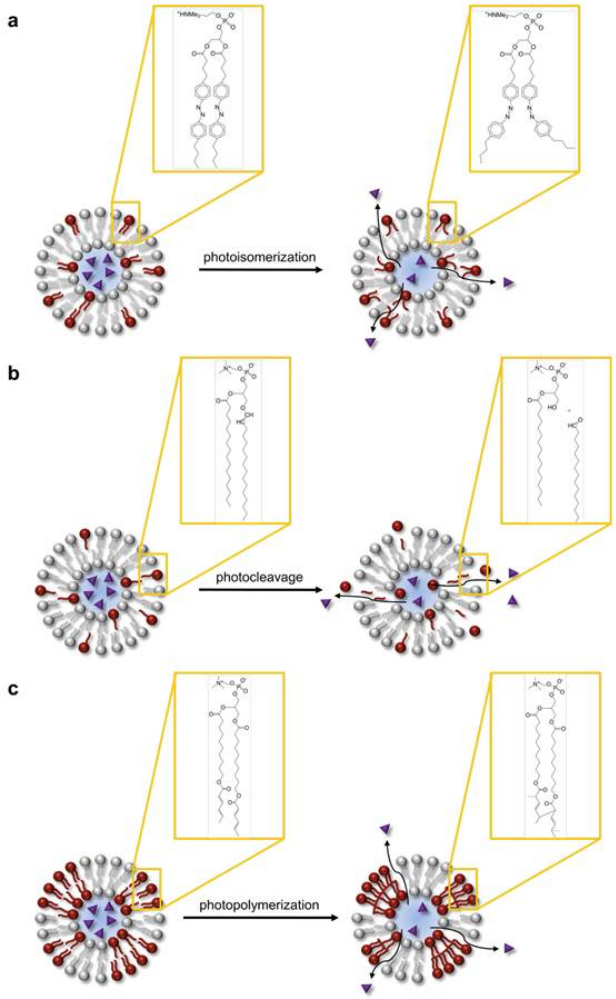

***Figure 1.8*- Mechanisms of light-activated release from liposomes: photoisomerization (a), photocleavage (b) and photopolymerization (c). Reproduced with permission from *Theranostics* 2012, 2, 1020-1036. © 2012 Ivyspring International Publisher.**

Liposome leakage by photoisomerization requires the presence of photochromic groups, such as retinoyl,[70] stilbene,[71] spyropyran[72] and azobenzene.[783]

Incorporation of azobenzene in phospholipid acyl chains,[74] amphiphiles,[75] cholesterol[76] and polymers[77] allows the fast and efficient carboxyfluorescein release, as well as the translocation of other species, such as QDs and peptides.[77a] It is reported that the insertion of polymeric species[78] in liposomal membranes are responsible for the formation of transient pores and that the *cis-trans* photoisomerization of pendant azobenzene moieties in methacrylic copolymers affects the binding ability of these polymeric species to the surface of phosphatidylcholine vesicles and, consequently, surface properties of liposomal membrane.[79] Release of liposomal contents by photocleavage requires the presence of photocleavable compounds, such as naturally occurring plasmalogens[80] (which are photocleaved by photodynamic sensitization in the presence of visible and near infrared light absorbers, such as zinc phtalocyanine and bacteriochlorophill A[81]). Moreover, photocleavable dithiane-based spacers[82] were inserted in the acyl chain of phospholipids, allowing unloading of pyridine from vesicles upon UV irradiation.

Photo-induced crosslinking of lipids represents another photochemical tool for inducing leakage of encapsulated material in liposomes. For example, photocrosslinking of 1,2-bis[10-(2',4'-hexadienoyloxy)-decanoyl]-*sn*-phosphatidylcholine[83] enhances the permeability of the marker present in liposomal interior and the addition photosynthesizers, such as cyanine dyes, allowed to achieve liposomal destabilization upon visible-light irradiation.[84]

Another possibility to achieve light-triggered release from liposomes lies in the photophysical activation of liposomal content, exploiting photothermal conversion of non-emitting or quenched dyes that are inserted in the phospholipid bilayer or encapsulated in the aqueous core: this approach proved to be very versatile, since it is possible to sensitize the liposomal content to a wide range of light wavelengths, making it highly effective for *in vivo* applications, such as the delivery of ophtalmic drugs.[85]

Photothermal conversion mediated by non-resonant gold nanoparticles allowed the release of berberin[86] from liposomes upon UV light irradiation. Moreover, leakage of small molecules from liposomal interior was observed in three different gold-liposome configurations: (i) gold nanoparticles covalently linked to lipid headgroups,(ii) gold nanoparticles protected with mercaptosuccinic acid

encapsulated in the aqueous interior of liposomes and (iii) hexanethiol-capped gold nanoparticles inserted in the phospholipid bilayer. In order to decrease the phototoxicity of the nanocarrier and to use excitation wavelengths in the visible region of the electromagnetic spectrum, liposomes surface was coated with plasmon resonant gold nanoparticles, yielding very stable structures, that are easy to store and manipulate and resulted in the photothermal release of entrapped doxorubicin and carboxyfluorescein.[87]

1.6 Azobenzene in supramolecular systems

Since the discovery of its photoreactivity by G.S. Hartley in 1937,[88] azobenzene photochromism has been extensively exploited in the design of artificial molecular systems.

Azobenzene undergoes an *E*⇄*Z* isomerization reaction (*Figure 1.9*) under UV light exposure and the reaction is reversible, fast, efficient and chemoselective, not leading to the formation of other products.

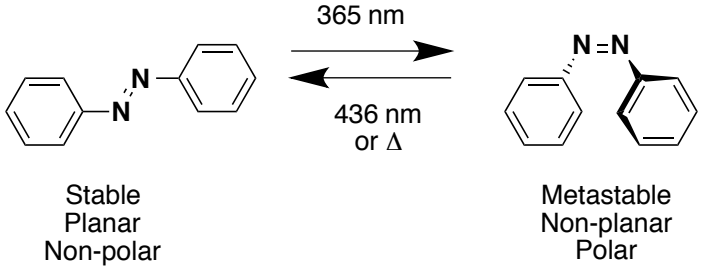

***Figure 1.9*- Isomerization of azobenzene.**

Among the two geometric isomers of azobenzene, the *E* one is the most thermodynamically stable, so that *Z*-azobenzene spontaneously reverts to the more stable *E* isomer if kept in the dark at room temperature.

Both azobenzene isomers exhibit different physical properties, such as geometry, dipole moment and absorption spectrum[89]: in fact, UV-Vis absorption spectrum of *E*-azobenzene exhibits an intense band in the near UV region that refers to π–π* transitions and a weak band located in the visible region, ascribable to n-π* transitions. Moreover, it has no dipole moment, whereas the one for *Z* isomer is 3 D. *E*→*Z* photoisomerization reduces the distance between two carbon atoms in

position 4 on the aromatic phenyl rings, passing from 9 Å to 5.5 Å and relevant changes in the absorption spectrum are seen (*Figure 1.10*): in fact, a decrease in the intensity of the π–π* transitions' band with a concomitant hypsochromic shift and an increase of the band referring to n-π* transitions are observed.

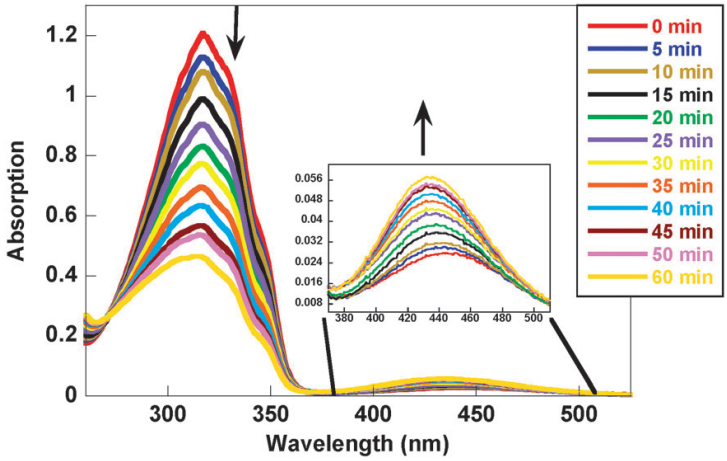

***Figure 1.10*- Changes in the absorption spectrum of azobenzene upon irradiation with UV light. Reproduced with permission from *Chem. Soc. Rev,* 2012, 41, 1809-1825 © 2012 Royal Society of Chemistry.**

The sum of photochemical quantum yields referring to $E \rightarrow Z$ and $Z \rightarrow E$ photoisomerization does not equal unity, as happens for other photochromic units, such as stilbene.[90] Azobenzene isomerization may occur according to multiple pathways (*Figure 1.11*) and among them the most accepted are inversion and rotation mechanisms.

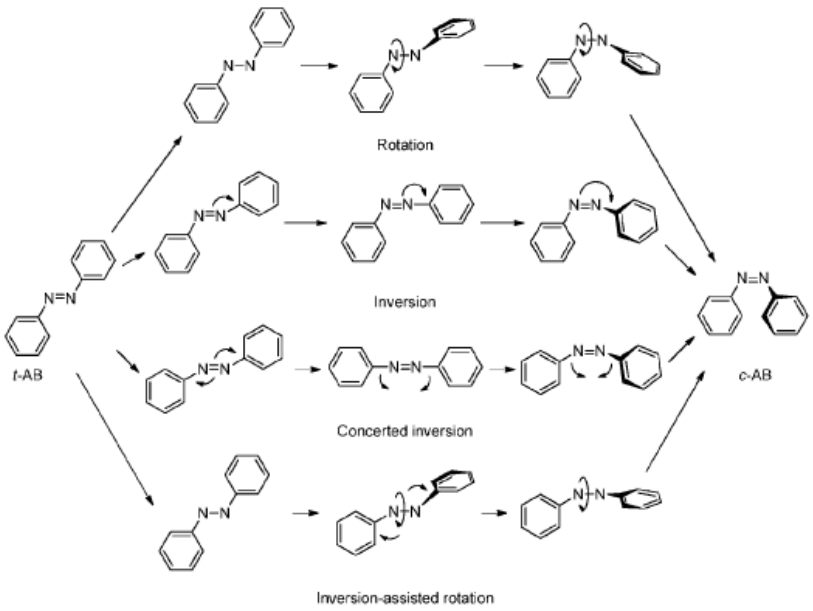

***Figure 1.11*- Proposed mechanisms for azobenzene isomerization. Reproduced with permission from *Chem. Soc. Rev,* 2012, 41, 1809-1825 © 2012 Royal Society of Chemistry.**

Since the basic condition for the development of a molecular switch is that it has to exist in two different and stable isomeric forms, azobenzene photochromic unit has incorporated in a myriad of supramolecular systems, comprising molecular devices and machines.[5]

More recently, azobenzene photoisomerization has been exploited in the development of molecular motors[91] and memories.[94] In the case of molecular motors, azobenzene photoisomerization enables the control over directionality of the transit of a macrocycle in a pseudorotaxane system[91a,b] (*Figure 1.12*), leading to the development of an autonomous supramolecular cycling system exploiting non-equilibrium processes[91b] and powered only by light input, resembling biomolecular motors.[93]

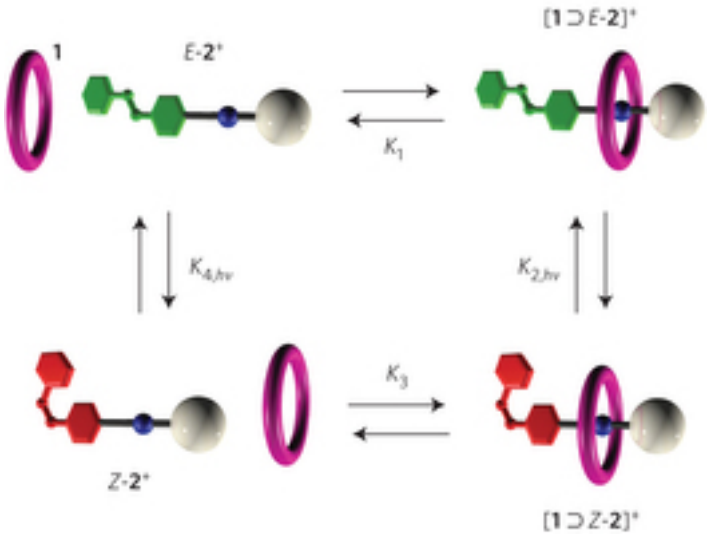

***Figure 1.12*- Square cycle of chemical and photochemical reactions representing operation of the system. Reproduced with permission from *Nature Nanotech.*, 2015, 10, 70-75. © 2015 Macmillan Publishers Limited.**

For kinetic reasons, the macrocyclic component enters from the *E*-azobenzene moiety of the axle and reaches the ammonium recognition site, leading to the formation of a [2]pseudorotaxane. Irradiation affords *Z*-azobenzene, that is bulkier than the *E* isomer and this destabilizes the pseudorotaxane and causes host ejection. This system resembles a light-triggered pump[92] that operates cyclically under photostationary conditions and can potentially induce concentration gradients when inserted in semipermeable membranes.

On the other hand, molecular memories are supramolecular systems able to process and store informations and azobenzene photoisomerization ensures to block and erase them, restoring the initial condition.

In the case of rotaxanes, orthogonal stimuli allow to completely control thermodynamics and kinetics of molecular shuttling. The molecular memory developed in 2012 by Avellini *et al.*[94] is composed of a photoactive axle bearing a central azobenzene unit and two different recognition sites and a π-electron deficient ring. The system is able to perform a "write-lock-erase" cycle, by means of redox and light inputs (*Figure 1.13*).

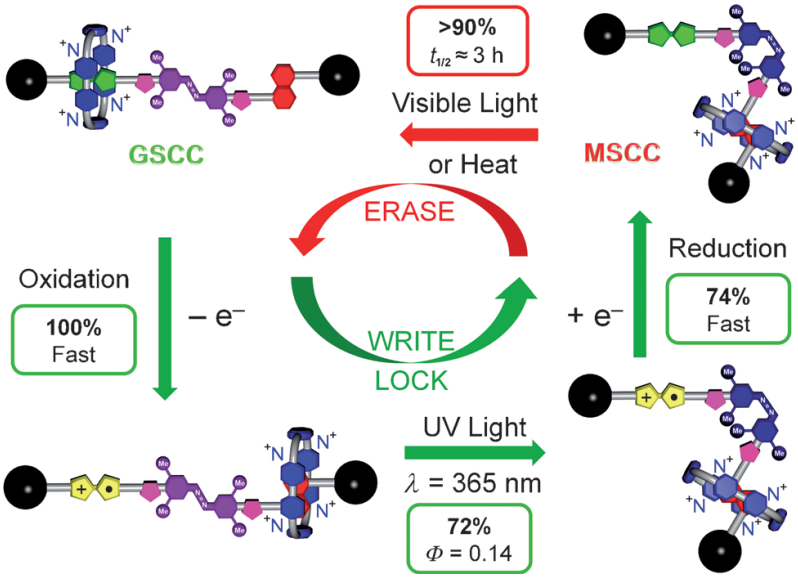

***Figure 1.13*- Chemically and photochemically triggered memory switching. Reproduced with permission from *Angew. Chem. Int. Ed.* 2012, 51, 7, 1611-1615.© 2012 Wiley-VCH Verlag GmbH & Co.**

In this system, the data are written by application of an oxidation stimulus and are then locked by photoisomerization of the azobenzene central unit. The oxidized species can be reduced back to the original form, without losing the written information: for this step, the kinetic of the $Z \rightarrow E$ thermal isomerization is essential in order to develop a molecular memory able to lock the written data in a metastable state co-conformation (MSCC). Moreover, irradiation of the *Z*-azobenzene moiety allows restoring of the ground state co-conformation (GSCC), erasing the written data.

1.6.1 Azobenzene in biological systems

Configurational isomerization of double bonds represents an important process in biological systems and it is involved in protein folding and in the mechanism of vision. For example, isomerases represent a category of enzymes able to catalyse isomerization processes, such as *cis-trans* peptidic bond in proline residues. Moreover, light is responsible for the isomerization of 11-*cis*-retinal in rhodopsin and the conformational change is responsible for the change in the electrochemical potential that leads to the subsequent transduction cascade that allows the vision process.[95]

Since isomerizations represent the basis for many important biological processes and azobenzene proved to be a versatile photochromic group in the development of molecular devices and machines, its incorporation in biologically relevant molecules can lead to develop light-controlled biomolecules.[96]

In the design of photocontrolled biomolecules, it is important to take into account some aspects referring to azobenzene photoisomerization:

- coupling of azobenzene photoisomerization must affect the activity or function of the biomolecule;
- since absorption spectra of *cis* and *trans* isomers of azobenzene overlap, irradiation leads to a photostationary state in which one isomer is not totally converted in the other one; in contrast, thermal *cis-trans* isomerization affords 100% of *trans* isomer, so it is preferable to use this last approach to reset the photoswitch;
- to achieve photo-control *in vivo*, it is necessary to choose a wavelength compatible with cells and biological tissues and in this case the choose of substituents in the resulting switch is essential in order to tune photochemical properties[97] and kinetics of thermal relaxation of the azobenzene unit.

Photocontrol of biomolecules, thus, allows to obtain a large change in the structure and function of the targeted biomolecule after the application of a light stimulus.

For example, insertion of azobenzene in proteins results in the triggering of their folding/unfolding transitions[98] by applying light inputs in a reversible manner.

Moreover, azobenzene photoisomerization allows the modulation of ion channels,[99] such as gramicidin ion channels[100] by creation of a molecular gate (*Figure 1.14*).

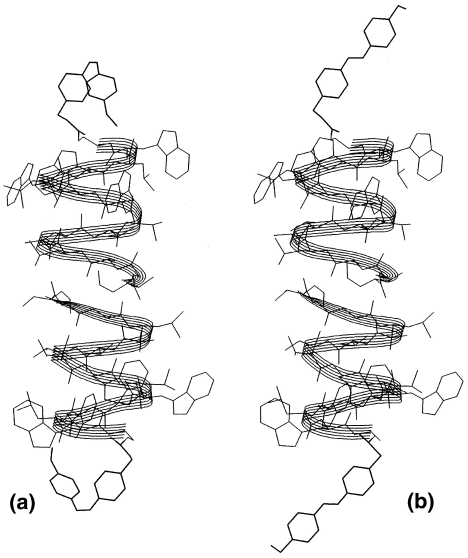

***Figure 1.14*- Structure of azobenzene-modified gramicidin channels, exhibiting azobenzene in its *cis* (a) and *trans* (b) conformation. Reproduced with permission from *J. Am. Chem. Soc.*1996, 118, 48, 12222-12223. © 1996 American Chemical Society.**

In this case, insertion of azobenzene did not modify the structure of gramicidin channel, but *trans-cis* isomerization resulted in alteration of conductance in these channels in a reversible fashion.

A more powerful effect in the photo-regulation of proteins is obtained when azobenzene is embedded in enzymes: in the case of non-specific labelling of papain,[101] azobenzene photoisomerization led to a 3-fold change of its activity. Schierling *et al.* presented a more elegant example of photoregulation of enzymatic activity: in this example, employment of a bifunctional azobenzene derivative for the cross-linking of cystein residues in a restriction endonuclease,[102] allowed to obtain a construct containing two photoactive cross-linkers located at the proximity of the enzymatic active site and this modified endonuclease exhibited a 16-fold increase in its DNA cleavage activity.

It is interesting that azobenzene photoisomerization is potentially able to turn off/on gene expression, by means of creation of a DNA photoswitchable molecular glue.[103] This glue allows a reversible and bidirectional photocontrol of adhesion of single-stranded DNAs that do not reciprocally hybridize.

In addition to the abovementioned applications, azobenzene photoisomerization is able to perform more sophisticated operations: for example, it allows to induce alteration in the membrane of DOPC liposomes,[104] mimicking some important cellular processes, such as budding-fission-fusion sequence observed in

phagocytosis. Moreover, insertion of azobenzene in RGD (arginine-glycine-aspartate) receptors grafted on self-assembled monolayers (SAMs) of alkane thiols on Au, allows to photocontrol cell adhesion reversibly on a molecularly-defined surface[105]: in fact, when the azobenzene unit is in its *cis* form, the RGD tripeptide is masked, thus inhibiting cell adhesion; in contrast, switching to the *trans* form enables cells to recognize the RGD ligand and to adhere to SAMs surface (*Figure 1.15*).

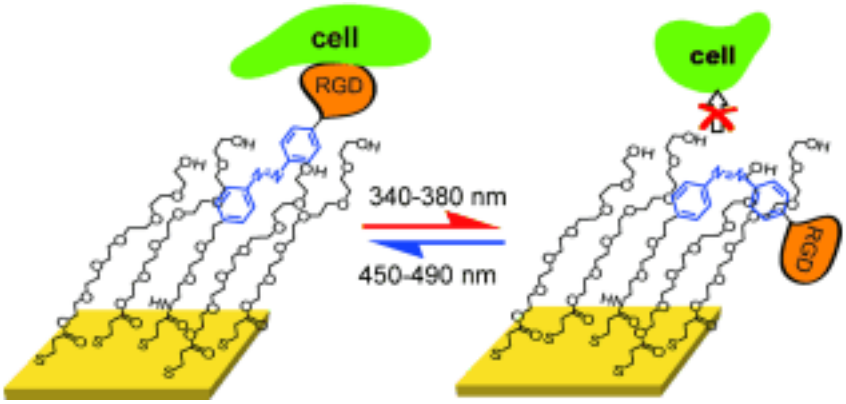

***Figure 1.15*- Photochemically triggered cell adhesion on SAMs surface. The azobenzene moiety can be converted photochemically between the E and Z configurations to either present or mask the RGD ligand and hence modulate biospecific cell adhesion. Reproduced with permission from *Angew. Chem. Int. Ed.* 2009, 48, 24, 4406-4408. © 2009 Wiley-VCH Verlag GmbH & Co.**

Recently, incorporation of azobenzene unit in the molecular structure of bioactive compounds is responsible for the dynamic control of its biological activity and gave birth to the concept of photopharmacology.[106] Incorporation of an azobenzene photoswitch into the structure of different pharmaceutical agents, such as chemotherapeutic agents[107] and antibiotics allowed the photocontrol over bacterial growth (*Figure 1.16*).[108]

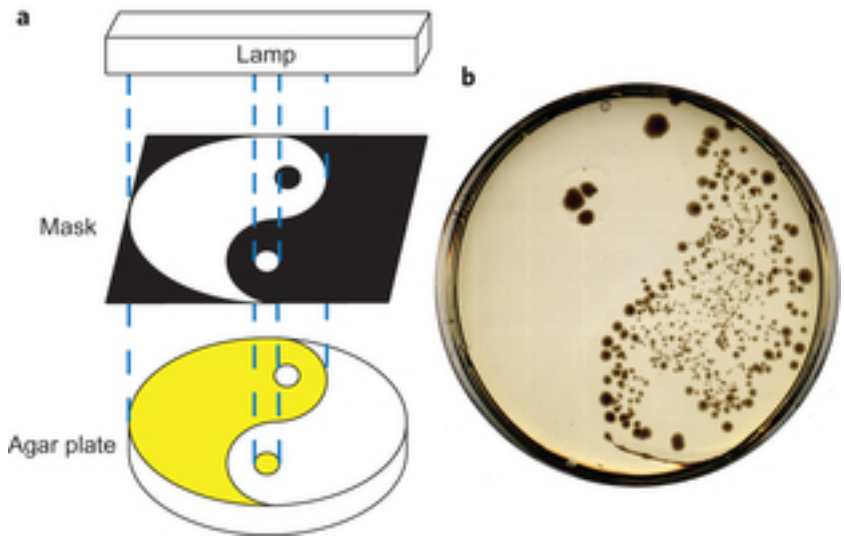

***Figure 1.16*- Bacterial patterning with light. Reproduced with permission from *Nature Chem.* 2013, 5, 11, 924-928. © 2013 Macmillan Publishers Ltd.**

The antibacterial activity of *trans* and *cis* isomers is different and among them the *cis* isomer exhibited high antibacterial activity against both Gram-positive and Gram-negative bacteria, whereas the *trans* isomer resulted inactive.

1.7 DNA-small molecules interaction

DNA represents the tool used by biological systems for storage of the genetic information and the genetic code is expressed during the transcription process: the result of this process is the phenotype, which is substantially made of proteins that reflect the observable physical and biochemical characteristics found in living organisms. The main phase in transcription is the copy of the DNA sequence to be translated as a sequence of RNA and this involves the interaction between a specific portion of DNA with specific enzymes.

Interaction between DNA and external ligands represents and effective tool in the development of therapeutic agents, since ligands, once complexed, are able to determine a structural change in the double helix of DNA.

External ligands can exhibit different binding modes to DNA double helix, by undergoing covalent or non-covalent interactions. Ligands that are able to covalently interact with DNA are known as alkylating agents[109] and among them the most popular is the anticancer drug cisplatin.[110] These agents

specifically bind to N-7 position of guanine and N-3 position of adenine bases, leading to base pairing inhibition and DNA fragmentation by repairing enzymes. Another possibility lies in the formation of cross-bridges between two complementary DNA bases that are located in opposite sides of the double helix, as a consequence of the presence of an alkylating agent bearing two alkylating sites.

In addition to covalent interactions, external ligands can bind to DNA by means of non-covalent interactions,[109,111] namely hydrogen bonding, π-stacking, van der Waals, hydrophobic and electrostatic interactions.

Groove binding and intercalation of external ligands to DNA requires that the ligand meets certain precise structural criteria: in fact, groove binders usually consist of at least two aromatic or heteroaromatic rings whose connections allow the required flexibility in order to fit perfectly into the groove. Moreover, groove binders can bind to minor or major groove of DNA, depending on the dimensions of the binder. In fact, the size of the two grooves is different; usually the major groove is the preferred binding site for DNA-interacting proteins. Typical minor groove-binders are Hoechst 33258 (*Figure 1.17*, **1**) netropsin (*Figure 1.17*, **2**) and furamidines (*Figure 1.17*, **3**).

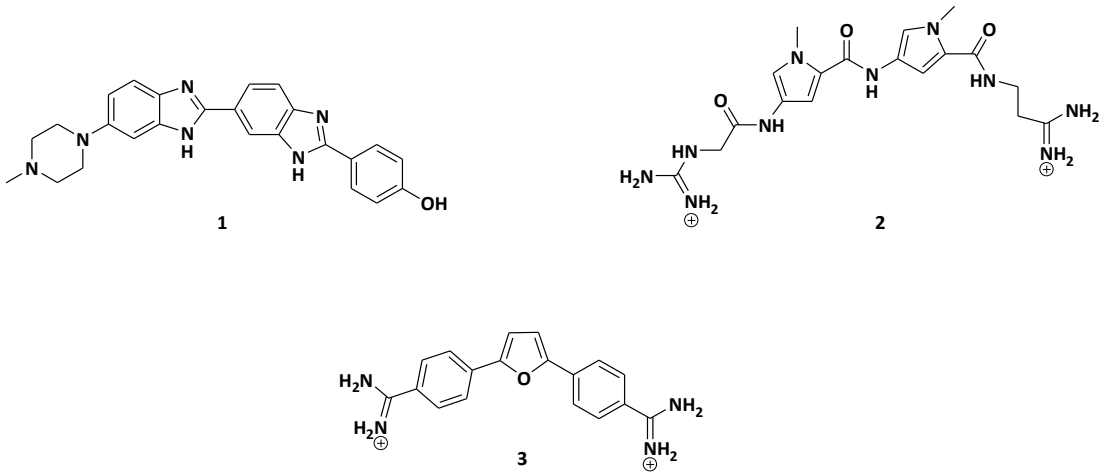

***Figure 1.17*- Typical minor groove binders.**

Intercalation of a small molecule in the DNA interior occurs upon unwinding of DNA and separation of two neighbouring base pairs. Hence, this binding mode results in dramatic perturbation of DNA structure. Such a structural change can suppress important recognition processes that are essential for DNA-based

cellular processes and thus can be used as a chemotherapeutic principle. Generally, a small molecule may act as an intercalator if its structure consists of a flat aromatic system made of at least two fused arene units, thus providing a maximal overlap of π surfaces. Moreover, it is reported that cationic intercalators exhibit larger stabilization energy compared to that of neutral ones: this arises from the larger energy contributions based on electrostatic interactions provided by charged ligands.[112] In this regard, the most popular intercalator is ethydium bromide (*Figure 1.18*, **4**), but recently, it was found that other polycyclic system,[113] such as diethinylethenes[114] (*Figure 1.15*, **5**) are able to bind to DNA enantioselectively in a reversible and photocontrolled fashion.

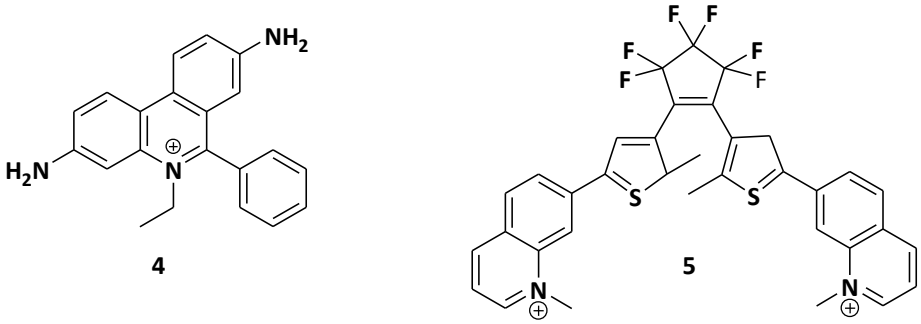

***Figure 1.18*- Typical DNA intercalators.**

As mentioned before, the intercalation event gives rise to drastic changes in DNA structure and reduces significantly the rotational, translational and vibrational freedom of the intercalator itself. On the other hand, the torsional angles of deoxyribose residues in DNA backbone, in which the intercalator is going to settle, have to change, thus reducing the helical twisting. At the same time, lengthening of the double helix occurs, due to separation of base pairs at the intercalation site. These structural changes are reflected into modifications in the spectroscopic properties of both the intercalator and DNA. In particular, upon intercalation induced dichroic signals (ICD) in the CD spectrum of DNA appear, as well as changes of its absorption/emission properties.

1.8 Aim of the work

This work refers to the study of biocompatible supramolecular species able to interact with light, in order to develop systems exhibiting potential applications for bioimaging and drug delivery.

In the first part, the photophysical, photochemical and electrochemical properties of water-soluble blue-emitting triazolopyridinium and triazoloquinolinium salts have been explored and their interaction of DNA, for the development of water-soluble systems for bioimaging applications (Chapter 3).

The second part of the work concerns the study of the effect exerted by the presence of light-driven supramolecular species in liposomes, inserted both in the phospholipid bilayer and in the in the aqueous core of vesicles, in order to develop light-triggered drug delivery systems (Chapter 4). Moreover, the possibility of photocontrolling efflux of ions from vesicles has been explored by synthesizing a photoactive anion transporter and by testing its anionophoric activity (Chapter 5).

In the last part, conjugated oligoazobenzene were evaluated for their insertion in liposomal bilayers, but their poor photoreactivity made them inadequate candidates for this purpose. In contrast, their electrochemical properties made them interesting candidates as electron acceptor materials for photovoltaic applications (Chapter 6).

References

[1] Fischer, H. E., *Chem. Ber.*,**1894**, 27, 2985-2993.

[2] a) Lehn, J.M., *Angew. Chem. Int. Ed. Engl.*,**1988**, 27, 1, 89-112.b) Lehn, J.M., *PNAS*, **2002**, 99, 8, 4763-4768.

[3] Nobel Prize Chemistry http://www.nobelprize.org/nobel_prizes/chemistry/laureates/1987/.

[4] Lehninger, A.L.; Nelson, D.L.; Cox, M.M., *Principi di Biochimica*, V edizione, Zanichelli: Bologna, **2010**.

[5] Balzani, V.;Credi, A.; Venturi, M., *Molecular Devices and Machines—Concepts and Perspectives for the Nanoworld*, Wiley-VCH, 2008.

[6] a) Israelachvili, J.N.; Mitchell, D.J.; Ninham, B.W. *J. Chem. Soc. Perkin Trans 2*, **1976**, 72, 1525-1568. b) Israelachvili, J.N.; Marcelja, R.G.; Horn, R.G., *Q. Rev. Biophys.*, **1980**, 13, 2, 121-200.

[7] Ohvo-Rekilä, H.; Ramstedt, B.; Leppimäki, P.; Slotte, P., *Progr. Lipid Res.*, **2002**, 41, 66-97.

[8] Demel, R.A.; De Kruyff, B., *Biochim. Biophys. Acta: Biomembranes*, **1976**, 457, 2, 109-132.

[9] a) Yeagle, P.L., *Biochim. Biophys. Acta: Biomembranes*, **1985**, 822, 3-4, 267-287. b) Needham, D.; Nunn, R.S., *Biophys. J.*, **1990**, 58, 4, 997-1009.

[10] Stockton, B.W.; Smith, I.C.P., *Chem. Phys. Lipids*, **1976**, 17, 251-263.

[11] Singer, S.J.; Nicholson, G.L., *Science*, **1972**, 175, 4023, 720-731.

[12] a) Cruciani, O.; Mannina, L.; Sobolev, A.P.; Cametti, C.; Segre, A.L., *Molecules*, **2006**, 11, 334-344. b) Gawrisch, K.; Gaede, H.C.; Mihailescu, M.; White, S.H., *Eur. Biophys. J.*, **2007**, 36, 281-291.

[13] Bangham, A.D.; Horne, R.W., *J. Mol. Biol.*, **1964**, 8, 5, 660-668.

[14] Immordino, M.L.; Dosio, F.; Cattel, L., *Int. J. Nanomed.*, **2006**, 1, 3, 297-315.

[15] Senior, J.; Gregoriadis, G., *Life Sci.*, **1982**, 30, 24, 2123-2136.

[16] a) Grit, M.; Crommelin, D.J.A., *Chem. Phys. Lipids*, **1993**, 64, 1-3, 3-18.
b) Porter, N.A.; Caldwell, S.E; Mills, K.A., *Lipids*, **1995**, 30, 4, 277-290.
c) Ytzhak, S.; Weitman, H.; Ehrenberg, B, *Photochem. Photobiol.*,**2013**, 89, 619-624.

[17] a) Barenholz, Y.; Crommelin, D.J.A, *Encyclopedia of Pharmaceutical*

Technology, Marcel Dekker: New York, **1994**. b) Akbarzadeh, A.; Razaei Sadabady, R.; Davaran, S.; Joo, S.W.; Zarghami, N.; Hanifehpour, Y.; Samiei, M; Kouhi, M.; Nejati-Koshki, K., *Nanoscale Res. Lett.*, **2013**, 8, 102-110.

[18] Ye, C.; Wang, Y.; Li, C.; Yu, J.; Hu, Y., *Microchim. Acta*, **2013**, 180, 117-125.

[19] Meunier, F.; Prentice, H,G,; Ringdén, O., *J. Antimicrob. Chemotherap.*, **1991**, 28, 83-91.

[20] Olson, J.A.; Adler-Moore, J.P.; Jensen, G.M.; Schwartz, J.; Dignani, M.C.; Proffitt, R.T., *Antimicrob. Agents Chemotherap.*,**2008**, 52, 259-268.

[21] Rivera, E.; *Oncologist*, **2009**, 8, 3-9.

[22] Barenholz, Y.; *J. Contr. Rel.*, **2012**, 160, 117-134.

[23] Park, J.; *Breast Canc. Res.*, **2002**, 4, 95-99.

[24] Hong, R.L.; *J. Chin. Oncol. Soc.*, **2004**, 20, 10-21.

[25] Chowdary, R.K.; Shariff, I.; Dolphin, D., *J. Pharm. Pharm. Sci.*, **2003**, 6, 13-19.

[26] Fahr, A.; Van Hoogevest, P.; May, S.; Bergstrand, N.; Leigh, M.L., *Eur. J. Pharm. Sci.*, **2005**, 26, 251-265.

[27] Usonis, V.; Bakasenas, V.; Valentelis, R.; Katiliene, G.; Vidzeniene, D.; Herzog, C., *Vaccine*, **2003**, 21, 4588-4592.

[28] Herzog, C.; Hartmann, K.; Kunzi, V.; Kursteiner, O.; Mischler, R.; Lazar, H.; Gluck, R., *Vaccine*, **2009**, 27, 4381-4387.

[29] Wasan, K.M.; Lopez-Berestein, G., *Clin. Infect. Dis.*, **1996**, 23, 1126-1138.

[30] Guo, L.S.; *Adv. Drug.Deliv. Rev.*, **2001**, 47, 149-163.

[31] Chang, H.-I.; Yeh, M.-K., *Int. J. Nanomed.*, **2007**, 7, 49-60.

[32] a) Storm, G.; Crommelin, D.J.A., *Phram. Sci. & Tech.*, 1998, 1, 19-31. b) Torchilin, V.P.; *Nature Rev. Drug Disc.*,**2005**, 4, 145-160. c) Natarajan, J.V.; Nugraha,C.; Ng, X.W.; Venkatraman, S., *J. Contr. Rel.*, **2014**, 193, 122-138.

[33] Eloy, J.O.; De Souza, M.C.; Petrilli, R.; Barcellos, J.P.A.; Lee, R.J.; Marchetti, J.M., *Coll. Surf. B*, **2014**, 123, 345-363.

[34] Torchilin, V.P.; *CRC Crit. Rev. Ther. Drug Carr. Syst.*, **1985**, 1, 65-115

[35] a) Gabizon, A.A.; *Cancer Invest.*, **2001**, 19, 424-436. b) Torchilin, V.P.; Omelyanenko, V.G.; Papisov, M.I.; Bogdanov, A.A; Trubetskoy, V.S.; Herron, J.N.; Gentry, C.A., *Biochim. Biophys. Acta*, **1994**, 1195, 1, 11-20. c) Torchilin, V.P.; Trubetskoy, V.S., *Adv. Drug. Del. Rev.*, **1995**, 16, 141-155. d) Allen, T.M.; Hansen, C., *Biochim. Biophys. Acta*, **1991**, 1068, 133-141.

[36] Yang, F.; Jin, C.; Jiang, Y.; Li, J.; Di, Y.; Ni, Q.; Fu, D., *Cancer Treat. Rev.*, **2011**, 37, 633-642.

[37] Lukyanov, A.N.; Elbayoumi, T.A.; Chakilam, A.R.; Torchilin, V.P., *J. Contr. Rel.*, **2004**, 100, 135-144.

[38] a) Gabizon, A.; Shmeeda, H.; Horowitz, A.T.; Zalipsky, S., *Adv. Drug Deliv. Rev.*, **2004**, 56, 1177-1192. b) Ni, S.; Stephenson, S.M.; Lee, R.J., *Anticancer Res.*, **2002**, 22, 2131-2135. c) Pan, X.Q.; Wang, H.; Lee, R.J., *Pharm. Res*, **2003**, 20, 417-422. d) Pan, X.Q.; Zheng, X.; Shi, G.; Wang, H.; Ratnam, M.; Lee, R.J., *Blood*, **2002**, 100, 594-602.

[39] a) Hatakeyama, H.; Akita, H.; Maruyama, K.; Suhara, T.; Harashima, H., *Int. J. Pharm.*, **2004**, 281, 25-33. b) Ishida, O.; Maruyama, K.; Tanahashi, H.; Iwatsuru, M.; Sasaki, K.; Eriguchi, M.; Yanagle, H., *Pharm. Res.*, **2001**, 18, 1042-1048.

[40] Drummond, D.C.; Hong, K., Park, J.W.; Benz, C.C.; Kirpotin, D.B., *Vitam. Horm.*, **2000**, 60, 285-332.

[41] Loose, M.; Schwille, P., *J. Struct.Biol.*, **2009**, 168, 1, 143-151.

[42] a) Kinoshita, T.; *Prog. Polym. Sci.*, **1995**, 20, 527-583. b) Mann, S.; *Angew. Chem. Int. Ed.*, **2008**, 47, 29, 5306-5320.

[43] a) Sharma, N.K.; Kumar, V., *Drug Del. Lett.*, **2014**, 4, 12-20. b) Gerasimov, O.V.; Boomer, J.A.; Qualls, M.M.; Thompson, D.H., *Adv. Drug Del. Rev.*, **1999**, 38, 317-338.

[44] a) Jentsch, T.J.; Hubner, C.A.; Fuhrmann, J.C., *Nature Cell Biol.*, **2004**, 6, 1039-1047. b) Cordat, E.; Casey, J.R., *Biochem. J.,* **2009**, 417, 423-439.

[45] a) Eggermont, J., *Proc. Am. Thorac. Soc.*, **2004**, 1, 22–27. b) Gadsby, D.C.; Vergani, P.; Csanádi, L., *Nature*, **2006**, 440, 477-483.

[46] Davis, J.T.; Okunola, O.; Quesada, R., *Chem. Soc. Rev.*, **2010**, 39, 3843-3862.

[47] Fürstner, A.; *Angew. Chem. Int. Ed.*, **2003**, 42, 31, 3582-3603.

[48] Harrell, W.A.; Bergmeyer, M.L.; Zavalij, P.Y.; Davis, J.T, *Chem. Comm.*, **2010**, 46, 3950-3952.

[49] Bahmanjah, S.; Zhang, N.; Davis, J.T., *Chem. Comm.*, **2012**, 48, 4432-4434.

[50] Busschaert, N.; Gale, P.A., *Angew. Chem. Int. Ed.*, **2013**, 52, 1374-1382.

[51] Sessler, J.L.; Eller, L.R.; Cho, W.-H.; Nicolau, S.; Aguillar, A.; Lee, J.T.; Lynch, V.M.; Magda, D.J., *Angew. Chem. Int. Ed.*, **2005**, 44, 37, 5989-5992.

[52] Hernández, P.I.; Moreno, D.; Javier, A.A.; Torroba, T.; Pérez-Tomás, R.; Quesada, R., *Chem. Comm.*, **2012**, 48, 1556-1558.

[53] McNally, B.A.; Koulov, A.V.; Lambert, T.N.; Smith, B.D.; Joos, J.B.; Sisson, A.L.; Clare, J.P.; Sgarlata, V.; Judd, L.W.; Magro, G.; Davis, A.P., *Chem. Eur. J.*, **2008**, 14, 31, 9599-9606.

[54] Judd, L.W.; Davis, A.P., *Chem. Comm.*, **2010**, 46, 2227-2229.

[55] a) Sidorov, V.; Kotch, F.W.; Abdrakhmanova, G.; Mizani, R.; Fettinger, J.C.; Davis,J.T., *J. Am. Chem. Soc.*, **2002**, 124, 2267-2278. b) Okunola, O.A.; Seganish, J.L.; Salimian, K.J.; Zavalij, P.Y.; Davis, J.T., *Tetrahedron*, **2007**, 63, 44, 10743-10750. c) Seganish, J.L.; Santacroce, P.V.; Salimian, K.J.; Fettinger, J.C.; Zavalij, P.Y.; Davis, J.T., *Angew. Chem. Int. Ed.*, **2006**, 45, 20, 3334-3338. d) Zappacosta, R.; Fontana, A.; Credi, A.; Arduini, A.; Secchi, A., *Asian J. Chem.*, just accepted, DOI: 10.1002/ajoc.201402244

[56] Tong, C.C.; Quesada, R.; Sessler, J.L.; Gale, P.A., *Chem. Comm.*, **2008**, 6321-6323.

[57] a) Madhavan, N.; Robert, E.C.; Gin, M.S., *Angew. Chem. Int. Ed.*, **2005**, 44, 46, 7584-7587. b) Jog, P.V.; Gin, M.S., *Org. Lett.*,**2008**, 10, 17, 3693-3696. c) Kauscher, U.; Samanta, A.; Ravoo, J.B., *Org. Biomol.Chem.*,**2014**, 12, 600-606.

[58] Ko, S.-K.; Kim, S.K.; Share, A.; Lynch, V.M.; Park, J.; Namkung, W.; Rossom, W.V.; Busschaert, N.; Gale, P.A.; Sessler, J.L.; Shin, I., *Nature Chem.*, **2014**, 6, 885-892.

[59] a) Dawson,R. E.; Hennig, A.; Weimann, D. P.; Emery,D.; Ravikumar, V.; Montenegro, J.; Takeuchi, T.; Gabutti, S.; Mayor, M.; Mareda, J.; Schalley, C. A.; Matile, S., *Nat. Chem.*, **2010**, 2, 533–538. b) Frontera,A.; Gamez, P.; Mascal, M.; Mooibroek, T. J.; Reedjik, J., *Angew. Chem. Int. Ed.*, **2011**, 50, 9564–9583. c) Salonen, L. M.; Ellermann, M.; Diederich, F., *Angew. Chem. Int. Ed.*, **2011**, 50,4808–4842. d) Chifotides, H. T.; Dunbar, K.R.,*Acc. Chem. Res.*, **2013**, 46, 894–906.

[60] Elie, C-R.; Charbonneau, M.; Schmitzer, A.R., *Med. Chem. Comm.*, **2012**, 3, 1231-1234.

[61] a) Smart, O.S.; Goodfellow, J.M.; Wallace, B.A., *Biophys. J.*, **1993**, 65, 2455-2460. b) Wallace, B.A.; *J. Struct. Biol.*, **1998**, 121, 123-141.

[62] Stankovic, C.J.; Heinemann, S.H.; Schreiber, S.L., *Biochim. Biophys. Acta*, **1991**, 1061, 163-170.

[63] Sato, T.; Kijima, M.; Shiga, Y., Yonezawa, Y., *Langmuir*, **1991**, 7, 2330-2335.

[64] a) Kaschiev, D.; Exerowa, D., *Biochim. Biophys. Acta*, **1983**, 732, 133-145. b) Zehl, T.; Wahab, M.; Mogel, H.-J.; Schiller, P., *Langmuir*, **2009**, 25, 13, 7313-7319. c) Ménager, C.; Cabouil, V., *J. Phys. Chem. B*, **2002**, 106, 7913-7918. d) D'Acunto, M.; *Mech. Res. Comm.*, **2011**, 38, 34-37. e) Fuhrmans, M.; Marelli, G.; Smirnova, Y.G.; Müller, M., *Chem. Phys. Lipids*, **2015**, 185, 109-128.

[65] Louhivuori, M.; Risselada, H.J.; Van der Giessen, E.; Marrink, S.J., *PNAS*, **2010**, 46, 19856-19860.

[66] a) Karanth, H.; Murthy, R.S., *J. Pharm. Pharmacol.*, **2007**, 59, 4, 469-483. b) Paliwal, S.R.; Paliwal, R.; Vyas, S.P., *Drug Del.*, **2014**, doi:10.3109/10717544.2014.882469

[67] Kneidl, B.; Peller, M.; Winter, G.; Lindner, L.H.; Hossann, M., *Int. J. Nanomed.*, **2014**, 9, 4387-4398.

[68] Leung, S.J.; Romanowski, M., *Theranostics*, **2012**, 2, 10, 1020-1036.

[69] a) Shum, P.; Kim, J.-M.; Thomson, D.H., *Adv. Drug. Del. Rev.*, **2001**, 53, 273-284. b) Fomina, N.; Sankaranarayanan, J.; Almutairi, A., *Adv. Drug. Del. Rev.*, **2012**, 64, 1003-1020.

[70] Pidgeon, C; Hunt, C.A., *Photochem. Photobiol.*,**1983**, 37, 491-494.

[71] Lei, Y.; Hurst, J.K., *Langmuir*, **1999**, 15, 3424-3429.

[72] a) Ohya, Y.; Okuyama, Y.; Fukunaga, A.; Ouchi, T., *Supramolec. Sci.*, **1998**, 5, 21-29. b) Zappacosta, R.; Siani, G.; Silvi, S.; Credi, A.; Fontana, A., *Langmuir*, **2014**, 30, 13667-13672.

[73] a) Kano, K.; Tanaka, Y. Ogawa, T.; Shimomura, M.; Kunitake, T., *Photochem. Photobiol.*,**1981**, 34, 323-329. b) Morgan, C.G.; Thomas, E.W.; Sandhu, S.S.; Yianni, P.P.; Mitchell, A.C., *Biochim. Biophys. Acta,* **1987**, 903, 504-509.

[74] a) Bisby, H.R.; Mead, C.; Morgan, C.G., *Photochem. Photobiol.*,**2000**, 72, 1, 57-61. b) Bisby, H.R.; Mead, C.; Morgan, C.G., *Biochem. Biophys. Res. Comm.,* **2000**, 276, 169-173.

[75] a) Liu, X.-M.; Yang, B.; Wang, Y.-L.; Wang, J.-Y., *Biochim. Biophys. Acta*, **2005**, 1720, 28-34. b) Liu, X.-M.; Yang, B.; Wang, Y.-L.; Wang, J.-Y., *Chem. Mater.*,

2005, 17, 2792-2795.

[76] a) Kano, K.; Tanaka, Y.; Ogawa, T.; Shimomura, M.; Kunitake, T., *Photochem. Photobiol.*, **1981**, 34, 323-329. b) Pidgeon, C.; Hunt, C.A., *Photochem. Photobiol.*, **1983**, 37, 5, 491-494.c) Sato, T.; Kijima, M.; Shiga, Y.; Yonezawa, Y., *Langmuir*, **1991**, 7, 2330-2335. d) Einaga, Y.; Sato, O.; Iyoda, T.; Fujishima, A.; Hashimoto, K., *J. Am. Chem. Soc.*, **1999**, 121, 3745-3750. e) Sakai, H.; Matsumura, A.; Yokoyama, S.; Saji, T.; Abe, M., *J. Phys. Chem. B*, **1999**, 103, 10737-10740.

[77] a) Sebai, S.C.; Milioni, D.; Walrant, A.; Alves, I.D.; Sagan, S.; Huin, C.; Auvray, L.; Massotte, D.; Cribier, S.; Tribet, C., *Angew. Chem. Int. Ed.*, **2012**, 51, 2132-2136. b) Sebai, S.C.; Cribier, S.; Karimi, A.; Massotte, D.; Tribet, C., *Langmuir*, **2010**, 26, 17, 14135-14141.

[78] Binder, W.H.; *Angew. Chem. Int Ed.*, **2008**, 47, 3092-3095.

[79] Ferritto, M.S.; Tirrell, D.A., *Biomaterials*, **1990**, 11, 9, 645-651.

[80] Anderson, V.C.; Thompson, D.H., *Biochim. Biophys. Acta,* **1992**, 1119, 33-42.

[81] Thompson, D.H.; Gerasimov, O.V.; Wheeler, J.J.; Yuanjinrui, Y.; Anderson, V.C., *Biochim. Biophys. Acta*, **1996**, 1279, 25-34.

[82] Li, Z.; Wan, Y.; Kutateladze, A.G., *Langmuir*, **2003**, 19, 6381-6391.

[83] Bondurant, B.; O'Brien, D.F., *J. Am. Chem. Soc.*, **1998**, 120, 13541-13542.

[84] a) Clapp, P.J.; Armitage, B.A.; O'Brien, D.F., *Macromol.*, **1997**, 30, 32-41. b) Randles, E.; Bergethon, P.R., *Langmuir*, **2013**, 29, 1490-1497.

[85] Khoobehi, B.; Char, C.A.; Peyman, G.A.; Schuele, K.M., *Lasers in Surgery and Medicine*, **1990**, 10, 303-309.

[86] An, X.; Zhang, F.; Zhub, Y.; Shena, W., *Chem. Comm.*, **2010**, 46, 7202-7204.

[87] a) Troutman, T.S.; Barton, J.K.; Romanowski, M., *Adv. Mat.*, **2008**, 20, 2604-2608. b) Jin, Y.; Gao, X., *J. Am. Chem. Soc.*, **2009**, 131, 17774-17776.

[88] Hartley, G.S., *Nature*, **1937**, 140, 3537, 281.

[89] Bandara, H.M.D.; Burdette, S.C.; *Chem. Soc. Rev.*, **2012**, 41, 1809-1825.

[90] Rodier, J.M.; Myers, A.B., *J. Am. Chem. Soc.*, **1993,** 115, 23, 10791-10795.

[91] a) Baroncini, M.; Silvi, S.; Venturi, M.; Credi, A.,*Angew. Chem. Int. Ed.***2012**, 51, 17, 4223-4226. b) Ragazzon, G.; Baroncini, M.; Silvi, S.; Venturi, M.; Credi, A., *Nature Nanotech.*,**2015**, 10, 70-75. c) Baroncini, M.; Ragazzon, G.; Silvi, S.; Venturi, M.; Credi, A.,*Pure and Appl. Chem.*, **2015**,10, 1, 70-75. d) Merino, E.;

Ribagorda, M., *Beilstein J. Org. Chem.*, **2012**, 8, 1071-1090.

[92] Sevick, E., *Nature Nanotech.*, **2015**, 10, 18-19.

[93] Goodsell, D. S., *Bionanotechnology: Lessons from Nature*, Wiley: Hoboken, **2004**.

[94] Avellini, T.; Li, H.; Coskun, A.; Barin, G.; Trabolsi, A.; Basuray, A.N.; Dey, S.K.; Credi, A.;Silvi, S.; Stoddart, J.F.; Venturi, M., *Angew. Chem. Int. Ed.***2012**, 51, 7, 1611-1615.

[95] Baylor, D., *PNAS*, **1996**, 93, 2, 560-565.

[96] Beharry, A.A.; Woolley, G.A., *Chem. Soc. Rev.*, **2011**, 40, 4422-4437.

[97] a) Hallas, G.; Jalil, M.A., *Dyes Pigm.*, **1992**, 20, 1, 13-23. b) Sadovsky, O.; Beharry, A.A.; Zhang, F.; Woolley, G.A., *Angew. Chem. Int. Ed.***2009**, 48, 8, 1484-1486.

[98] a) Kusebauch, U.; Cadamuro, S.A.; Musiol, H.-J.; Lenz, M.O.; Wachtveitl, J.; Moroder, L.; Renner, C., *Angew.Chem. Int. Ed.*, **2006**, 45, 7015-7018.b) Zhang, F.; Zarrine-Afsar, A.; Al-Abdul-Wahind, M.S.; Prosser, R.S.; Davidson, A.R.; Woolley, G.A., *J. Am. Chem. Soc.*, **2009**, 131, 2283-2289.

[99] Banghart, M.R.; Volgraf, M.; Trauner, D., *Biochemistry*, **2006**, 45, 51, 15129-15141.

[100] a) Lien, L.; Jaikaran, D.C.J.; Zhang, Z.; Woolley, G.A., *J. Am. Chem. Soc.*, **1996**, 118, 12222-12223. b) Borisenko, V.; Burns, D.C.; Zhang, Z.; Woolley, G.A., *J. Am. Chem. Soc.*, **2000**, 122, 6364-6370.

[101] Willner, J.; Rubin, S.; Riklin, A., *J. Am. Chem. Soc.*, **1991**, 113, 3321-3325.

[102] Schierling, B.; Noël, A.-J.; Wende, W.; Hien, L.T.; Volkov, E.; Kubareva, E.; Oretskaya, T.; Kokkidinis, M.; Römpp, A.; Spengler, B.; Pingoud, A., *PNAS*, **2010**, 107, 4, 1361-1366.

[103] Dohno, C.; Uno, S.-N.; Nakatani, K., *J. Am. Chem. Soc.*, **2007**, 129, 11898-11899.

[104] Ishii, K.-I.; Hamada, T.; Hatakeyama, M.; Sugimoto, R.; Nagasaki, T.; Takagi, M., *ChemBioChem*, **2009**, 10, 251-256.

[105] Liu, D; Xie, Y.; Shao, H.; Jiang, X., *Angew. Chem. Int. Ed.*, **2009**, 48, 24, 4406-4408.

[106] Velema, W.A.; Szymanski, W.; Feringa, B.L., *J. Am. Chem. Soc.*, **2014**, 136, 6, 2178-2191.

[107] Hansen, M.J.; Velema, W.A.; De Bruin, G.; Overkleeft, H.S.; Szymanski, W.; Feringa, B.L., *ChemBioChem*, **2014**, 15, 12, 2053-2057.

[108] Velema, W.A.; Van Der Berg, J.P.; Hansen, M.J.; Szymanski, W.; Driessen, A.J.M.; Feringa, B.L., *Nature Chem.*, **2013,** 5, 11, 924-928.

[109] Paul, A.; Bhattacharya, S., *Curr.Science*, **2012**, 102, 212-231.

[110] Jamieson, E.R.; Lippard. S.J., *Chem. Rev.*, **1999**, 99, 2467-2498.

[111] a) Ihmels, H.; Thomas, L., *Materials Science of DNA*, CRC Press: Boca Raton, **2011**. b) Rescifina, A.; Zagni, C.; Varrica, M.G.; Pistarà, V.; Corsaro, A., *Eur. J. Med. Chem.*, **2014**, 74, 95-115.

[112] Kubar, T.M.; Hanus, F.; Ryjacek, F.; Hobza, P., *Chem. Eur. J.*, **2006**, 12, 280-290.

[113] Andersson, J.; Li, S.; Lincoln, P.; Andréasson, J., *J. Am. Chem. Soc.*, **2008**, 130, 11836-11837.

[114] Pace, T.C.S.; Müller, V.; Li, S.; Lincoln, P.; Andréasson, J., *Angew. Chem. Int. Ed.*, **2013**, 52, 4393-4396.

Chapter 2

Experimental Techniques

2.1 Chemicals

All triazolopyridiunium and triazoloquinoliumsalts were synthesized and fully characterized in Prof. I. Aprahamian's group (Dartmouth College, Hanover). Polyazobenzene derivatives were synthesized and fully characterized in Prof. Hecht's group (Humboldt University, Berlin).

Conjugated polyazobenzene derivatives were synthesized and fully characterized in Prof. S. Masiero's group (University of Bologna, Bologna).

Any model compound used exhibited the highest purity commercially available.

POPC was purchased from Avanti Polar Lipids (Alabaster, AL) and CF^{3-}(95% purity), Triton X100, Sephadex G-25 and calf-thymus DNA were purchased from Sigma Aldrich. Calf-thymus DNA solutions were prepared in PBS 1x buffer (pH=7) and filtered with a Minisart RC 0.45 μM filter. DNA concentration was determined spectrophotometrically (ε_{260nm}= 6600 $M^{-1}cm^{-1}$ with respect to phosphate groups) and its purity was verified by checking the ratio of absorbance at 260 and 280 nm.

The solvents used for photophysical, photochemical and electrochemical characterization of all compounds were chloroform (Merck Uvasol™),

dichloromethane (Merck Uvasol™), methanol (Merck Uvasol™), ethanol (Merck Uvasol™) and acetonitrile (Romil).

2.2 Electronic absorption spectra

The acquisition of electronic absorption spectra was carried out at room temperature on air-equilibrated solutions of the samples included in quartz cuvettes (optical path length of 1 cm or 0.5 cm). When necessary, oxygen was removed by performing three freeze-pump-thaw cycles. The concentration of the solutions was ranging between 10^{-6} and 10^{-4} M.

The absorption spectrum of each compound in the 900-190 nm range was performed by using a UV/Vis Perkin Elmer Lambda-650 and an Agilent Technology Cary 300 double beam spectrophotometers. The precision on the wavelength values was ± 1 nm. Molar extinction coefficient values were determined using the Lambert-Beer law and the experimental error associated to each value is estimated to be ±5%. Spectrophotometric titrations were performed by the addition of small aliquots (usually in the range 5-20 μL) of a concentrated solution (1 mM) of titrating species by using a microsyringe. Titrating species were added to a known volume of a dilute solution of the titrated species contained in a quartz cuvette. Dedicated spectrophotometric cells composed of two compartments separated by a quartz wall were employed for a careful determination of the sum of the absorption spectra of the separated components (unmixed solutions) and the absorption spectrum of their complex (mixed solutions).

Spectrophotometric kinetic experiments were performed using a Varian Cary 50 Bio single beam spectrophotometer and the obtained time-dependent absorption variations were fitted by means of SPECFIT software[1] using a suitable kinetic model.

The general set-up for a spectrophotometer is shown in *Figure 2.1*.

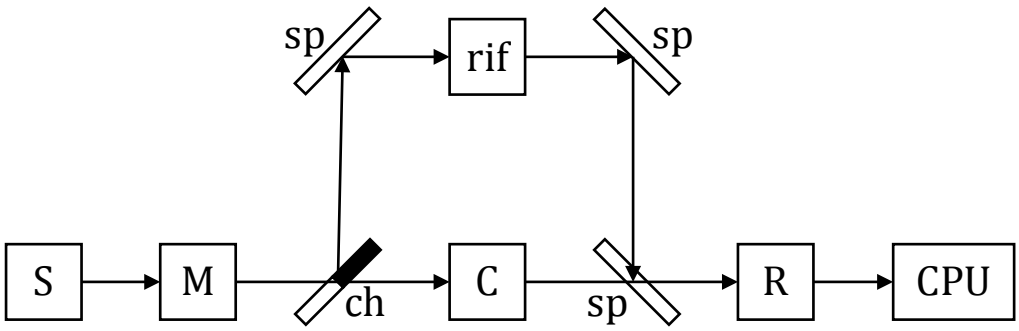

***Figure 2.1*- Block diagram of a UV-Vis double-beam spectrophotometer.**

The main components of the instruments are:

- *source (S)*: composed of two lamps, a tungsten filament lamp (1100-320 nm) and a deuterium lamp (320-190 nm);
- *monochromator (M);*
- *reference (rif);*
- *sample (C);*
- *chopper (ch);*
- *mirrors (sp);*
- *detector (R)*: photomultiplier tube.

The amount of light absorbed by the sample is expressed in terms of *transmittance (T)* that is defined as the ratio between the intensities of transmitted (I_t) and incident light (I_i):

$$T = \frac{I_t}{I_i}$$

It can be expressed in terms of absorbance (A):

$$A = -\log_{10} T$$

The spectrophotometer measures the absorbance of the solution of the sample as a function of the wavelength and it subtracts the absorbance of the reference, allowing to distinguish the electronic transitions responsible for the passage from the electronic ground state to electronic excited states. The obtained absorption spectrum allows the determination of the *molar absorption coefficient* (ε), that represents the probability associated to every electronic transition. It is expressed in $M^{-1}cm^{-1}$ and it is determined following *Lambert-Beer's law*:

$$A = \varepsilon c l$$

where $c$is the molar concentration of the sample and$l$is the optical path length of

the cuvette used in the measurement.

2.3 Luminescence spectra

Fluorescence emission spectra, excitation spectra and kinetic measurements were performed at room temperature on a Perkin Elmer LS55 spectrofluorimeter equipped with a Hamamatsu R928 photomultiplier and a 4-position automatic cell holder. Kinetic measurements were also performed on a Varian Cary Eclipse at 298 K. For both instruments, the precision on wavelength values ranges from ± 1nm to ± 2 nm.

Fluorescence emission spectra and excitation spectra on drop casted films of triazolopyridinium and triazoloquinolinium salts were recorded at room temperature on a Perkin Elmer LS55 spectrofluorimeter equipped with a Hamamatsu R928 photomultiplier and a front-face solid sample holder.

Fluorescence and phosphorescence emission spectra at 77 K were recorded on a Perkin Elmer LS55 spectrofluorimeter equipped with a Hamamatsu R928 photomultiplier.

The general scheme for the instrumental setup for a spectrofluorimeter is reported in *Figure 2.2*.

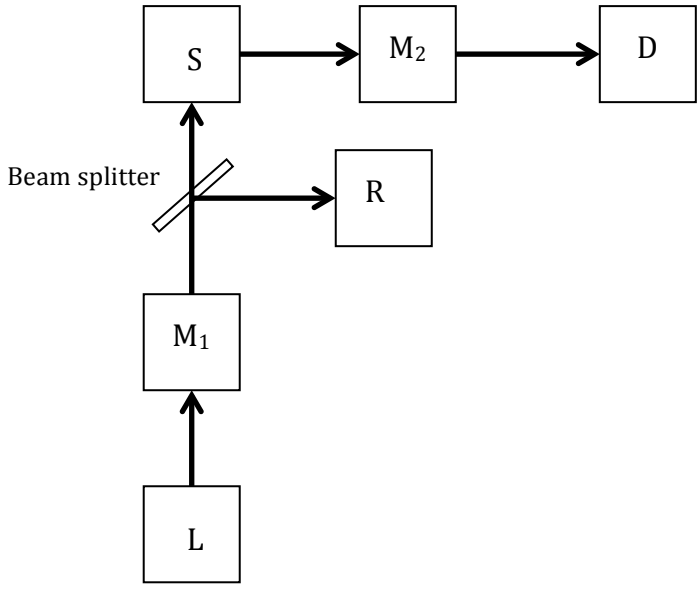

***Figure 2.2*- Block diagram of a spectrofluorimeter.**

The instrument is made up by the following components:

- *source* (L): a pulsed xenon lamp;
- two *monochromators*, one for the selection of the excitation light (M_1) and the other for emission light (M_2);
- two *photomultipliers*, a *reference detector* (R) for the correction of the light emitted by the source and a *detector* (D) for detecting the light emitted by the sample;
- *sample* (S);
- *excitation and emission slits.*

2.3.1 Luminescence quantum yield measurement

Luminescence quantum yield represents a useful parameter in photophysics, since it allows the direct comparison between photons emitted and absorbed by a luminescent species for a precise excitation wavelength.

The most employed method for the assessment of the luminescence quantum yield in solution is based on the direct comparison with a reference standard, whose quantum yield (Φ_r) is known. The equation that allows its determination is given by

$$\Phi = \Phi_r \times \frac{S}{S_r} \times \frac{n^2}{n_r^2}$$

where *S* and *n* represent the area beneath the emission profile and the refractive index of the solvent used to prepare both the solution of the sample and the reference, respectively. This equation is valid only if the absorbance values referring to the excitation wavelength of both the reference and the sample are the same and are below 0.1.

The spectral region of its emission has to be superimposable to the one of the sample, in order to obtain emission spectra using the same experimental conditions. The determination of the luminescence quantum yield was performed by following the experimental procedure proposed by Demas and Crosby[3] and the most suitable standard for the measurement was chosen depending on the spectral region related to the emission of the sample. [4]

For the luminescence quantum yield determination of triazolopyridinium and triazoloquinolinium salts, a sodium salt of quinine sulphate in H_2SO_4 50 mM was used as reference standard.

2.3.2 Luminescence lifetime determination

Fluorescence lifetime measurements were carried out at room temperature and at 77 K on air equilibrated solutions and on solid films obtained by drop casting technique. Measurements were performed by using an Edinburgh Analytical Instruments *time-correlated single photon counting* (TCSPC) equipment, which allows the assessment of lifetimes in a time range between 0.5 ns and 30 μs. Like other time-domain measurements, TCSPC technique measures sample luminescence as a function of time, in terms of a direct proportionality between the number of emitted photons and the concentration of excited states of samples.

The block diagram of TCSPC is depicted in *Figure 2.3*.

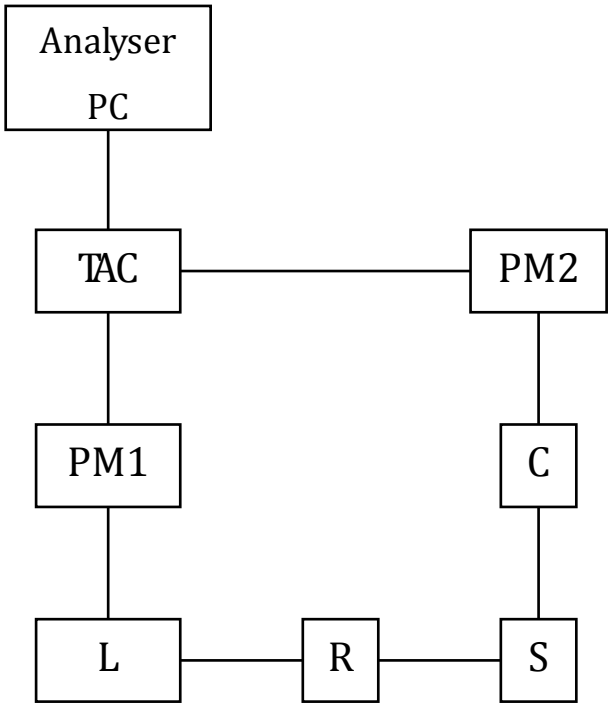

***Figure 2.3*- Block diagram of a time-correlated single photon counting device.**

By observing the scheme, it is possible to distinguish the main components of the

apparatus:

- *sources* (L): they can be a pulsed diode laser or a low-pressure discharge lamp (nF900, filled with nitrogen or deuterium), which is able to deliver 0.5 ns pulses at a frequency in the range 1-100 kHz;
- two *monochromators* (R,C);
- two *photomultipliers* (PM1, PM2);
- *sample* (S);
- *time-to-amplitude converter* (TAC);
- *multichannel analyser* (MCA);
- *computer* (CPU).

In principle, the measurement starts with the emission of a short pulse (1-5 ns) and at the same time the *start photomultiplier* sends a signal to the TAC. The TAC starts a linear voltage ramp until the photon emitted by the sample after the excitation pulse is detected by the *stop photomultiplier* and sends a stop signal to the TAC, thus blocking the voltage ramp. The TAC resembles a chronometer since it measures the time elapsed from the start and the stop signals and this time interval is sent to the MCA as an electrical signal. Repetition of many excitation-emission cycles allows the MCA to accumulate and organize the obtained signals in different channels on the basis of their delay form the excitation.

For statistical reasons, the frequency of the registered events has to be less than 2% of the working frequency of the lamp. In this way, it is possible to avoid to detect only the contribution of photons that are emitted immediately after the excitation: these photons have a high detection probability and this results in a shift of the luminescence decay curve towards shorter times.[4]

Fluorescence lifetimes were determined by applying mono and biexponential fitting were models and the factor χ^2 was employed as quality parameter of the fits.

Phosphorescence lifetime measurements were performed at 77 K on a Perkin Elmer LS55 spectrofluorimeter equipped with a Hamamatsu R928 photomultiplier.

2.4 Fluorescence anisotropy measurements

Fluorescence anisotropy measurements were carried out on a spectrofluorimeter Edinburgh Analytical Instruments FLS920.

Generally, fluorescence anisotropy allows to investigate processes involved in the change of the orientation of the dipole moment referring to the electronic distribution of an excited state: these processes concern the rotation dynamics of a fluorophore in the space and energy transfer processes. The main application field of this technique refers to the study of the dynamics of deactivation processes and passage of energy, as a consequence of supramolecular interactions. It represents a quantity able to determine the polarization of the emitted light from a sample previously excited by polarized light. Thus, the measurement is performed at different wavelengths and the fluorescence excitation spectrum is obtained by fixing the excitation wavelenght.

The instrumental setup is shown in *Figure 2.4*.

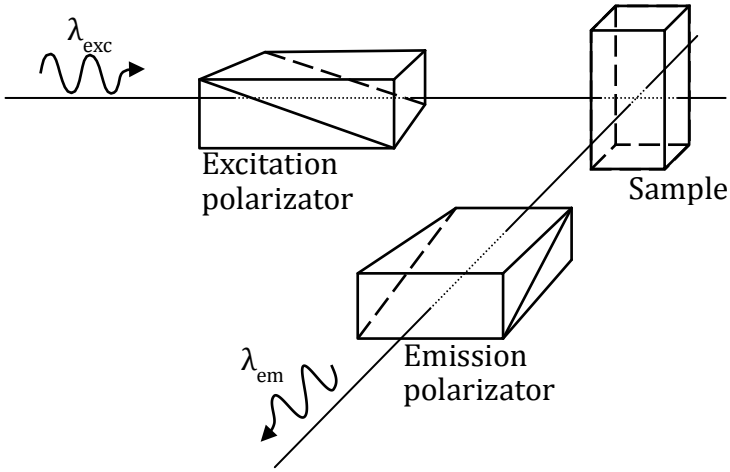

***Figure 2.4*- Instrumental configuration for fluorescence anisotropy measurements.**

The presence of a couple of polarizers placed in the excitation and emission beams, allows to measure the extent of polarization of the sample emission, that is assessed by the anisotropy *r*, which is defined as

$$r = \frac{I_{\parallel} - I_{\perp}}{I_{\parallel} + 2I_{\perp}}$$

where $I_{\parallel}$ is the intensity registered when the emission polarizer is parallel to the excitation one and $I_{\perp}$ correspond to the intensity measured when the emission

polarizer is perpendicular to the excitation one.

Fluorescence anisotropy measured in solution is lower than the maximum theoretical value (+0.4) because of the occurrence of several depolarization processes, such as energy migration, rotational diffusion, light scattering and radiative energy transfer. In the case of depolarization by rotational diffusion, the anisotropy value is given by Perrin equation[5]

$$r = \frac{r_0}{1 + {\theta}/{\tau}}$$

where r_0 denotes the fundamental anisotropy, θ is rotational correlation time andτ stands for the excited state lifetime.

2.5 Photochemical experiments

Irradiation of samples were performed at room temperature in a spectrophotometric quartz cuvette (1 cm path length) containing 2.5 mL of sample solutions under gently stirring and using a 125 W Hg medium pressure lamp and an interference filter as light source. Variations in the absorption spectrum were recorded using a Varian Cary 50 Bio single beam spectrophotometer.

2.5.1 Photochemical quantum yield assessment

The efficiency of a given photochemical process is expressed by its photochemical quantum yield (Φ_P) that is

$$\Phi_P = \frac{\Delta C \times V}{q_{p,in} \times f_m \times t}$$

where ΔC represents the concentration of photoproduct obtained during the irradiation, V is the volume of the irradiated solution, $q_{p,in}$ is the number of photons emitted by the source and f_m is the mean value of the fraction of absorbed light at the irradiation wavelenght. The number of incident photons is measured by using chemical actinometers and, more specifically, in this work it was estimated on dilute sample solutions at room temperature by using potassium ferrioxalate and potassium reineckate (Reinecke's salt) as chemical

actinometers.

Potassium ferrioxalate[6] represents the most practical actinometer for UV and visible light and can be used up to 500 nm.

The photochemical reaction involved is a photodecomposition described in the following equation:

$$[Fe(C_2O_4)_3]^{3-} + h\nu \rightarrow Fe^{2+} + C_2O_4^{\bullet -} + 2\ C_2O_4^{2-}$$

$$[Fe(C_2O_4)_3]^{3-} + C_2O_4^{\bullet -} \rightarrow Fe^{2+} + 2CO_2 + 3\ C_2O_4^{2-}$$

The amount of Fe^{2+} is determined spectrophotometrically by adding *o*-phenantroline and monitoring the formation of the colored tris-phenantroline complex (ε=11100 $M^{-1}cm^{-1}$ at 510 nm), since potassium ferrioxalate is transparent to that wavelength and $Fe^{3+}$is not appreciably complexed by *o*-phenantroline. Since the reaction vessel consists of a spectrophotometric quartz cell having a 1cm path length and containing 3 ml of 12 mM ferrioxalate solution, a microversion of the actinometer was performed.[7]

The number of incident photons is given by

$$q_{p,in} = \frac{\Delta A_{510\ nm}}{\mathrm{t}} \times Y \times N_A$$

where the factor Y includes the yield of the actinometer at a precise irradiation wavelength, the ε of the complex $[Fe(phen)_3]^{2+}$ at 510 nm and the ratio between the product of the irradiated volume and the final volume after addition of *o*-phenantroline and the aliquot of the irradiated solution used for Fe^{2+} determination.

The main advantage related to the use of potassium ferrioxalate resides in the quantum yield independence of temperature and concentration, but the main drawbacks concern the poor absorbance and change of the quantum yield upon shifting the irradiation wavelength towards higher values in the visible region, limiting its applicability: in this case, it is necessary to use another chemical actinometer and Reinecke's salt represents a valid alternative.

In aqueous solution, potassium reineckate experiences the following photoaquation reaction:

$$[Cr(NH_3)_2(SCN)_4]^- + H_2O + h\nu \rightarrow [Cr(H_2O)(NH_3)_2(SCN)_3] + SCN^-$$

The amount of SCN^- produced is determined spectrophotometrically after formation of a colored complex (ε=4300 $M^{-1}cm^{-1}$ at 450 nm) with $Fe(NO_3)_3$ which

allows to monitor the photoreaction and to determine the number of incident photons. Unlike potassium ferrioxalate, the quantum yield for this actinometer does not depend on irradiation wavelenght and it is constant in the range 315-750 nm,[8] even if the absorbance of this actinometric solution (~ 50 mM) is almost complete up to 600 nm for an optical path of 1 cm. Since the quantum yield depends on temperature and pH, it is necessary to prepare the actinometric solution before performing the irradiation. Moreover, SCN^- is released also thermally so it is necessary to subtract the contribution of this thermal reaction by comparing the absorbance value at 450 nm obtained upon irradiation with that of the same solution stored in the dark.

2.6 Electrochemical techniques

Electrochemical measurements were carried out in argon-purged solutions of samples dissolved in water, anhydrous acetonitrile or anhydrous dichloromethane at 298 K. For cyclic voltammetry and differential pulse voltammetry the working electrode was a glassy carbon electrode (0.08 cm^2), the counter electrode was a Pt spiral and a SCE reference electrode for measurements in aqueous solutions, whereas for solutions in solvents other than water an Ag wire was used as a quasi reference electrode, ferrocene (100 mM in acetonitrile) and decamethylferrocene (100 mM in dichloromethane) were used as internal references. The electrochemical cell was linked to an Autolab PGSTAT 12 potentiostat/galvanostat.

The concentration of compounds examined was of 0.5mM and 1 mM; $TEAPF_6$ (50 mM in acetonitrile), $TBAPF_6$ (100 mM in dichloromethane) and $NaClO_4$ (100 mM in water) were added as supporting electrolytes. Cyclic voltammograms were obtained with scan rates in the range 10-500 mV/s and differential pulse voltammograms were obtained applying a modulation time of 40 s, a modulation amplitude of 75 mV and a scan rate of 20 mV/s.

2.6.1 Cyclic voltammetry

Among potentiostatic methods, voltammetric techniques [9] consist on the application of a potential scan to the working electrode and then the current response of the cell is measured. In cyclic voltammetry the potential applied to the working electrode is changed linearly with time within a defined potential range then a reverse scan is applied, as shown in *Figure 2.5*.

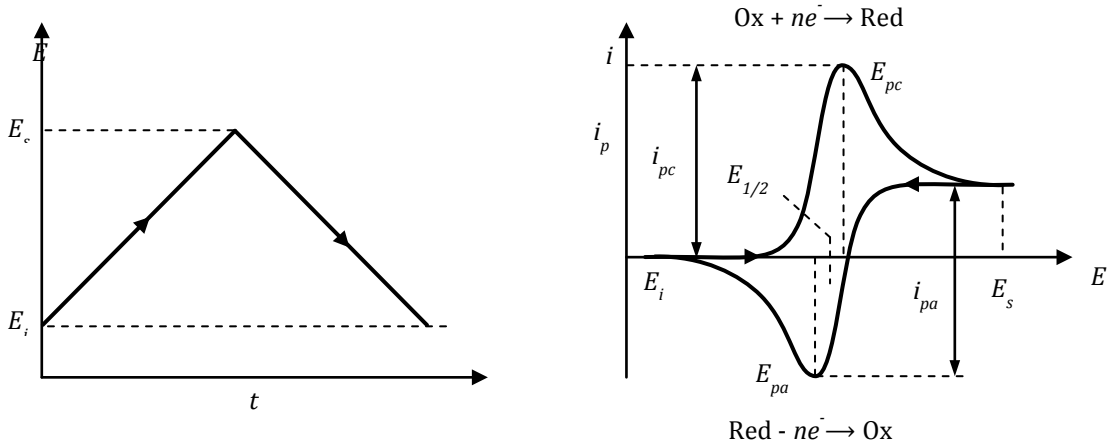

***Figure 2.5*- Potential excitation function and current vs potential response for cyclic voltammetry.**

For an electrochemically reversible redox process in an unstirred solution containing a supporting electrolyte, hypothesizing a condition of semi-infinite linear diffusion (that is the case found with planar electrode of conventional size), the peak current i_p is given by

$$i_p = 0.4463\ (nF)^{3/2}(RT)^{-1/2}AD_{ox}^{1/2}C_{ox}v^{1/2}$$

where A represents the surface area of the electrode, D_{ox} and C_{ox} are the diffusion coefficient of the electroactive species and its concentration respectively, v is the scan rate and n refers to the number of transferred electrons. In this case, the current depends on the square root of the applied scan rate (which represents the slope of the excitation function), but the peak potential does not change its position by varying the scan rate and the ratio of the values of the couple peak currents (i_a and i_c) equals 1. Moreover, the potential difference between cathodic and anodic peaks is equal to $57/n$ mV at 298 K. The average of the cathodic and anodic peak potential yields the *halfwave potential* ($E_{1/2}$) for the redox couple.

In contrast, when an irreversible process (for which the voltammogram may or

may not exhibit a peak) takes place, the peak potential does not remain fixed by changing the scan rate and so all the considerations above are not applicable.

2.6.2 Differential pulse voltammetry

In contrast to cyclic voltammetry, differential pulse voltammetry (DPV) is a more sensitive technique, having a detection limit of 10^{-8} M. This voltammetric technique[10] is based on the application of a series of regular potential pulses over a base potential: in this case the value of the applied voltage is stepped from the imposed potential range by applying small increments (*step potential*). The applied pulses have the same height with respect to the base potential and the same time duration, as depicted in *Figure 2.6*.

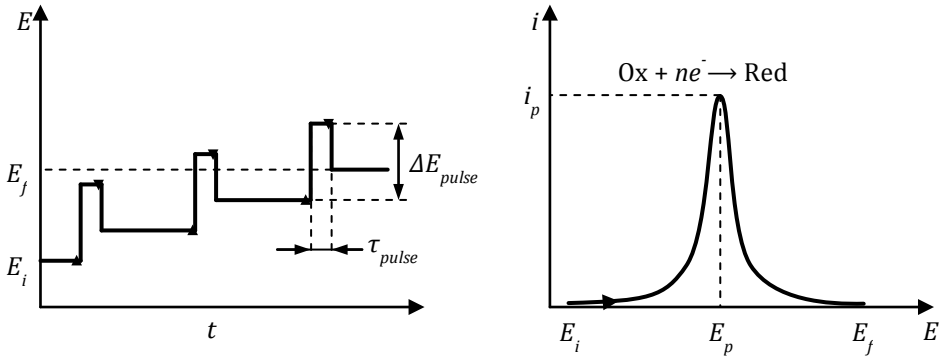

***Figure 2.6*- Potential excitation function and current vs potential response for differential pulse voltammetry.**

The most important parameters for DPV are:

- *modulation amplitude* (ΔE_p): is the height of the potential pulse
- *modulation time* (τ_p): is the duration of the potential pulse

In this case, the scan rate is defined as the ratio between the potential increment and the period of the cycle.

In the case of a reversible process, the potential corresponding to the peak in the voltammogram is independent on the scan rate and is related to the *halfwave potential* by

$$E_p = E_{1/2} - \frac{\Delta E_{pulse}}{2}$$

and the peak on the voltammogram exhibits a symmetrical shape.

As for CV, in a diffusion-controlled experiment the current depends on the

surface area of the electrode, on the square root of diffusion coefficient of the electroactive species, on its concentration, but also on the height and duration of the applied pulse.
In the case of irreversible processes (chemically or electrochemically), the DPV peak is weaker and broader and its shape is not symmetric anymore.

2.7 Circular dichroism

Circular dichroism measurements were performed at room temperature in a spectrophotometric quartz cuvette (1 cm path length) containing 2 mL of sample solutions and spectra were acquired on a Jasco J-810 single beam spectropolarimeter.
In general, circular dichroism (CD) spectroscopy concerns the different absorption of the two chiral components (*left-handed* and *right-handed*) of the linearly polarized light experienced by chiral entities.
This spectroscopic technique is based on the principle that the two circularly polarized components of linearly polarized light have different absorption coefficients when they proceed through an optically active compound: so they are absorbed at different degrees by the chiral compound. The light passing through the compound is elliptically polarized and the compound has "chiral dichroism". Molar ellipticity (θ) is the parameter used to express the extent of circular dichroism and it is defined as

$$\theta = \frac{4500}{\pi} \Delta\varepsilon \log_e 10$$

where $\Delta\varepsilon$ denotes the difference between the molecular extinction coefficients for the two circularly polarized components of linearly polarized light, defined as *molar circular dichroism*.
The instrumental setup[11] for a Jasco J-810 spectropolarimeter is shown in *Figure 2.7*

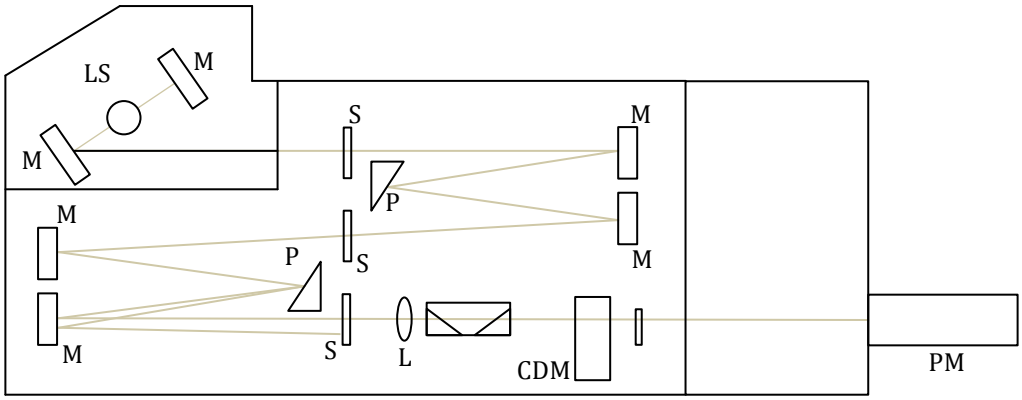

***Figure 2.7*- Instrumental setup of a Jasco J-810 spectropolarimeter.**

The main components are:

- *source* (LS): a xenon lamp;
- *mirrors* (M);
- *optical system*: composed by a double monochromator;
- *slits* (S);
- *prisms* (P): allow to obtain linearly polarized light;
- *modulator* (CDM): splits the linearly polarized light in its two circularly polarized components;
- *detector* (PM): a photomultiplier tube.

2.8 Liposomes preparation

Large unilamellar vesicles were prepared by rehydration of a thin film of 1-palmitoyl-2-oleoyl-*sn*-glycero-3-phosphocholine (POPC).[12]

In order to obtain liposomes having a molecular guest in their phospholipid bilayer, an appropriate amount of a POPC solution in chloroform (25 mg/mL, Avanti Polar Lipids) and guest were placed in a 5 mL round-bottom flask and the mixture was evaporated under reduced pressure at 40°C to produce a thin film that was dried under vacuum for 1 hour. The phospholipid film was kept overnight at 4°C before rehydration.

In both cases, the lipid film was rehydrated with an aqueous buffer solution [made of 174mM NaCl, 105 mM Na_2HPO_4, 20 mm KH_2PO_4 (pH 7.4, 578 mOsm) or made of made of 121.5 mM NaCl, 25.2 mM Na_2HPO_4, 4.8 mm KH_2PO_4 for

microviscosity measurements (pH 7.4, 578 mOsm)] or with a 50 mM CF^{3-} buffered aqueous solution [made of 121.5 mM NaCl, 25.2 mM Na_2HPO_4, 4.8 mM KH_2PO_4 and 50 mM CF^{3-} (pH 7.4, 578 mOsm)]. The resulting liposomal suspension was extruded 20 times through a polycarbonate membrane with 100-nm pores on an Avanti Polar Lipids (Alabaster, AL, USA) mini-extruder. For dequenching measurements, the obtained liposomal suspension was passed through a Sephadex G-25 column in order to get rid of the unentrapped dye. Prior to be used, the liposomal solutions were diluted with the appropriate buffer (isosmotic with the one used for the rehydration step), in order o achieve a final concentration of POPC equal to $1.32*10^{-5}$ M for stability measurements and $2.64*10^{-5}$ M for viscosity measurements, assuming 100% elution of phospholipids during the gel permeation process.

The same procedure was followed for the entrapment of guests in the liposomal aqueous core, but in this case the phospholipid film was rehydrated with a $1.7*10^{-4}$ M and $8.5*10^{-5}$ M aqueous solutions of *E,E*-**1**$^{2+}$ and CB7 in 5 mM NaCl. The obtained liposomal suspension was extruded 20 times through a polycarbonate membrane with 100-nm pores on an Avanti Polar Lipids (Alabaster, AL, USA) mini-extruder and the unentrapped guest was removed by gel permeation on Sephadex G-25 columns. Liposomes eluted from columns were diluted with a 5mM NaCl solution (pH 7.4).

For chloride transport assays in Egg Yolk Phosphatidylcholine (EYPC) liposomes, a lipid film was formed by evaporating a chloroform solution containing 50 mg or 25 mg of lipids (EYPC) under reduced pressure at 25°C for at least 2 hours. The lipid film was then hydrated with 500 µL of a 2 mM lucigenin solution containing 100 mM NaCl and 10 mM NaH_2PO_4/Na_2HPO_4 buffer (pH 6.2). The resulting suspension was then subjected to at least 10 freeze/thaw cycles (1 minute at -78°C followed by 1 minute at 35°C) and vortexed for 30 seconds between each cycle. The suspension is then extruded through a 100 nm polycarbonate membrane 21 times. Liposomes are purified through a Sephadex G-25 column to remove the extravesicular lucigenin dye using a 100 mM $NaNO_3$ and 10 mM NaH_2PO_4/Na_2HPO_4 buffer (pH 6.2) as eluent. The isolated liposomes were diluted to 10 mM (50 mg of EYPC) or 5 mM (25 mg of EYPC) relative to the lipid, assuming all EYPC was conserved through manipulations.

2.9 Liposomes characterization

POPC liposomes were characterized on a Malvern Instruments DLS ZetaSizer Nano-ZS and their size and zeta potential were assessed. For size measurements PMMA disposable cuvettes containing 1 ml of diluted liposomal suspension in PBS (pH 7.4) were used, whereas for zeta potential determination disposable folded capillary cells containing 1 mL of diluted liposomal suspension in NaCl 10 mM (pH 7.4) were used (the diffusion barrier technique was employed to load the sample in the cell).

The instrumental setup for DLS measurement is shown in *Figure 2.8*.

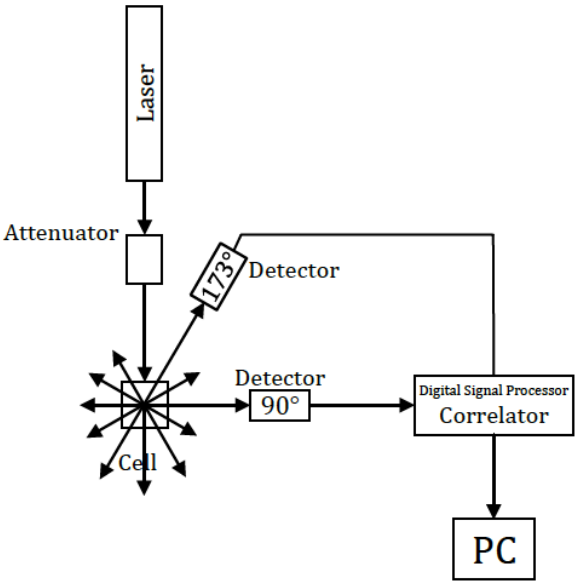

***Figure 2.8*- Block scheme of a Malvern Instruments DLS ZetaSizer Nano-ZS.**

The instrumental setup for zeta potential measurement is presented in *Figure 2.9.*

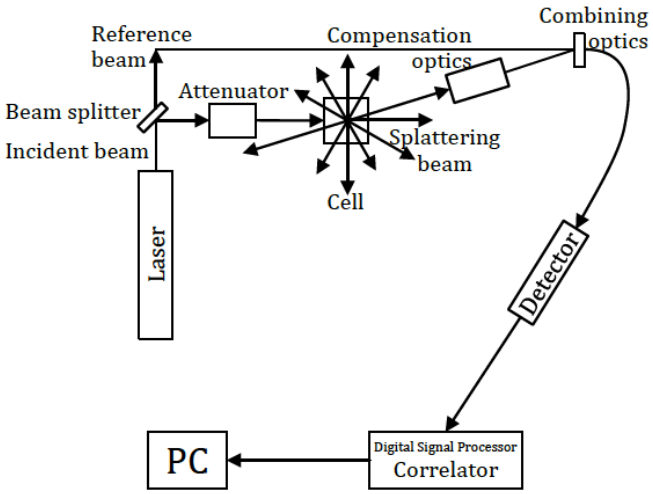

***Figure 2.9*-Instrumental setup for zeta potential measurements.**

In both cases, the main components of the instrument[13] are:

- *Laser*: He-Ne laser;
- *Attenuator*: reduces the intensity of the laser beam;
- *Detector*: registers the light scattered from the sample and its position can be at 173° or 90° with respect to the incident laser beam for DLS measurements. For zeta potential measurements it is at 17° with respect to the incident beam;
- *Correlator*: it is a digital signal processing board, that analyses the output signal;
- *Software*.

2.9.1 Size determination

Dynamic light scattering is a useful technique in size determination of particles having submicrometric dimensions. This technique correlates Brownian motion and particle dimension, expressed in terms of *hydrodynamic diameter*. The translational diffusion coefficient (D) allows derivation of the particle size, using the Stokes-Einstein equation

$$d(H) = \frac{kT}{3\pi\eta D}$$

where $d(H)$ stands for the hydrodynamic diameter, k is the Boltzmann constant,

T is the absolute temperature andη expresses the medium viscosity.

Since particles are in a solution environment, the hydrodynamic diameter is defined as the diameter of spherical rigid particle having the same diffusion coefficient and the same diffusion speed of the one that is under measurement. It is important to mention that this value depends on factors other than temperature and medium viscosity, but also on structure of particle's surface and ionic strength of the dispersant medium. *Rayleigh approximation* describes the relationship between the intensity of the scattered light (I), particles dimensions (d) and laser wavelength (λ). It states that

$$I \propto d^6$$

$$I \propto {}^1/_{\lambda^4}$$

if the dimension of particles irradiated by the source is negligible compared to wavelength of the source used and if the light scattered by the sample is isotropic.

A DLS measurement provides not only the value of the hydrodynamic diameter, but it gives information on some other important parameters that represent a valid indication of the quality of the sample under analysis. These parameters are:

- *Correlation function*: for a good measurement, it must have a sigmoidal shape and the y-axis intercept value has to approach 1. Moreover, the time required for the decay gives information on the dimension of particles: for small particles, the correlation of the signal takes a short time to decay, whereas for big ones, the decay is much slower. The angle of decay gives information about the polydispersity of the distribution and the baseline about the presence of aggregates;
- *Polydispersity Index (PDI)*: indicates the width of the distribution of populations in the sample. For a monodisperse sample it has to be as narrow as possible;
- *Count rate*: provides information on sample stability. A decreasing count rate indicates sample sedimentation, whereas an increasing count rate refers to particles' aggregation.

2.9.2 Zeta potential

Zeta potential is a physical property exhibited by particles in suspension that indicates the stability of a colloidal system. Generally, the threshold for instability is the potential range between -30 and +30 mV: above those values, particles are stabilized by electrostatic forces and do not flocculate.

When a particle bears a net charge on its surface and it is suspended in a solution environment, the liquid layer that surrounds it exists as two regions: the *Stern layer*, in which ions having opposite charge are strongly bound to the surface of the particle and a *diffuse layer*, where ions are less firmly associated. Within this layer, a theoretical boundary layer exists, in which ions and particles form a stable entity: when the particle moves, ions within this layer move with it, whereas ions beyond this layer stay with the bulk dispersant. Zeta potential is defined as the potential at this surface of hydrodynamic shear, as shown in *Figure 2.10.*

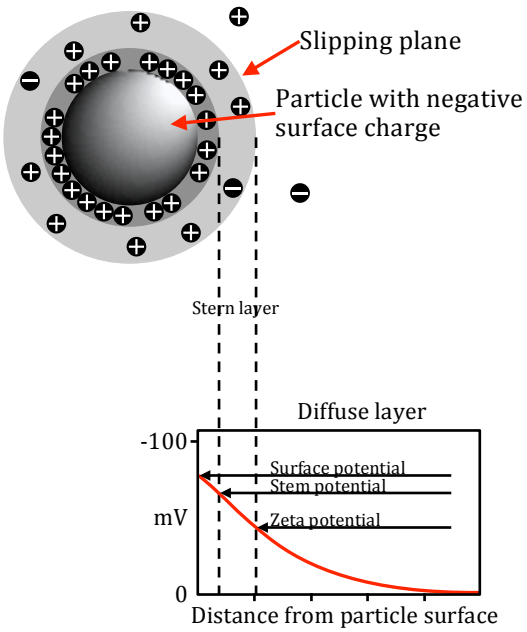

***Figure 2.10*-Schematic representation of zeta potential.**

Zeta potential depends on pH, ionic strength and conductivity of the dispersing medium and, of course, on superficial charge of the particle. The main consequence of having a colloidal system, in which the dispersed particles are charged, is that they interact with an applied electric field, yielding *electrokinetic*

effects. Among them, *electrophoresis* is very important since the *Henry equation* correlates the electrophoretic mobility (U_E) and zeta potential (z):

$$U_E = \frac{2\varepsilon z f(\kappa a)}{3\eta}$$

where ε is the dielectric constant, η is the viscosity and $f(\kappa a)$ is the Henry's function, whose value is 1.5 in the Smoluchowski's approximation.

Electrophoretic mobility is measured by using the *laser Doppler electrophoresis technique* together with *M3-PALS* (that is a combination of *laser Doppler velocimetry* and *phase analysis light scattering*): as a consequence of the applied electric field, motion of particles causes a fluctuation of the light scattered by the sample and the fluctuation frequency is proportional to the particle speed, allowing to derive zeta potential.

References

[1] Binstead, R.A.; SPECFIT, Spectrum Software Associates, Chapel Hill, NC (USA), **1996**.

[2] Balzani, V., Ceroni, P., Juris, A.; *Photochemistry and Photophysics: concepts, research, applications*, Wiley-VCH Verlag: Weinheim, **2014**.

[3] Demas, J.N.; Crosby, G.A.,*J. Phys. Chem.*, **1971**, 75, 991-1024.

[4] a) Moggi, L.; Juris, A.; Gandolfi, M.T.,*Manuale del Fotochimico, Tecniche e Metodologie*, BononiaUniversity Press, Bologna, **2006**. b) Montalti, M.; Credi, A.; Prodi, L.; Gandolfi, M.T., *Handbook of Photochemistry, 3rd ed.*, CRC Taylor & Francis: Boca Raton, **2006**.

[5] Lackowicz, J.R.; *Principles of Fluorescence Spectroscopy*, Springer, New York, **2006**.

[6] Hatchard, C.G.; Parker, C.A., *Proc. Roy. Soc. London*, **A235**, 518-536.

[7] Fisher, E.,*EPA Newsletters*, **1984**, 21, 33-34.

[8] Wegner, E.; Adamson, A.W., *J. Am. Chem. Soc.*, **1966**, 88, 394-404.

[9] Bard, A.J.; Faulkner, L. R., *Electrochemical Methods: fundamental and applications 2nd Ed.*, John Wiley & Sons, New York, **2000**.

[10] Ceroni, P.; Credi, A.; Venturi, M., *Analytical Methods in Supramolecular Chemistry 2nd Ed.*, Wiley-VCH Verlag: Weinheim, **2012**.

[11] Jasco J-810 spectropolarimeter Hardware/Function Manual http://brc.boisestate.edu/wp-content/blogs.dir/1/files/2014/04/J-810-Series-Hardware-Function-Manual.pdf

[12] a) De Maria, P.; Filippone, P.; Fontana, A.; Gasbarri, C.; Siani, A.; Velluto, D., *Colloid Surf. B.-Biointerfaces*, **2005**, 40, 11-18. b) De Maria, P.; Fontana, A.; Gasbarri, C.; Velluto, D.; *Soft Matter*, **2006**, 2, 595-602. c) Zappacosta, R.; Semeraro, M.; Baroncini, M.; Silvi, S.; Aschi, M.; Credi, A.; Fontana, A., *Small*, **2010**, 6, 8, 952-959.

[13] Zetasizer Nano Series User Manual http://www.malvern.com/en/support/resource-center/user-manuals/MAN0485EN.aspx

Chapter 3

Triazolopyridinium and triazoloquinolinium salts as biocompatible blue emitters

3.1 Introduction

The development of blue light fluorophores has attracted much attention because of their application in many application fields, such as OLED technology [1], Förster resonance energy transfer (FRET),[2] bio imaging and bioassays. The main limitation in their design and development resides in the large energy gap required between their excited- and ground-state energy levels and this often translates in low quantum yields and poor photostability.[3]

In addition to the properties mentioned above, self-quenching suppression represents another important feature that makes a compound a useful blue light emitter: in this sense, compounds exhibiting a large Stokes shift constitute good candidates for this purpose. Among blue emitting organic compounds, N-2-aryl-triazoles (NAT)[4] and [1,2,3]triazolo[1,5-*a*]-pyridines[5] represent an important family of blue emitting fluorophores, but the main limitation in their use as

biological probes concerns their poor water solubility. To overcome this issue, hydrophilic substituents can be introduced, leading to synthetic complications. Another solution could be to switch the attention towards systems intrinsically water soluble, namely [1,2,3]triazolo[1,5-*a*]-pyridinium salts.[6] The synthesis of this family of water soluble organic salts exploits the benefits deriving from the use of Cu(II)-promoted oxidative cycloadditions performed in CH_3CN, starting from the corresponding hydrazone and the oxidation step proved to be very easy and accessible, affording the product in high yields (*Figure 3.1*).[7]

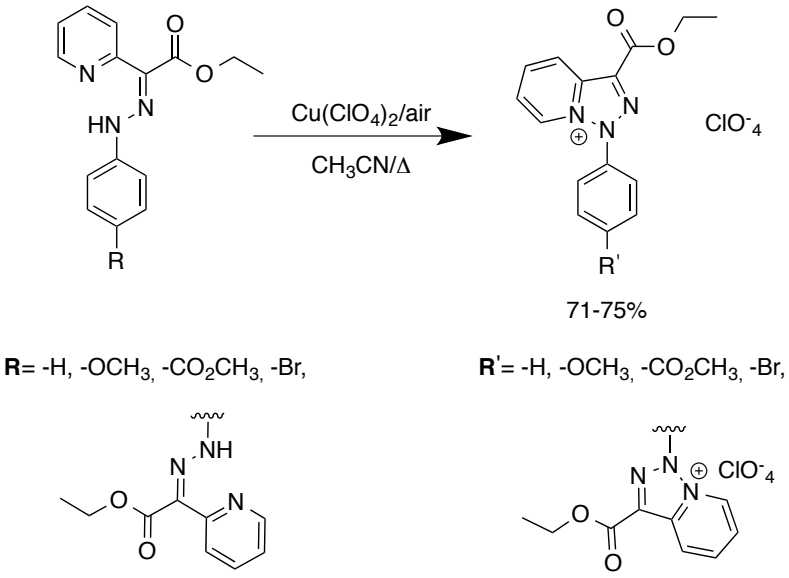

***Figure3.1*- Synthesis of [1,2,3]triazolo[1,5-*a*]-pyridinium salts.**

These compounds exhibit interesting photophysical properties both in solution and in the solid state, such as tunable blue light emission with "mega" Stokes shift [8] and they recently have been employed as turn-on chemodosimeters for CN^- detection in solution under mild conditions.[9] This novel class of chemodosimeters exploits the pseudopericyclic ring opening reaction that occurs between the bridgehead nitrogen atom and CN^- anion (*Figure 3.2*).

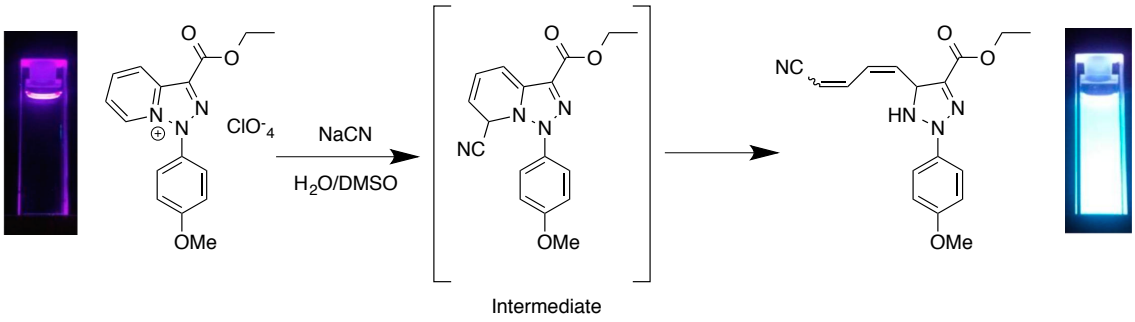

***Figure 3.2*-Reaction-based detection of CN^-.Reproduced with permission from *Org. Lett.*,2013, 15, 10,2386-2389. © 2013 American Chemical Society.**

In this Chapter, the results concerning the photophysical, photochemical and electrochemical characterization of a family of *p*-substituted1-phenyl-[1,2,3]triazolo[1,5-*a*]-pyridinium and triazoloquinolinium salts (*Figure 3.3*) are reported.

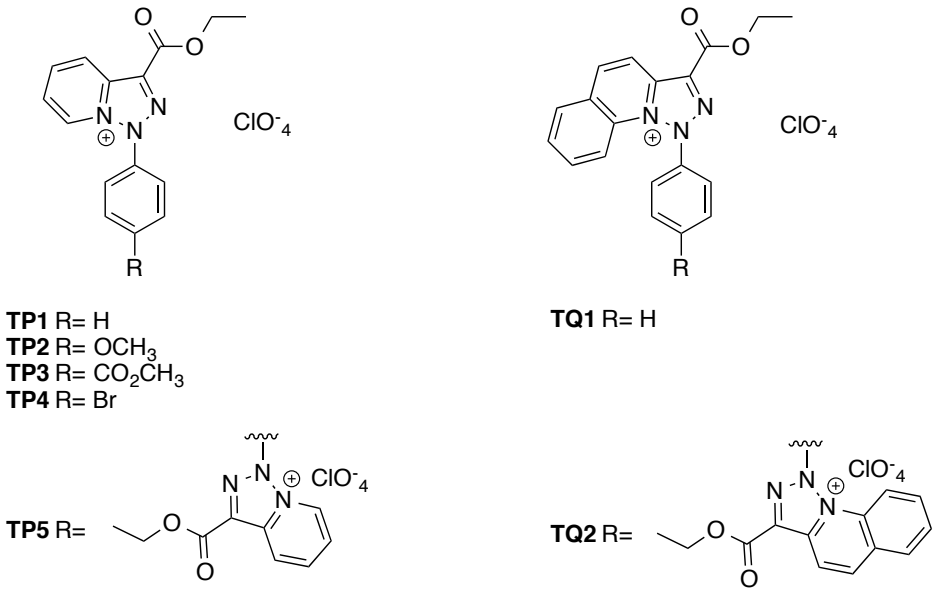

***Figure 3.3*- Structure of triazolopyridinium and triazoloquinolinium salts.**

In order to establish the role exerted by the 3-ethoxycarbonyl substituent and by the phenyl ring linked to the triazolopyridinium moiety in their photophysical and electrochemical properties, the results obtained were compared with those obtained for two reference compounds (*Figure 3.4*).

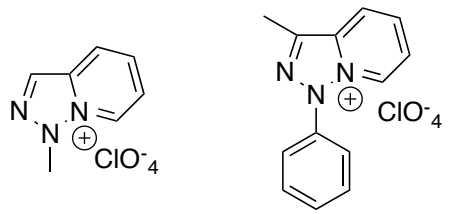

TPR1 **TPR2**

***Figure 3.4*- Structure of reference compounds.**

Among the studied triazolopyridinium salts, compounds **TP1**, **TP3** and **TP4** were chosen (since they exhibit the highest fluorescence quantum yield and water solubility) to study their interaction with DNA.

This work was performed in collaboration with the group of Prof. I. Aprahamian, Dartmouth College, Hanover, New Hampshire (USA), who made the synthesis of the studied compounds.

3.2 Photophysical characterization

3.2.1 Solution measurements

The absorption and emission spectra of triazolopyridinium and triazoloquinolinium salts are mainly due to the presence of the phenyl in the 1-phenyl-1H-[1,2,3]triazolo[1,5-*a*]pyridinium and 1-phenyl-1H-[1,2,3]triazolo[1,5-*a*]quinolinium units: the single triazolopyridinium unit, in fact, exhibits a more structured absorption spectrum and proved to be non emissive.

The absorption spectra (*Figure 3.5*) of TP1-5 in H_2O are have a similar shape compared to the one of TPR2 and show three main bands in the near UV region, located approximately at 220, 250 and 300 nm. The presence of different substituents affects the position and the magnitude of bands located at 250 and 300 nm, which can be attributed to the 3-(ethoxycarbonyl)-1H-[1,2,3]triazolo[1,5-*a*]pyridin-8-ium unit.

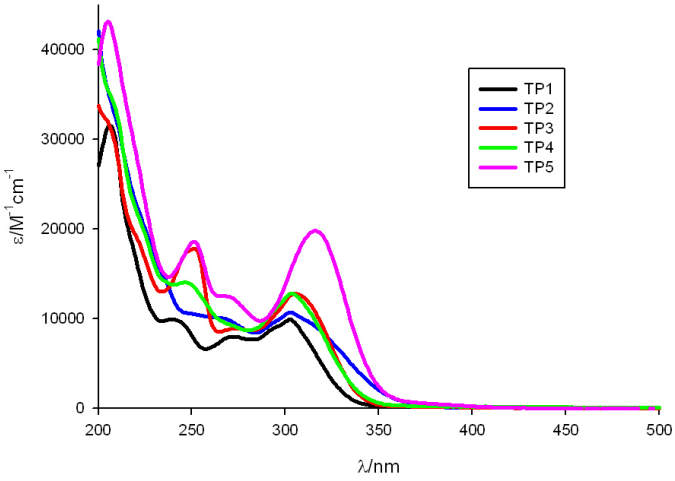

***Figure 3.5*- Absorption spectra of triazolopyridinium salts in H_2O at r.t.**

In general, the presence of substituents determines two main effects: an auxochromic effect of bands at 200, 250, 270 and 300 nm and a batochromic effect on the bands at 250 and 300 nm.

In particular, the presence of a second unit of 3-(ethoxycarbonyl)-1H-[1,2,3]triazolo[1,5-*a*]pyridin-8-ium determines a red shift of the absorption maximum at 300 nm and determines also a doubling in the values of the molar absorption coefficient and the same trend is also observed for the maximum at 250 nm. The presence of an additional fused ring, as in the case of triazoloquinolinium salts, exerts a drastic change in solubility, but do not affect significantly the shape of absorption spectra.

In fact, absorption spectra (*Figure 3.6*) of the compounds show three main bands in the UV region, located at 220, 255 and 340 nm. The two spectra have a very similar shape, whereas the intensity of the bands in the case of TQ2 is about twice as that of the bands of TQ1 (*Table 3.2*).

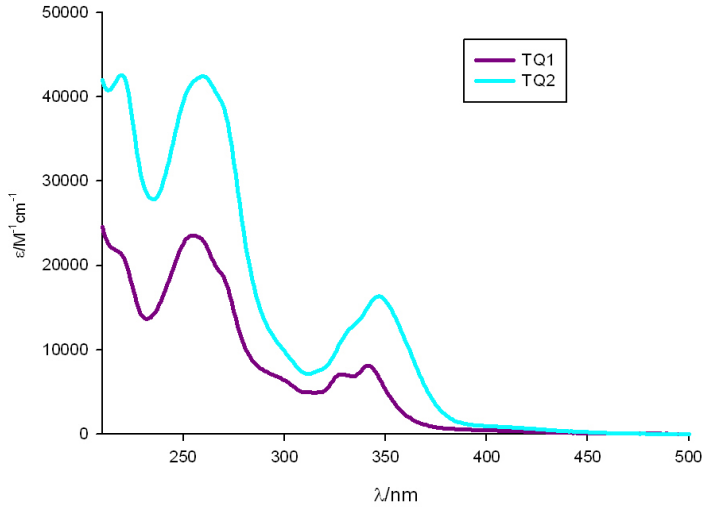

***Figure 3.6*- Absorption spectra of triazoloquinolinium salts in CH_3OH and CH_3CN at r.t.**

These observations indicate that the triazoloquinolinium unit is the chromophore responsible of the UV-visible absorption, and that the two triazoloquinolinium units of TQ2 are practically independent from one another, as also suggested by molecular modeling (see Section 3.5).

The shape of emission spectra is similar for all compounds (*Figure 3.7*): regarding the presence of both a triazolopyridinium and triazoloquinolinium chromophores, they all show a broad and structureless fluorescence band, whose maxima are located between 406 and 498 nm, depending on the nature of both the cation and the substituent in *para* position on the phenyl ring.

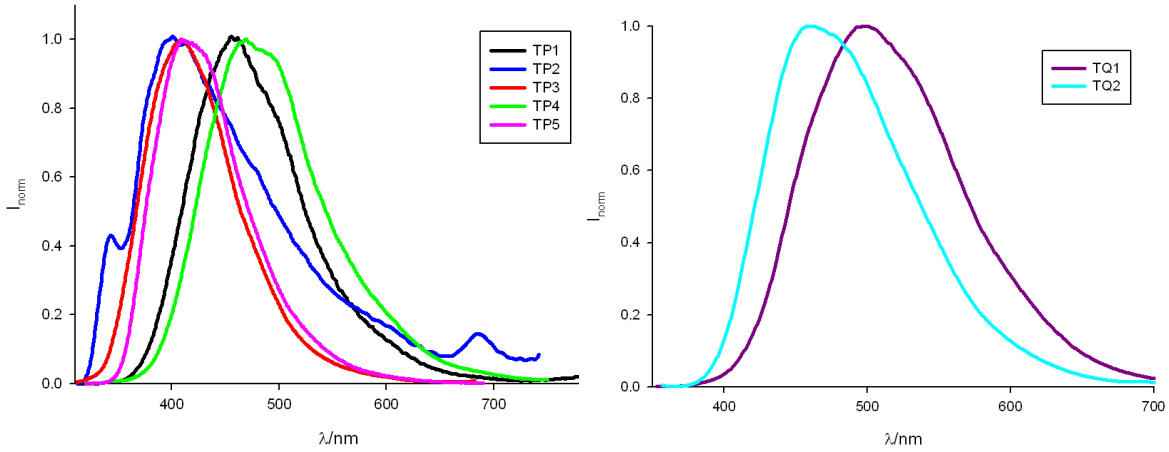

***Figure 3.7*- Fluorescence emission spectra of triazolopyridinium in H_2O (left) and triazoloquinolinium (right) salts in CH_3OH and CH_3CN at r.t.**

The presence of different substituents and the nature of the pyridinium ion also affect the emission wavelength and, consequently, the magnitude of the Stokes shift. The presence of electron withdrawing substituents (e.g., Br) determines a bathochromic effect on the emission, whereas the presence of electron donating ones (e.g., OMe) is responsible for an emission at shorter wavelengths, reducing the Stokes shift (*Table 3.1*). This observation is in contradiction with a partial charge transfer (phenyl-to-triazolopyridinium) character of the electronic transition, as suggested by quantum chemical calculations (see Section 3.5), as the presence of electron donors in the phenyl ring should make the charge transfer easier. In the case of triazoloquinolinium derivatives, the reduced Stokes shift in TQ2 may be related to the larger tilt angle of the phenyl substituent with respect to the triazoloquinolinium plane in the bichromophoric species TQ2 due to steric repulsions, as shown by molecular modeling (see Section 3.5), resulting in a smaller electron delocalization. In the end, the nature of substituents on the phenyl moiety also affects the quantum yield: in the presence of electron donating substituents, it is decreased by one order of magnitude (*Table 3.1*).

***Table 3.1*- Photophysical properties of TP and TQ derivatives in solution.**

Compound	**λ_{max}/nm (ε /M^{-1} cm^{-1})**	**λ_{em}/nm**	**Φ**	**τ /ns**	**Stokes Shift/nm**
TPR1	213 (24200) 214 (25200) 289 (7700) 294 (7200) 300 (8700)	/	/	/	/
TPR2	305 (11200)	460	$2.55*10^{-3}$	< 0.2[#]	155
TP1	207 (31400) 302 (9900)	460	0.029	0.9	158

TP2	303 (10700)	406	$1.03*10^{-3}$	< 0.2#	103
TP3	251 (17800)	427	0.066	0.6	122
	305 (12800)				
TP4	247 (14100)	469	0.023	0.6	163
	305 (12500)				
TP5	205 (43100)	419	0.22	1.28	114
	251 (18600)				
	305 (19800)				
TQ1	255 (23500)	498	0.04	τ_1=1.4	157
(solvent:	329 (7100)			τ_2=2.3	
CH_3OH)	341 (8100)				
TQ2	220 (42600)	460	0.11	τ_1=1.7	113
(solvent:	260 (42500)			τ_2< 0.2#	
CH_3CN)	347 (16400)				

3.2.2 Solid state measurements

The emission spectra were recorded by exciting different regions of the sample at different excitation wavelengths and were then normalized at the emission maximum (*Figure 3.8*). Unlike reference compounds TPR1 and TPR2, all triazolopyridinium and triazoloquinolinium salts proved to be emissive in the solid state and the observed emission bands are reproducible and assigned to genuine luminescence from the investigated compounds.

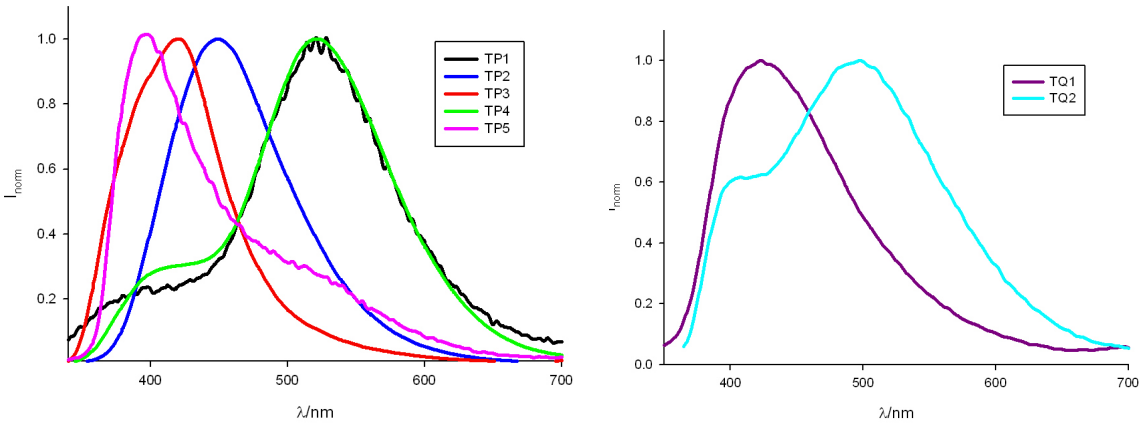

***Figure 3.8*- Fluorescence emission spectra of triazolopyridinium (left) and triazoloquinolinium (right) salts in a glass-deposited solid state film.**

Compared with the emission spectrum in aqueous solution, there is a red shift of the emission band in the solid state for TP1, TP2 and TP4, as shown in *Figure 3.6*, and in *Table 3.2*. On the other hand, TP3, TP5 and TQ1 exhibit a blue shift of the emission maximum in the solid state (*Figure 3.8*). This effect may be due to the lack of solvation (polar water molecules can stabilize electronic levels with a charge-transfer character) and/or decreased conformational freedom of the chromophore in the condensed phase. In the case of TQ2 the emission from the film takes place in the same spectral region as that of the solution; the maximum is slightly red shifted but the emission onset occurs at higher energies than in solution.

The passage from solution to solid state causes also a change in the emission kinetics: in fact, the decay becomes biexponential for TP1, TP4 and TP3. TP5 experiences a decrease in the lifetime, whereas the emission of TP2 becomes longer lived. In the case of triazoloquinolinium salts, the excited state becomes shorter lived and the decay is monoexponential, as shown in *Table 3.2*.

***Table 3.2*- Photophysical properties in solid films.**

Compound	**λ_{em} /nm**	**τ /ns**
TP1	520	τ_1=0.25 τ_2=2

TP2	449	τ=3.1
TP3	418	τ_1< 0.2#
		τ_2=0.68
TP4	524	τ_1=4
		τ_2=0.55
TP5	392	< 0.2#
TQ1	520	< 0.2#
TQ2	524	< 0.2#

3.2.3 Spectroscopic experiments in a frozen solvent at 77 K

All compounds exhibit fluorescence and phosphorescence emission (*Figure 3.9*); fluorescence bands are blue shifted respect to the fluorescence detected in solution, except for TP2 and TP5. In all cases, the fluorescence band in the glass matrix at 77K is blue shifted with respect to that observed on solid films at room temperature (*Table 3.3*).

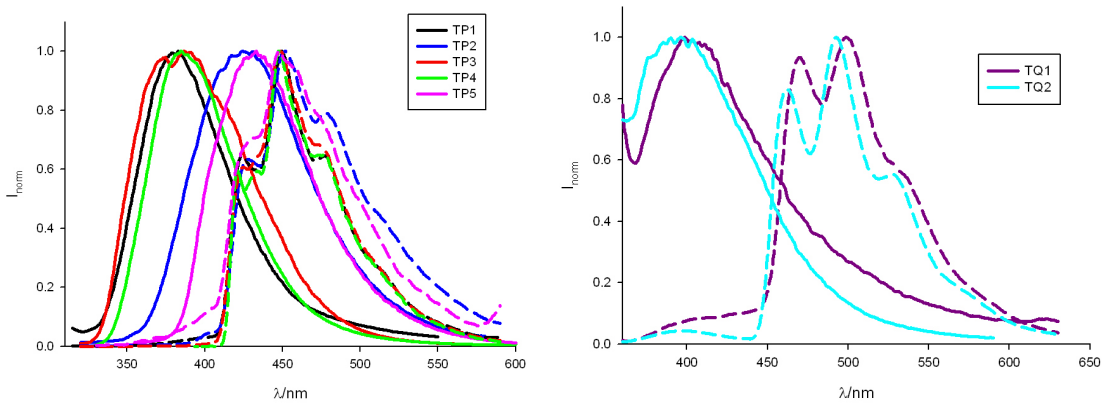

***Figure 3.9*- Normalized fluorescence (straight line) and phosphorescence (dashed line) emission spectra of triazolopyridinium (left) and triazoloquinolinium (right) salts at 77 K.**

The comparison between emission wavelengths and lifetimes in solution, solid state and at low temperature is presented in *Table 3.3*.

Table 3.3- **Comparison between photophysical properties in solution, solid state and 77 K.**

Compound	Solution		Solid state		77 K			
	λ_{em}/nm	τ/ns	λ_{em}/nm	τ/ns	λ_{fluo}/nm	τ/ns	λ_{phos}/nm	τ/s
TP1	460	0.9	520	τ_1=0.25 τ_2=2	384	τ_1=0.8 τ_2=2.4	450	2.4
TP2	406	<0.2#	449	3.1	424	τ_1=0.6 τ_2=2.6	448	τ_1=0.9 τ_2=2.3
TP3	427	0.6	418	τ_1<0.2# τ_2=2.3	387	1.9	452	τ_1=1.4 τ_2=2.9
TP4	469	0.6	524	τ_1=4 τ_2=0.55	385	τ_1=0.6 τ_2=2.6	448	τ_1=0.9 τ_2=2.3
TP5	419	1.3	392	<0.2#	433	3.9	448	2.1
TQ1	498	τ_1=1.4 τ_2=2.3	415	<0.2#	396	1.9	493	3.49
TQ2	460	τ_1=1.7 τ_2<0.2#	495	<0.2#	399	τ_1=1.4 τ_2=6.8	499	2.65

3.3 Photochemical experiments

Triazolopyridinium and triazoloquinolinium salts exhibited different photoreactivity: in fact, triazoloquinolinium derivatives proved to be photochemically inert, whereas some of the triazolopyridinium salts studied showed a good photoreactivity.

Among reference compounds, TPR1 experienced a photochemical reaction when irradiate at 287 nm: in fact, remarkable variations in the absorption spectrum were observed both in the presence and in the absence of O_2 (*Figure 3.10*). In both cases, the same spectral variations were observed and the isosbestic points at 271 and 222 nm remained constant during the whole irradiation time.

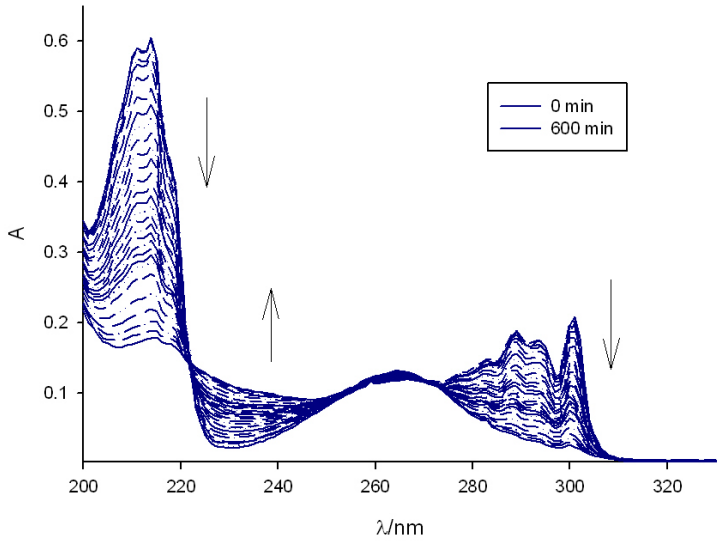

***Figure 3.10*- Variations in the absorption spectrum during irradiation at 287 nm of TPR1 in aqueous solution at r.t.**

For this reaction the quantum yield was found to be 0.034 in air equilibrated solution and 0.017 in the absence of oxygen, suggesting that it plays an active role in the reaction.

Other triazolopyridinium salts (TP1 and TP4) are not stable under light exposure, but in this case the photoreactivity is much lower and different from that observed for TPR1, indicating that the presence of a phenyl ring in 1-position and an ester group in 3-position on the triazolopyridinium ion affects the photoreactivity of these compounds. In fact, for TP1 and TP4 a slight decrease of the bands at 207 and 302 nm is observed (*Figure 3.11*).

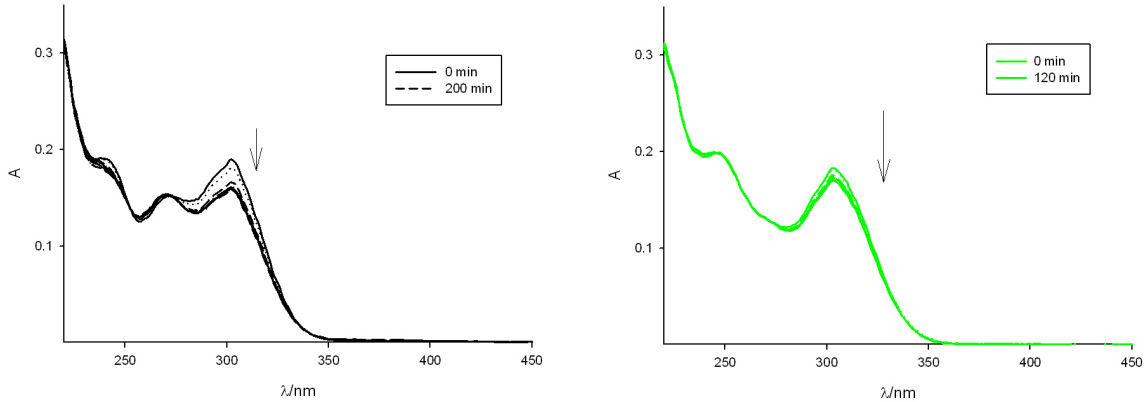

***Figure 3.11*- Variations in the absorption spectrum during irradiation at 313 nm of TP1 (left) and TP4 (right) in aqueous solution at r.t.**

The absorption changes observed on irradiation of TP3 at 313 nm are more complex: in fact, the band peaking at 251 nm decreases and shifts to the red, the band at 276 nm increases, and the band at 305 nm experiences an increase and a blue shift. Moreover, three isosbestic points (218, 257 and 297 nm) are observed (*Figure 3.12*), suggesting that a single product is formed. The quantum yield for this photoreaction is 0.019.

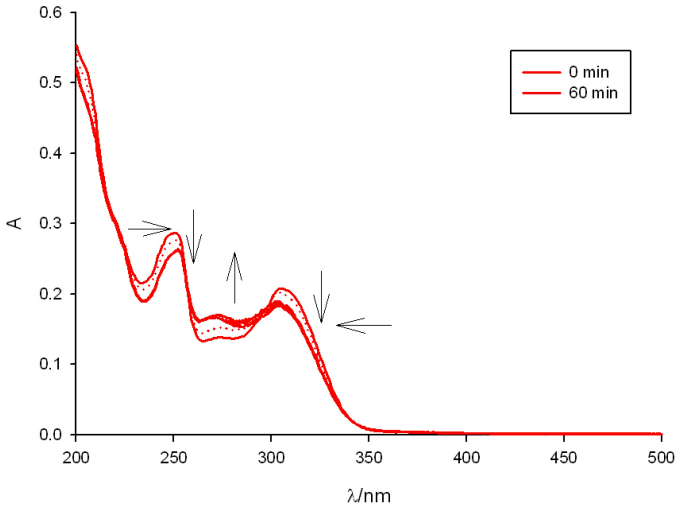

***Figure 3.12*- Variations in the absorption spectrum during irradiation at 313 nm of TP3 in aqueous solution at r.t.**

Also in this case, the irradiation of TP3 was performed on a deoxygenated solution in order to clarify the possible role of O_2 in this reaction. The absorption changes (*Figure 3.13*) are qualitatively similar to those observed in the presence of O_2 (isosbestic points are maintained) but the reaction is faster and proceeds to a greater extent (the quantum yield is 0.069). This suggests that a triplet excited state, which is efficiently quenched by oxygen, may be involved in the photoreaction.

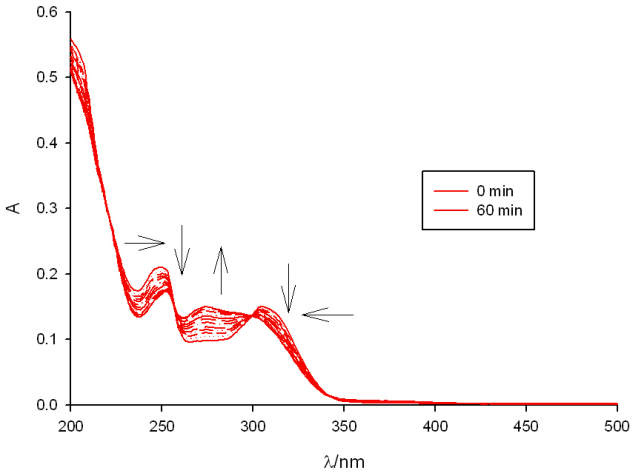

***Figure 3.13*- Variations in the absorption spectrum during irradiation at 313 nm of TP3 in aqueous solution at r.t. in the absence of O_2.**

In the end, the presence of an additional 3-(ethoxycarbonyl)- 1H-[1,2,3] triazolo[1,5-*a*]pyridin-8-ium results in an enhancement of the photoreactivity: in fact, relevant changes in the absorption spectrum of TP5 occur upon irradiation at 313 nm (*Figure 3.14*): the bands at 205, 251 and 316 nm decrease while that at 374 nm increases. Moreover, two isosbestic points (276 and 341 nm) are observed.

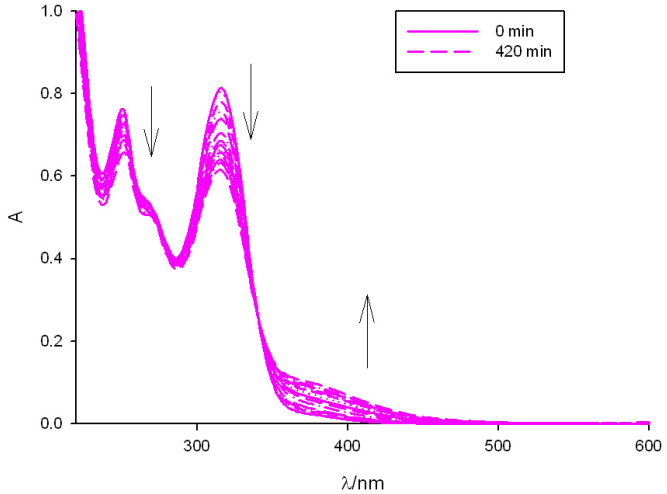

***Figure 3.14*- Variations in the absorption spectrum during irradiation at 313 nm of TP5 in aqueous solution at r.t.**

3.4 Electrochemical characterization

Triazolopyridinium and triazoloquinolinium do not undergo oxidation processes: in fact, by observing the obtained voltammograms and DPV peaks (*Figure 3.13- 3.15*), it is possible to observe only reduction processes. In the case of triazolopyridinium derivative, these processes are irreversible; triazoloquinolinium salts exhibited poorly reversible or irreversible reduction processes.

All compounds exhibit two reduction processes: the first one, occurring at potential values around –1 V vs SCE (*Figure 3.15*), can be assigned to reduction of the triazolopyridinium unit, by comparing these voltammograms with those obtained for TPR1 and TPR2.

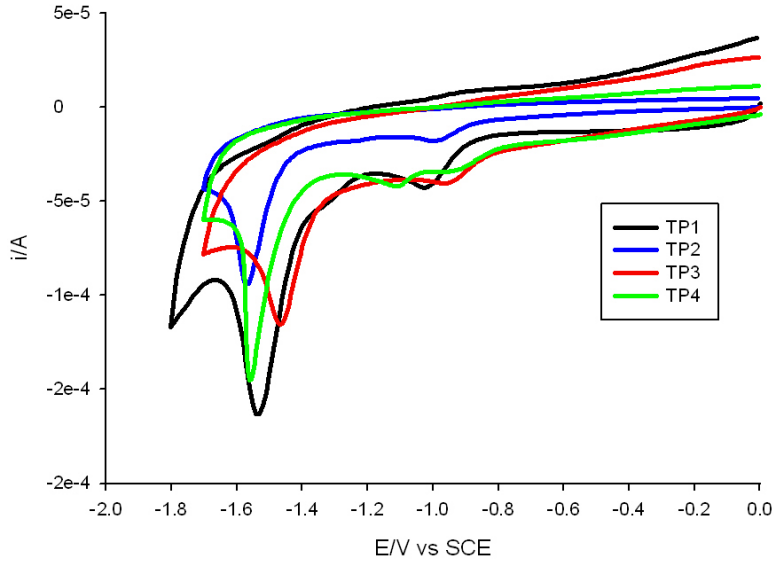

***Figure 3.15*- Cyclic voltammograms of an aqueous solution of triazolopyridinium salts. Working electrode: glassy carbon; supporting electrolyte 0.1 M $NaClO_4$; reference electrode: SCE; scan rate 200 mV/s.**

The second process takes place at much more negative values and is often accompanied by precipitation and deposition of the product on the electrode surface, as shown by the sharp profile of the DPV peaks (see *Figure 3.16*).

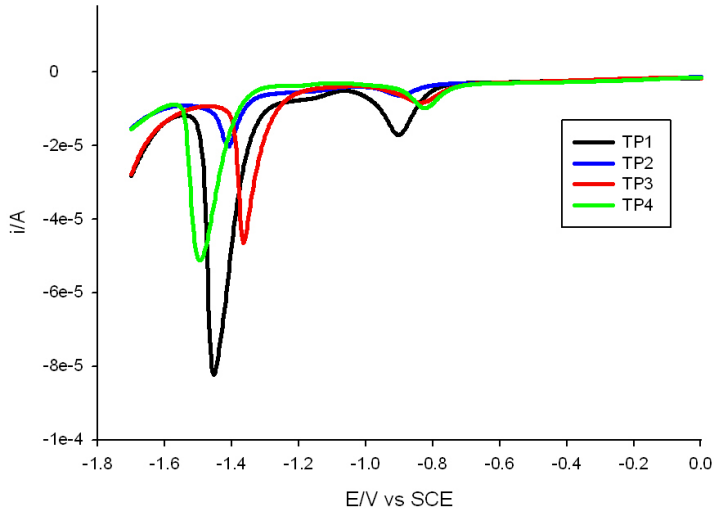

***Figure 3.16*- Differential pulse voltammetry of triazolopyridinium salts . Working electrode: glassy carbon; supporting electrolyte: $NaClO_4$; reference electrode: SCE. Modulation time: 40 ms, modulation amplitude: 75 mV, scan rate: 20 mV/s.**

A comparison between the reduction potential values obtained from DPV measurements (*Table 3.4*) for the various compounds indicates that the triazolopyridinium moiety and the phenyl ring are not electronically insulated: this behaviour supports the partial charge-transfer character of the HOMO-LUMO transitions associated with fluorescence. In fact, it can be observed that electron donating substituents on the phenyl ring shift the reduction potential to more negative values, whereas electron withdrawing ones cause a shift to less negative potentials. The same trend is not observed for the second reduction process, which is not present in TPR1 and TPR2, and can thus be tentatively assigned to the irreversible reduction of the pendant ester group.

In the case of triazoloquinolinium salts, the electrochemistry is more complex: in fact, both compounds exhibit several reduction processes, as shown in *Figure 3.17*.

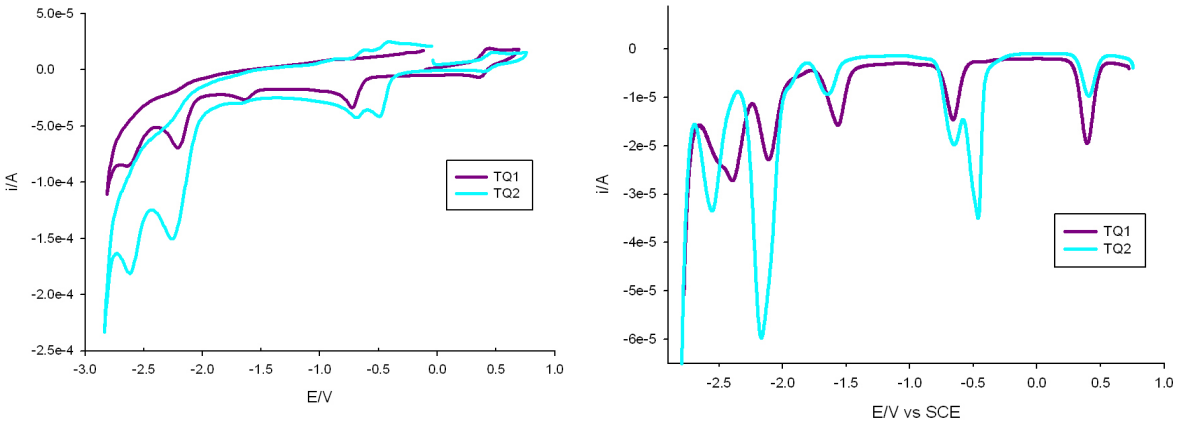

***Figure 3.17*- Cyclic voltammograms (left) and DPV peaks (right) of a CH_3CN ($5*10^{-4}$ M)/$TEAPF_6$ ($5*10^{-3}$ M) solution of TQ1 and TQ2. Working electrode: glassy carbon; internal reference: ferrocene 0.1 M, CH_3CN. Potential values are referred to the SCE. In DPV peaks the peak at +0.4 V is the oxidation of ferrocene.**

The first reduction of TQ1 is relatively facile (–0.66 V vs SCE, *Table 3.4*) and it is obviously assigned to the uptake of one electron by the triazoloquinolinium moiety. The second reduction corresponds to the introduction of a further electron into the LUMO and therefore occurs at a considerable more negative potential (–1.57 V). The third reduction signal should involve the LUMO+1 orbital and is observed at –2.1 V.

In the case of TQ2 the first reduction occurs (–0.44 V) at a considerably less negative potential compared with TQ1, suggesting a much higher degree of delocalization of the injected electron in the former compound. In fact, semi-empirical quantum chemical calculations (see Section 3.5) indicate that the LUMO of TQ2 encompasses both triazoloquinolinium moieties as well as the phenylene bridge. Such an extensive delocalization is in agreement with the fact that the second reduction occurs at a potential only 150 mV more negative than for the first process. The third process (–2.18 V) occurs approximately at the same potential as for TQ1; the current intensity of its CV signal, however, is about twice as that observed for TQ1, suggesting that in TQ2 the process involves the exchange of two electrons. In fact, quantum chemical calculations show that in TQ2 the LUMO+1 is centred onto each triazoloquinolinium moiety (see Section 3.5). Hence, it can be hypothesized that at –2.18 V two electrons are simultaneously injected in TQ2 (one for each triazolopyridinium unit). A similar

discussion can be made for the fourth process (–2.39 V in TQ1 and –2.59 V in TQ2).

***Table 3.4*- Electrochemical data.**

Compound	E_{OX} (V vs SCE)	E_{RED} (V vs SCE)
TPR1	/	–1.40
TPR2	/	–1.11
TP1	/	–0.90
		–1.44
TP2	/	–0.89
		–1.41
TP3	/	–0.83
		–1.37
TP4	/	–0.82
		–1.49
TQ1	/	–0.66
		–1.57
		–2.1
		–2.39
TQ2	/	–0.44
		–0.59
		–1.61#
		–2.18
		–2.59

 # Very weak signal in the CV and DPV scans; process assigned to an electroactive impurity.

3.5 Molecular Modeling

Molecular modeling was performed using molecular mechanics (MM2 force field) and semi-empirical quantum calculations (MOPAC/MNDO method), as implemented in the Chem3D Pro software.

The molecular structure was first energy-minimized by molecular mechanics, and successively the HOMO and LUMO surfaces were determined by semi-empirical calculations.

In the case of triazolopyridinium salts, the HOMO is mainly located onto the phenyl unit, whereas the LUMO is centered onto the electron-poor triazolopyridinium moiety (*Figure 3.18*).

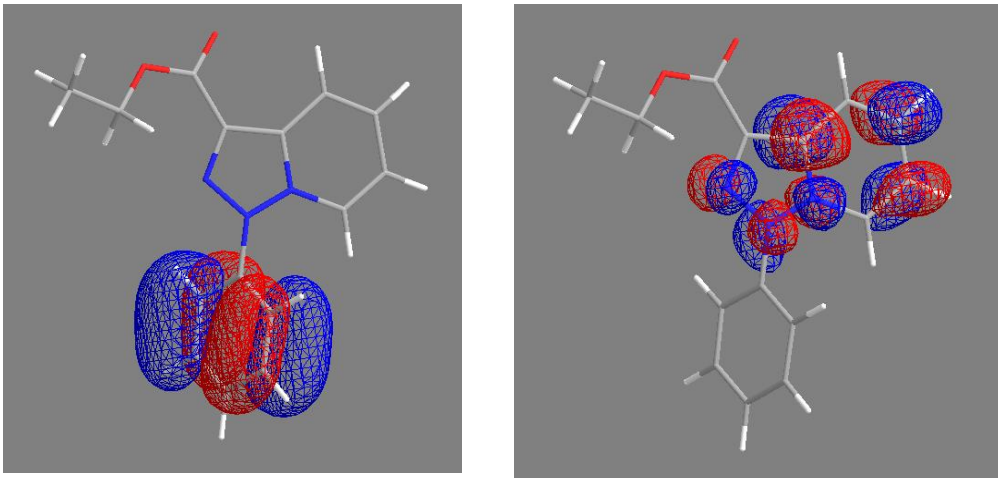

***Figure 3.18*- Representation of the HOMO (left) and LUMO (right) orbitals for triazolopyridinium salts (MOPAC/MNDO).**

Hence, the phenyl ring and the triazolopyridinium moiety are not electronically insulated, supporting partial charge-transfer character of the HOMO-LUMO transitions associated with fluorescence and the dependence of the reduction potential for the triazolopyridinium unit with substituents on the phenyl ring (*Table 3.4*). In fact, the frontier orbitals in TPR1 are both located onto the planar triazolopyridinium chromophore (*Figure 3.19*), leading to different spectroscopic properties as well as more negative reduction potential.

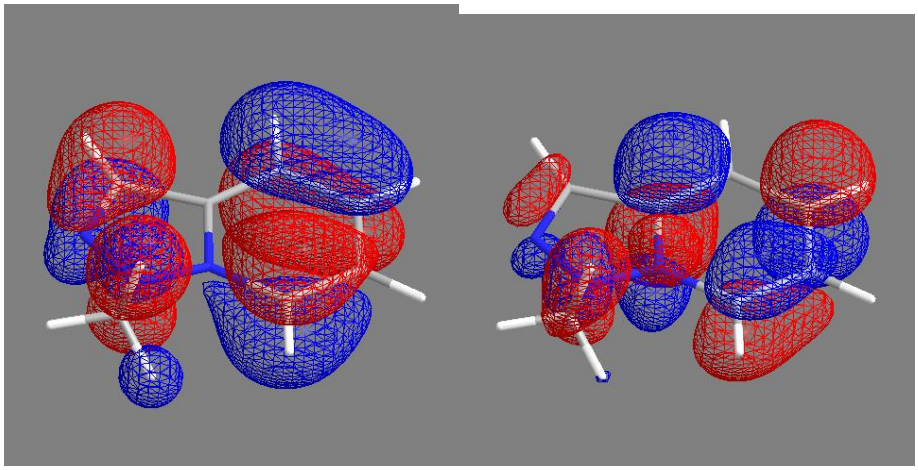

***Figure 3.19*-Representation of the HOMO (left) and LUMO (right) orbitals for TPR1 (MOPAC/MNDO).**

In the case of triazoloquinolinium salts, the situation is more complex: in fact the HOMO is not merely located on the phenyl ring, but it extends on the triazoloquinolinium unit too. Indeed, the LUMO is located on the triazoloquinolinium unit (*Figure 3.20*).

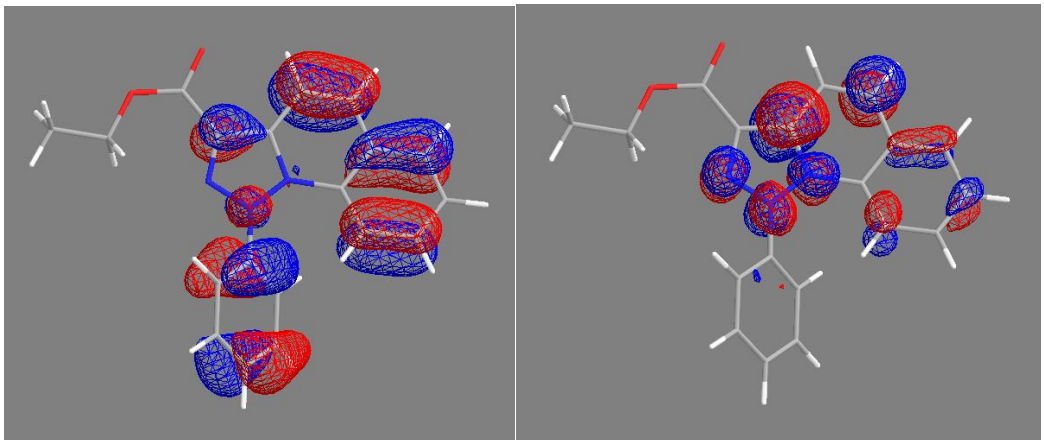

***Figure 3.20*- Representation of the HOMO (left) and LUMO (right) orbitals for TQ1 (MOPAC/MNDO).**

The presence of an additional triazoloquinolinium unit results in a more extended LUMO orbital, whereas the HOMO is less delocalized and is located onto triazoloquinolinium units (*Figure 3.21*).

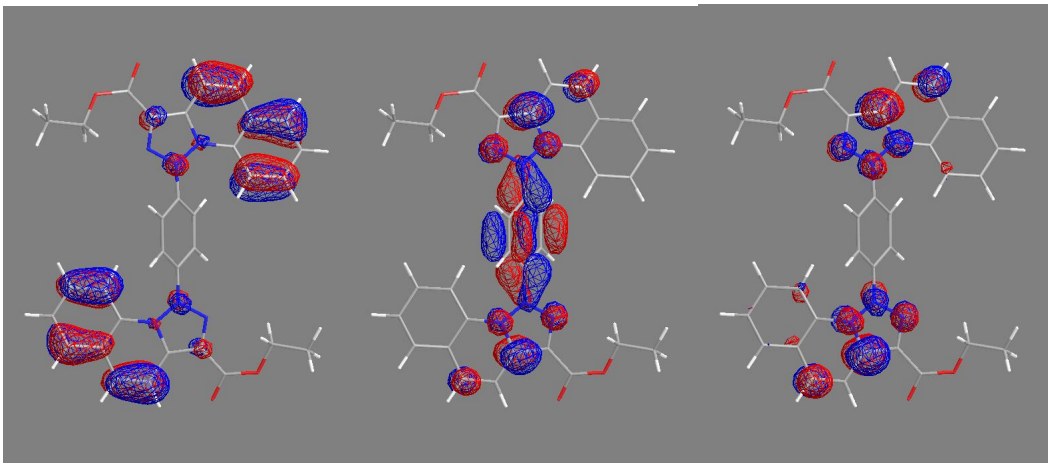

***Figure 3.21*- Representation of the HOMO (left), LUMO (center) and LUMO+1 (right) orbitals for TQ2 (MOPAC/MNDO).**

These observations help in the interpretation of spectroscopic and electrochemical data obtained: in fact, the intensity of the absorption bands in the case of TQ2 is about twice as that of the bands of TQ1, supporting the hypothesis that the two triazoloquinolinium units in TQ2 are independent. Moreover, the extensive delocalization of the LUMO orbital in TQ2 results in a higher delocalization of the injected electron and makes the second reduction process easier.

3.6 DNA binding studies

3.6.1 Introduction

DNA represents the unique tool used by living organism for the storage of the genetic information, which produces evident physical and biochemical traits, constituting the phenotype. DNA is involved in the biosynthesis of proteins and, more specifically, the aminoacidic sequence that composes them is written in the genetic code that refers to the oligonucleotide sequence forming DNA double helix. It is interesting and amazing that birth, proliferation and death of living organisms relies on the transcription process, whose key player is DNA. Therefore, living organisms' fate depends on the recognition of specific sites in DNA structure by specific enzymes and, more precisely, on their interaction.
This highlights the essential role played by this macromolecule in biological system and makes it the long-standing target for treatment and diagnosis for

human illness. On the other hand, small molecules are able to recognize specific DNA sequences and to interact with them in several ways and this paved the way for their employment as tool for genome interpretation as well as therapeutic agents. [10] In fact, regulation of the transcription process represents one of the most effective way to achieve control over gene expression and in this sense ligand-DNA interaction can result in a dramatic structural change in the double helix so that essential and specific recognition processes between DNA and enzymes are annihilated.

Organic molecules as well as organometallic compounds[11] can undergo covalent interactions with DNA as alkylating agents, leading to its fragmentation by repairing enzymes in their attempt to replace alkylated bases. Moreover, establishment of non- covalent interactions, such as electrostatic, van Der Waals, hydrophobic forces and hydrogen bonding results in other binding modes such as intercalation, outside-edge binding and minor/major groove binding.[12]

It should be emphasized that intercalation and groove binding may exert a deep influence on the physiological function of the nucleic acid and thus they are extensively employed as chemotherapeutic strategies. It follows that the intercalating and groove binding ability are strictly linked to their molecular structure and design [13]: generally, this behaviour is observed for flat aromatic systems consisting of at least two aromatic or heteroaromatic fused rings and the presence of a positive charge (namely, the presence of a quaternary nitrogen atom conjugated with an aromatic π system) determines a further benefit, since charged ligands considerably stabilize the final DNA-ligand complex by a mean of charge-transfer and electrostatic interactions. [14]

Since triazolopyridinium and triazoloquinolinium satisfy structural criteria mentioned above, those endowed with the highest emission quantum yield in solution and the best solubility in water were chosen and their interaction with DNA was investigated, in terms of changes in their photophysical properties, such as emission/absorption spectra, emission lifetimes, emission anisotropy and circular dichroism.

3.6.2 Results and discussion

All triazolopyridinium salts show no variations in their absorption spectra, that are ascribable to the formation of a DNA-molecule complex (*Insets Figure 3.20*): in fact, absorption spectra obtained after the addition of 10 eq. of DNA are equal to the sum of the single absorption spectra of triazolopyridinium salts and DNA alone. On the other hand, a decrease in their emission intensity (ca. 40%) was observed upon addition of DNA (*Figure 3.22*). In order to exclude kinetic effects, the same spectra were recorded after waiting one hour and no changes in theirshape was observed.

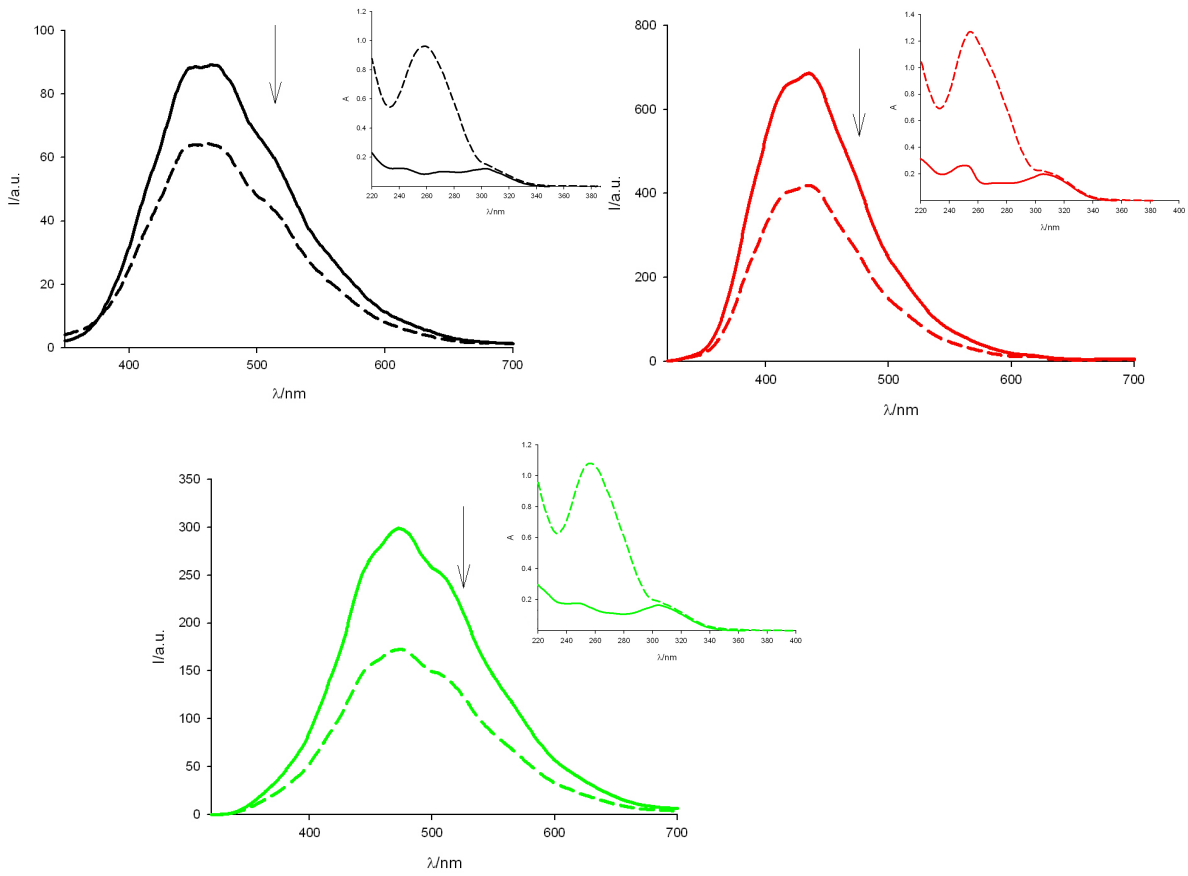

***Figure 3.22*- Fluorescence quenching of TP1 (black), TP3 (red) and TP4 (green) upon addition of 10 eq. of DNA (dashed line). Inset: absorption spectra of TP1 (black), TP3 (red) and TP4 (green) in the absence (solid line) and after the addition of 10 eq. of DNA**

For all compounds, fluorescence quenching is accompanied by a change in the emission kinetics, passing from a monoexponential to a biexponential trend (*Table 3.5*).

***Table 3.5*- Emission quenching percentage and emission lifetime change upon addition of DNA.**

Compound	eq. DNA added	% Emission quenching	τ/ns
TP1	0		τ_0 =0.5
	10	42%	τ_1 =0.4
			τ_2 =3.7
TP2	0		τ_0 =0.8
	10	30%	τ_1 =0.9
			τ_2 =0.3
TP3	0		τ_0 =0.4
	10	40%	τ_1 =0.3
			τ_2 =2.9

Emission quenching and change in emission lifetime lead to the conclusion that an interaction between DNA and all triazolopyridinium salts takes place, but these data alone do not give enough information about the kind of this interaction.

Moreover, emission anisotropy was measured in the presence of increasing amounts of DNA and it is possible to observe that all compounds do not increase significantly their emission anisotropy, except for TP1, which experiences a 10-fold change of its anisotropy value (*Table 3.6*).

Table 3.6- **Emission anisotropy values after the addition of several amounts of DNA.**

eq. DNA added	TP1 (460 nm)	TP3 (427 nm)	TP4 (469 nm)
0 eq.	$4.46*10^{-3}$	$7.72*10^{-2}$	$1.08*10^{-1}$
1 eq.	$1.63*10^{-2}$	$8.93*10^{-2}$	$6.65*10^{-2}$
3 eq.	$3.76*10^{-2}$	$8.11*10^{-2}$	$1.12*10^{-1}$
5 eq.	$2.5*10^{-2}$	$8.16*10^{-2}$	$8.5*10^{-2}$
10 eq.	$4.42*10^{-2}$	$6.62*10^{-2}$	$7.43*10^{-2}$

By comparing data obtained and the molecular structures of the studied compounds, it is possible to hypothesize that the interaction between this compound and DNA is easier, since TP1 does not exhibit any substituent in *para* position on the phenyl ring. Moreover, this supports the conclusion that the interaction between these organic salts and DNA is basically electrostatic and refers to the phosphate backbone of DNA and the triazolopyridinium moiety, since compound bearing substituents on the phenyl ring do not increase their anisotropy values. A further confirmation of the kind of interaction occurring is given by circular dichroism measurements: in fact, these measurements proved to be highly diagnostic in stating which kind of interaction between triazolopyridinium derivatives and DNA takes place. If an intercalation or a minor groove binding interaction occurs, induced dichroic bands (ICD) are normally observed.[12] In the presence of a ligand, a significant alteration of DNA CD spectrum can be observed and it is ascribable to coupling of DNA and ligand transitions, or changes in base coupling because of changes in DNA geometry due to ligand binding; this effects are translated in considerable increases in intensity accompanied by shifts in the maximum/minimum of DNA bands.[15] By observing circular dichroism spectra (*Figure 3.23*) an increase of the positive band at 268 nm can be observed and the same trend is observed for the negative band located at 245 nm, accompanied with the presence of isoelliptic points at 256

and 287 nm. These two bands are ascribable to stacking interaction between bases and helical B conformation of DNA.[16]

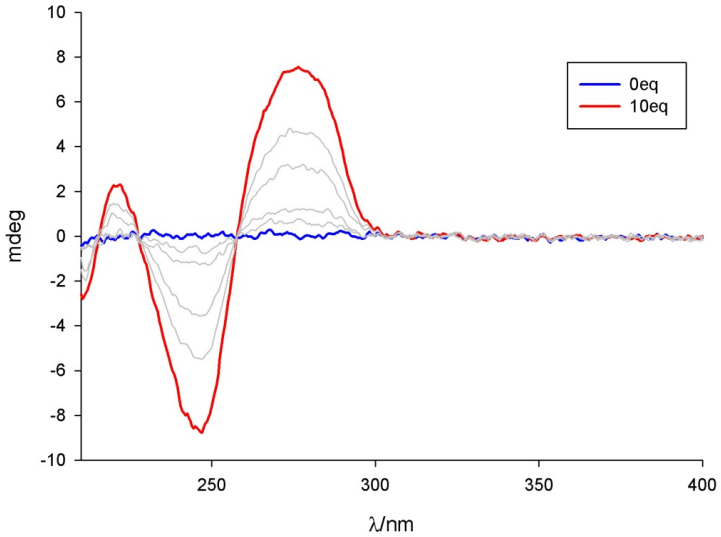

Figure 3.23 **- Circular dichroism spectrum of triazolopyridinium salts in the presence of increasing amounts of DNA.**

Hence, the absence of bands referring to an induced dichroic signal suggests that neither intercalation nor minor groove binding interaction between the three triazolopyridinium derivatives and DNA takes place, but only an outside-edge interaction between phosphate backbone of DNA and the triazolopyridinium moiety.

3.7 Conclusion

In this chapter the photophysical, photochemical and electrochemical properties of triazolopyridinium and triazoloquinolinium were studied and it was shown their tunability by changing the substituents in *para* position on the phenyl ring. These compounds exhibited tunable blue light emission with "mega" Stokes shift both in solution and in the solid state. Moreover, they exhibited phosphorescence by performing 77 K measurements and it was found that lifetime of triplet states is quite long compared to that found for other blue emitting organic compounds. Among them, only triazolopyridinium derivatives proved to be soluble in water and this make them attractive for biological applications, such as bioimaging.

Moreover, since they exhibited the typical structural features of known DNA binders, their interaction with DNA was investigated but the obtained results did not show groove binding nor intercalation.

References

[1] Sasabe, H.; Kido, J., *Chem. Mater.*, **2011**, 23, 621-630.

[2] a) Sapsford, K.E.; Berti, L.; Medintz, I.L., *Angew. Chem., Int. Ed.*, **2006**, 45, 4562-4588. b) Kikuchi, K.; *Chem. Soc. Rev.*, **2010**, 39, 2048-2053.

[3] Gaal, M.; List, E.; Scherf, U., *Macromolecules*, **2003**, 36, 4236–4237.

[4] Yan, W.; Wang, Q.; Lin, K.; Li, M.; Petersen, J.L.; Shi, X., *Chem. Eur. J.*, **2011**, 17, 5011-5018.

[5] Bower, J. D.; Ramage, G. R., *J. Chem. Soc.*, **1957**, 4506–4510.

[6] Kuhn, R.; Münzing, W., *Chem. Ber.*,**1952**, 85, 29–37.

[7] a) Su, X.; Liptak, M.; Aprahamian, I., *Chem. Commun.*, **2013**, 49, 4160-4162. b) Aprahamian, I.; Su, X., (**2013**); *Triazolium and tetrazolium derivatives as organic light emitters;* US20140336385.

[8] Martin, A.; Long, C.; Forster, R. J.; Keyes, T. E.,*Chem. Commun.*,**2012**, 48, 5617–5619.

[9] Robbins, T.F.; Qian, H.; Su, X.; Huges, R.; Aprahamian, I., *Org. Lett.*,**2013**, 15, 10, 2836-2839.

[10] Gottesfeld, J.M.; Neely, L.; Trauger, J.W.; Baird, E.E.; Dervan, P.B., *Nature*, **1997**, 387, 202-205.

[11] Paul, A.; Bhattacharya, S., *Curr.Science*, **2012**, 102, 212-231.

[12] Ihmels, H.; Thomas, L., *Materials Science of DNA*, CRC Press: Boca Raton, **2011**.

[13] a) Neto, B.A.D.; Lapis, A.A.M., *Molecules*, **2009**, 14, 1725-1746. b) Rescifina, A.; Zagni, C.; Varrica, M.G.; Pistarà, V.; Corsaro, A., *Eur. J.Med. Chem.*, **2014**, 95-115.

[14] Kubar, T.; Hanus, M.; Ryjacek, F.; Hobza, P., *Chem. Eur. J.*, **2006**, 12, 280-290.

[15] a) Nordén, B.; Kurucsev, T., *J. Mol. Rec.*, **1994**, 7, 141-156. b) Garbett, N.C.; Ragazzon, P.A.; Chaires, J.B., *Nature Protocols*, **2007**, 2, 3166-3172.

[16] Kypr, J.; Kejnovskà, I.; Renčiuk, D.; Vorlìčkovà, M., *Nucleic Acids Res.*, **2009**, 37, 1713-1725.

Chapter 4
Photoactive and self-assembled biocompatible drug delivery systems

4.1 Introduction

Release of liposomal content represents the essential step in the development of biocompatible drug delivery systems: in order to state if the system under investigation is effective in its purpose, it is necessary to compare the exerted effect on liposomal membranes' permeability with the spontaneous one. Moreover, it is important to follow the enhancement on liposomal membrane permeability and, thus, to develop an effective experimental procedure to achieve this purpose.

In order to monitor the time evolution of liposomal membrane permeability, a commonly used experimental approach deals with the exploitation of change of photophysical properties of some fluorescent dyes upon release. Among them, 5(6)-carboxyfluorescein (CF^{3-}) is widely used for the determination of liposomal stability[1] for three main reasons. First, its permeability in the bilayer is low[2] and its photophysical properties depend on pH[3] and concentration. In fact, at high concentration the dye experiences a self-quenching of its fluorescence due to energy transfer to non fluorescent dimers[4] and this behaviour can be

exploited in order to monitor the time-dependent evolution of liposomal membrane destabilization.

In a typical experiment, the dye is entrapped in the aqueous core of vesicles in a high concentration (typically 50 mM, at which fluorescence self-quenching is significant) and its efflux from liposomes results in a dilution of the dye into the external dispersant medium and recovery of its fluorescence[5]: thus, a typical kinetic profile consists of a curve in which the time dependent increase of carboxyfluorescein fluorescence is reported. This profile is consistent with a first-order kinetic mechanism and usually an apparent first-order rate constant k_{obs} can be determined according to the following equation

$$\frac{d[CF^{3-}]}{dt} = k_{obs}[CF^{3-}]$$

It is important to note that the first-order kinetic model is not always adequate in describing the kinetics of CF^{3-} leakage from vesicles and that a stretched exponential function best fits data obtained. This kinetic model has been used to describe different kinetic behaviours observed in many different phenomena, such as the discharge of capacitors,[6] dielectric relaxation in polymeric materials,[7]luminescence decay of fluorophores incorporated in micelles, cyclodextrins, sol-gel matrices, polymers, proteins biological tissues and vesicles or membranes.[8]

Moreover, the efficiency of a drug delivery system is usually expressed in terms of percentage of CF^{3-} leakage, by comparing the effect obtained after the addition of Triton X-100 (who is known to enhance membrane permeability of living cells[9] and to lyse liposomes), according to the following equation

$$\%leakage = \ 100 * \frac{F(t) - F(0)}{F(Triton) \ - \ F(0)}$$

In this chapter, the effect of different polyazobenzene derivatives on membrane permeability of POPC liposomes is examined: in particular, both commercial azobenzene and polyazobenzene derivatives inserted in the phospholipid bilayer as well as a photoactive pseudorotaxane entrapped in the aqueous core were evaluated as potential candidates for the development of biocompatible photoactive systems for drug delivery purposes.

This work was performed in collaboration with the group of Prof. S. Hecht,

Humboldt-Universität zu Berlin, Berlin (Germany), who made the synthesis of the studied compounds.

4.2 Azobenzene

4.2.1 Photoinduced carboxyfluorescein leakage

Due to its interesting photochromism, the azobenzene unit has been widely exploited in order to create smart nanoscale objects able to perform different operations. Moreover, it has been used in the development of photoactive biocompatible drug delivery systems based on liposomes as biological carriers. First of all, it is interesting t evaluate the effect that plain azobenzene exerts on the permeabilization of membranes made of POPC phospholipids.

Azobenzene was inserted in the liposomal bilayer and, by using the method proposed by Iwata *et al.*[10], it was estimated to be 4% mol. respect to moles of POPC phospholipids.

One sample of POPC liposomes containing self-quenched CF^{3-} in their core and azobenzene in their bilayer was irradiated at 365 nm. The observed spectral variations (*Figure 4.*1) are typical for the *trans-cis* photoisomerization of azobenzene.[11]

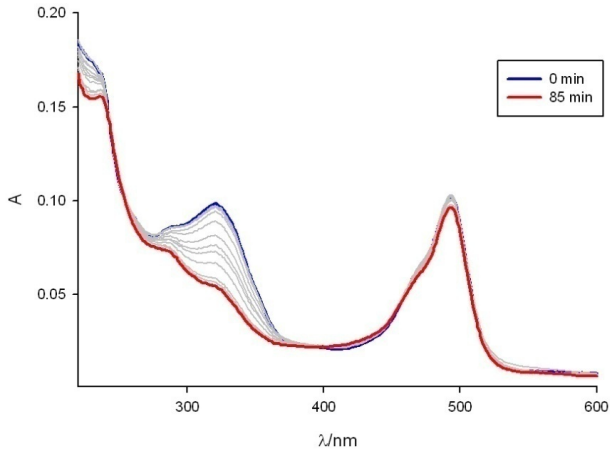

Figure 4.1 **- Time-dependent variations in the absorption spectrum of POPC liposomes ([POPC= 62 µM) containing CF^{3-} (50 mM in PBS pH=7.4) and azobenzene (4%mol) in their bilayer during the irradiation at 365 nm.**

Liposomes stability was evaluated in terms of efflux of the entrapped dye and, more specifically, the value of the observed kinetic constant was used as a

quantification of the level of permeabilization achieved, since the higher the kinetic constant the more effective would be the compound inserted in the bilayer.

In this case, CF^{3-} leakage at the end of irradiation was compared with that obtained for a sample kept in the dark and with the one referring to spontaneous release.

By comparing the values of the kinetic constants (*Table 4.1*) and the kinetic profiles obtained (*Figure 4.2*), it is possible to state that both the presence of *trans*-azobenzene and, even more, its photoisomerization leads to a faster efflux of the entrapped dye. Moreover, it is interesting to observe that the presence of azobenzene as well its photoisomerization does not change vesicles' dimensions (*Table 4.1*).

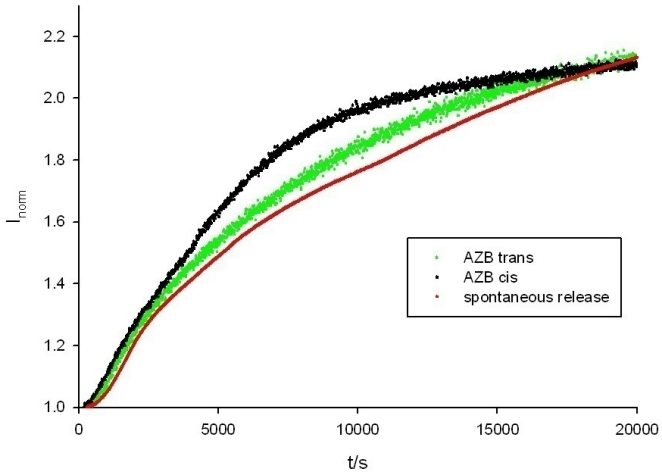

***Figure 4.2* - Normalized kinetic profiles of CF^{3-} (50 mM in PBS pH=7.4) leakage from POPC liposomes ([POPC= 13μM). The curves refer to spontaneous (red), *trans* (green) and *cis*(black) azobenzene-mediated CF^{3-} leakage.**

***Table 4.1*- Hydrodynamic diameter and kinetic constants.**

	Time (min.)	Hydrodynamic Diameter (nm)	k_{obs} (s^{-1})
No AZB	0	130.3	$6.87*10^{-5} \pm 3.4*10^{-6}$
	/	/	
trans-AZB	0	154	$1.65*10^{-4} \pm 4.5*10^{-5}$
	85	154	

***cis*-AZB**	0	154	$2.1*10^{-4} \pm 7*10^{-5}$
	85	154	

Thus, these results are a useful premise for the successive investigation on the effect exerted by more azobenzene units in an organic compound embedded in the phospholipid bilayer.

4.3 Polyazobenzene derivatives: a new perspective in liposomal destabilization

4.3.1 Decoupled polyazobenzenes

4.3.1.1 Introduction

Azobenzene represent an appealing photoactive unit to make opto-mechanical materials, which converts photon energy into mechanical work.[12] The basic requirement to construct efficient materials is that the constituting units are able to undergo a dramatic change of their shape and dimension upon irradiation and it is clear that azobenzene represent the ideal structural motif found in many different photoswitchable materials. Polyazobenzene architectures are found for example in rigid-rod polymers,[13] which are able to undergo reversible shrinkage and stretching of their polymeric backbone upon irradiation (*Figure 4.3*).

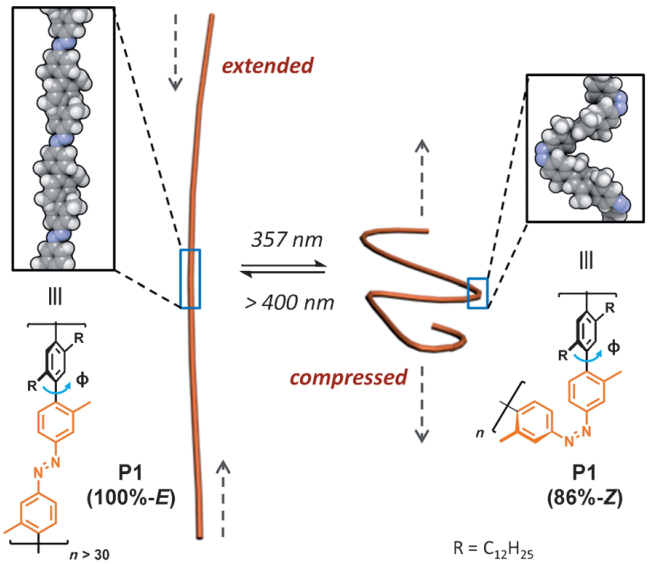

Figure 4.3 **- Schematic representation of rigid-rod polymer in the extended (left) and compressed (right) state. Molecularly dissolved polymer can reversibly shrink and stretch upon exposure to UV and visible light irradiation. Reproduced with permission from *Angew. Chem. Int. Ed.*, 2011, 50, 12559-12563. © 2011 Wiley-VCH Verlag GmbH & Co.**

The key of their morphological behaviour resides in the electronic separation of the constituents azobenzene units: this point is not trivial since conjugated azobenzenes do not exhibit *Z*-rich photostationary states when irradiated.[14]

In fact, there is a deep connection between electronic conjugation and the degree of separation of azo units, expressed in terms of dihedral angle of the biphenyl linkage units. In fact, as the dihedral angle increases, the electronic conjugation decreases,[15] leading to an enhancement of photoswitching characteristics. Moreover, it has been found that when biphenyl linkers are perpendicular, azobenzene units operate independently:[16] since the presence of an azo moiety leads to an almost 3-fold increase of CF^{3-} leakage form POPC liposomes, it would be interesting to analyse which would be the effect exerted by many independent azo units in the same compound inserted in the phospholipid bilayer, especially if the embedded compound has a molecular length comparable with bilayer thickness of POPC vesicles. In this paragraph, the results concerning the insertion of a polyazobenzene derivative bearing three separated azo units (AZO-3) in POPC phospholipid bilayers are shown.

4.3.1.2 Photophysical and photochemical characterization

Photophysical and photochemical properties of AZO-3 were compared with those of other azobenzene derivative, having one (AZO-1) and two (AZO-2) azobenzene photochromic units (*Figure 4.4*).

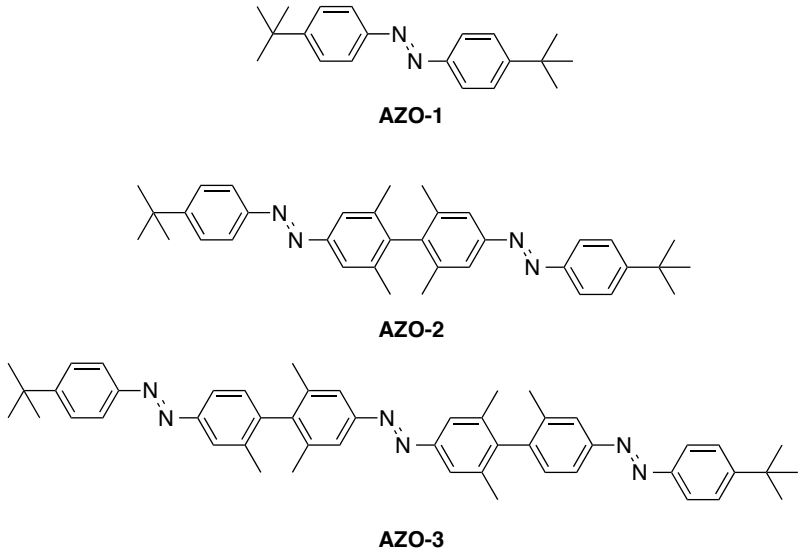

***Figure 4.4* - Chemical structure of azobenzene derivatives AZO-1, AZO-2 and AZO-3.**

Absorption spectra (*Figure 4.5*) show two main bands referring to π–π^* and n–π^* transitions of azobenzene and by comparing molar absorption coefficient values (*Table 4.2*) it is possible to notice that there is not a perfectly linear correlationwith the number of azo units in the compounds. This behaviour is remarkable, since for conjugated azobenzenes the trend is perfectly linear (see par.6.2.1). Moreover, absorption maximum related to π–π^*transitions is slightly *redshifted* by increasing the azobenzene units in the compound and the same trend is observed for the other absorption maximum. As usually found for azobenzene derivatives, all compounds are non emissive in solution.

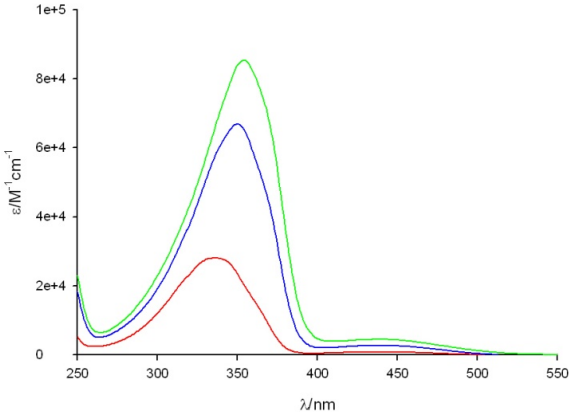

***Table 4.2*- Photophysical and photochemical parameters.**

	ε /M^{-1}cm^{-1}	Φ
AZO-1	ε_{336nm} = 28100	0.22
	ε_{438nm} = 480	
AZO-2	ε_{350nm} = 66900	0.11
	ε_{440nm} = 2700	
AZO-3	ε_{354nm} = 85600	0.08
	ε_{442nm} = 4500	

***Figure 4.5* - Absorption spectra of AZO-1 (red), AZO-2 (blue) and AZO-3 (green) in $CHCl_3$ at r.t.**

The proof of the separation of their photochromic units emerges from photochemical experiments: in fact, all compounds show time-dependent variations on their absorption spectra that are consistent with the bahaviour of azobenzene and with a full *trans-cis* isomerization (*Figure 4.6* and *Table 4.2*). Moreover, the strong decrease of the π–π^* transition band refers to the presence of a *Z*-rich photostationary state and the presence of well-defined isosbestic points indicates that AZO-2 and AZO-3 have the same photoreactivity of AZO-1 and, thus, that azobenzene chromophores are separated.

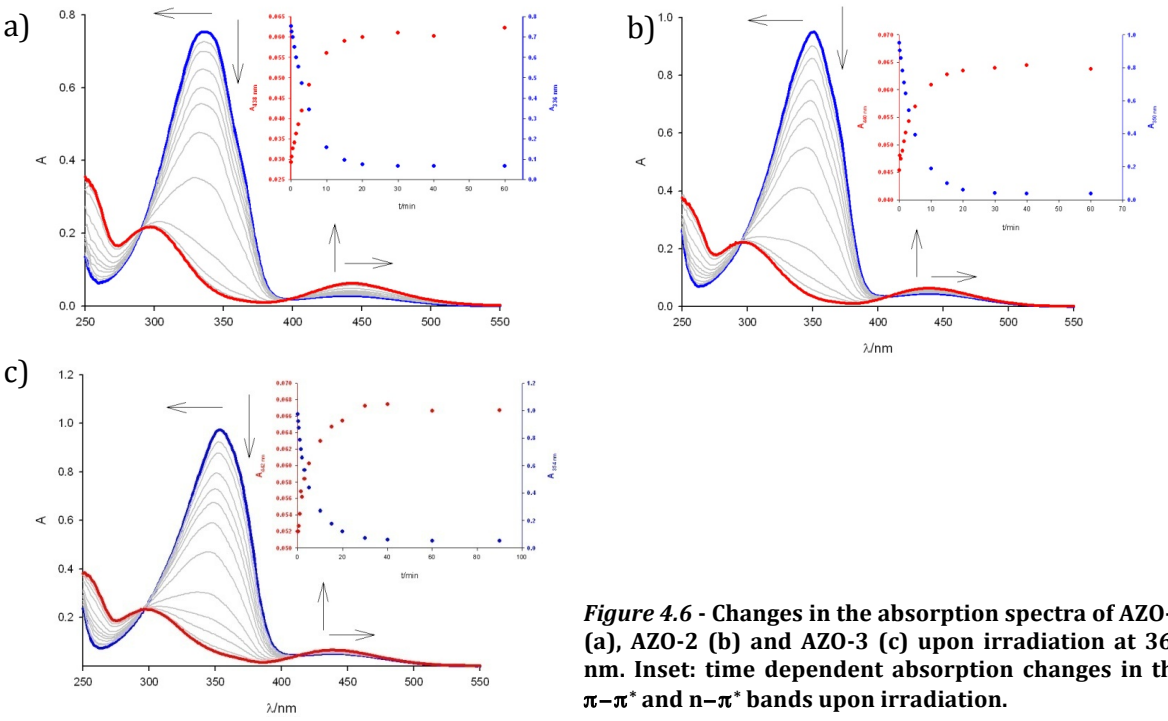

***Figure 4.6* - Changes in the absorption spectra of AZO-1 (a), AZO-2 (b) and AZO-3 (c) upon irradiation at 365 nm. Inset: time dependent absorption changes in the π–π^* and n–π^* bands upon irradiation.**

Among these three photoactive compounds, AZO-3 was chosen since its molecular length is comparable with bilayer thickness of POPC bilayers (39.8 Å at 20°C)[17] and its ability in destabilizing liposomal membranes was explored.

4.3.1.3 Membrane insertion of AZO-3

Insertion of AZO-3 in POPC bilayers was performed following two different approaches:

1. Guest insertion in the lipid film and rehydration;
2. Guest addition to preformed liposomes.

The application of the first protocol leads to a non-homogeneous sample: the absorption spectrum (*Figure 4.7*) shows a structured band at 350 nm that refers to the polyazobenzene guest, but the same band is not present anymore after filtration.

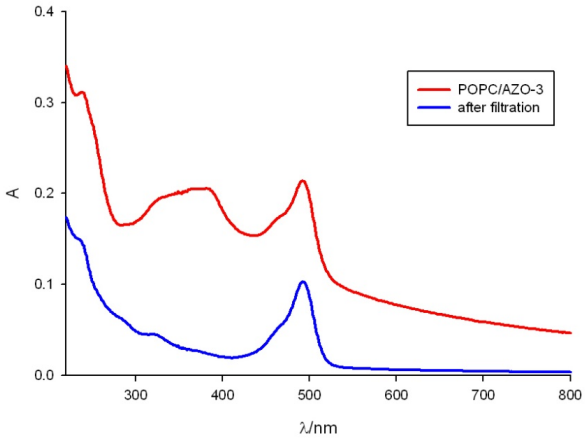

***Figure 4.7* - Absorption spectrum of POPC liposomes ([POPC]= 62 μM) containing AZO-3 in their bilayer and CF^{3-} (5o mM in PBS) in their aqueous core before (red) and after (blue) filtration.**

DLS measurements (*Figure 4.8*) show three different populations and liposomes do not represent the most abundant one in the sample: this suggests the hypothesis that the guest undergoes self-aggregation during the hydration and extrusion steps.

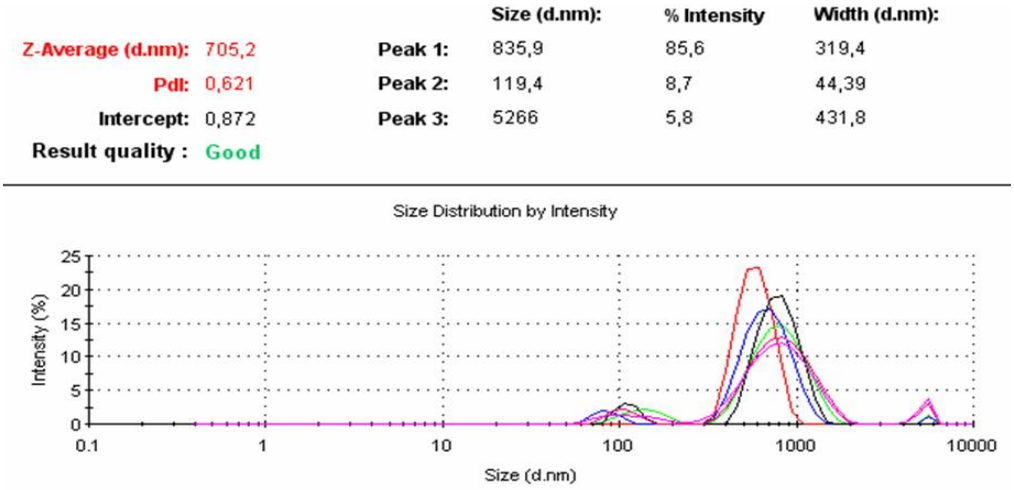

Figure 4.8 **- DLS measurements of POPC liposomes ([POPC]= 62 μM) containing AZO-3 in their bilayer and CF^{3-} (5o mM in PBS) in their aqueous core.**

The second approach was applied in order to overcome this issue, assuming that during solvent evaporation the hydrophobic guest inserts in the hydrophobic region of the phospholipid bilayer, but it led to the same results. In fact, its high hydrophobicity makes it totally insoluble in water, but, presumably because of its long size and rigid shape, it is not able to dissolve in the hydrophobic region of the phospholipid bilayer. On the other hand, its transverse insertion in the bilayer may be both thermodynamically and kinetically demanding, since its hydrophobic ends should deal with the zwitterionic region of the phospholipid at the membrane-water interface.

4.3.2 Decoupled polyazobenzene amphiphile

4.3.2.1 Introduction

Previous results concerning the insertion of AZO-3 in POPC bilayer, prompted Prof. Hecht's group to design a new guest, AZO-4, in which the photochemical activity of separated azobenzene units have to be joined with the presence of positively charged terminal groups (*Figure 4.9*), in order to improve the self-assembly of phospholipids and guest during hydration and extrusion steps and, thus, to enhance the insertion efficiency of the photoactive guest.

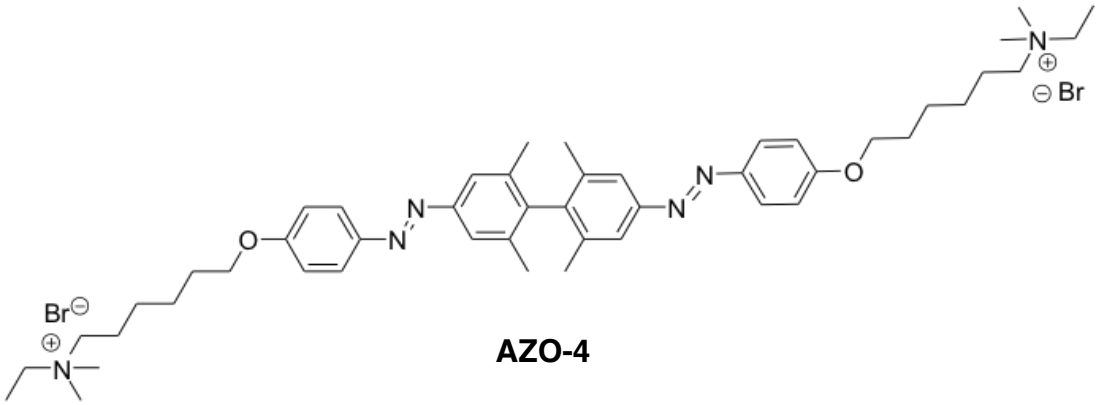

AZO-4

Figure 4.9 **- Chemical structure of azobenzene derivatives AZO-4.**

Many different photoactive compounds exhibiting the azobenzene core have been incorporated in liposomal membranes, in order to develop photoactive and biocompatible nanocarriers for drug delivery. Many different azobenzene-containing guests have been explored, including cholesterol derivatives,[18] polymers,[19] phospholipids,[20] and amphiphiles,[21] but all of them showed one or more azobenzene units that are far each other, whereas no one reported the effect exerted by two (or more) azobenzene units so spatially close.

Moreover, it is possible to obtain an efficient release using amphiphilic molecules, whose structure resembles the one of membrane-forming lipids: in fact, the structural analogy between them and these light-sensitive compounds may improve the encapsulation efficiency and overall stability of resulting liposomal suspensions.

4.3.2.2 Photophysical and photochemical characterization

The absorption spectrum (*Figure 4.10*) of AZO-4 shows one main band: a strong UV band related to π–π*, exhibiting an absorption maximum at 362 nm; this band overlaps with the one referring n-π* transitions of azobenzene.[22]

By comparing the absorption spectrum and the molar absorption coefficient value referring to the π–π* band (*Table 4.3*) with the one of plain azobenzene, it is possible to notice that the π–π* band is *redshifted* and that the molar absorption coefficient is almost twice than the one found for azobenzene. This

behaviour can be ascribed to the presence of *p*-methoxy substituents on phenyl rings. [23]

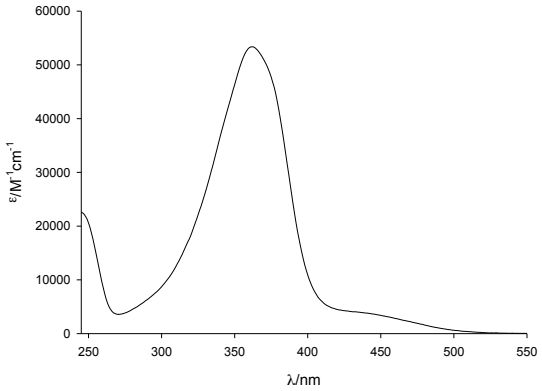

***Table 4.3*- Photophysical and photochemical parameters.**

	Value
ε /M^{-1}cm^{-1}	50600
E:Z	1:99
Φ /molecule	0.16
$k_{Z->E}$ (s^{-1})	1.03*10^{-5}

***Figure 4.10* - Absorption spectrum of AZO-4 in $CHCl_3$ at r.t.**

Moreover, the compound did not exhibit any emission in solution and upon irradiation at 365 nm it exhibited the typical photoreactivity and thermal *Z*→*E* isomerization of azobenzene parent compounds (*Figure 4.11*).

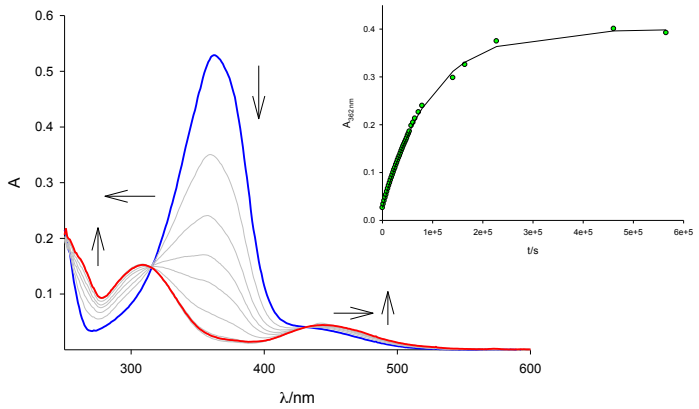

***Figure 4.10* - Changes in the absorption spectra of AZO-4 upon irradiation at 365 nm. Inset: time dependent absorption changes in thermal *Z/E* isomerization and first-order fitting.**

By observing *Table 4.3*, it emerges thatthe quantum yield is much higher (0.16) than the one found for azobenzene: this is consistent with the behaviour of substituted azobenzenes, expecially those bearing amino and alkoxy moieties in 2 and 4 position.[24]

The photostationary state is composed mainly by the *Z,Z* isomer (99%) and the thermal backward isomerization was monitored and fitted with a first order kinetic model, yielding a kinetic constant value of 1.03*10^{-5} s^{-1}.

4.3.2.3 Photoinduced carboxyfluorescein leakage

The absorption spectrum of POPC liposomes containinfg CF^{3-} in their aqueous compartment and 3% mol AZO-4 in their bilayer[25] exhibit a slight *blueshift* of the absorption maximum referring to the π–π^* transition of azobenzene, which is now located at 356 nm. Variations in the absorption spectrum during irradiation (*Figure 4.11, left*) are observed, leading to the conclusion that photoisomerization of the guest is possible even when it is inserted in the phospholipid bilayer. Moreover, another sample containing the same amount of veisicles was kept in the dark and the variation in its absoprtion spectrum were compared with that of the irradiated sample: no significant absorption changes occur in the darkduring the time needed for irradiation of the other sample (*Figure 4.11, right*).

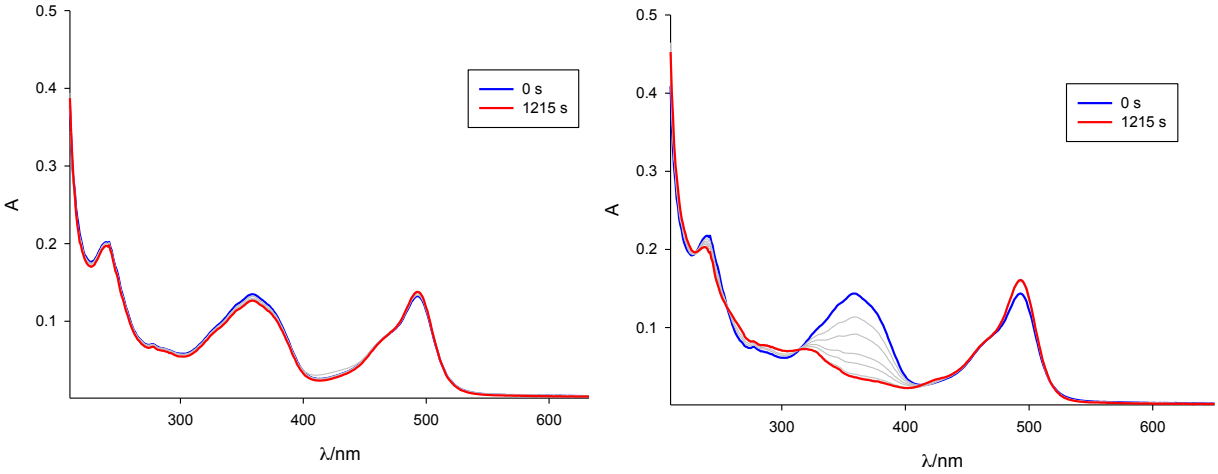

Figure 4.11 **- Time-dependent spectral variations of POPC liposomes containing CF^{3-} in their core and AZO-4 (3%mol) in their bilayer in the dark (left) and during the irradiation at 365 nm (right) ([POPC]=62 μM, CF 50 mM, pH PBS 7.4).**

DLS measurements (*Table 4.4*) show that the presence of a lipophilic guest leads to an increase of the dimension of the vesicles and, moreover, the photoisomerization of azo units exerts a slight increase of their hydrodynamic diameter.

***Table 4.4*- Hydrodynamic diameter of POPC liposomes containing CF^{3-} in their core and AZO-4 (3%mol) in their bilayer.**

	Hydrodynamic dimeter (nm)
AZO-4_cis	163±14
AZO-4_trans	160± 10

It is interesting to observe that the stability of liposomes is highly affected by AZO-4 photoisomerization: in fact, during irradiation a huge increase of CF^{3-} fluorescence is observed for the irradiated sample, compared to that observed for the other one (*Figure 4.12*).

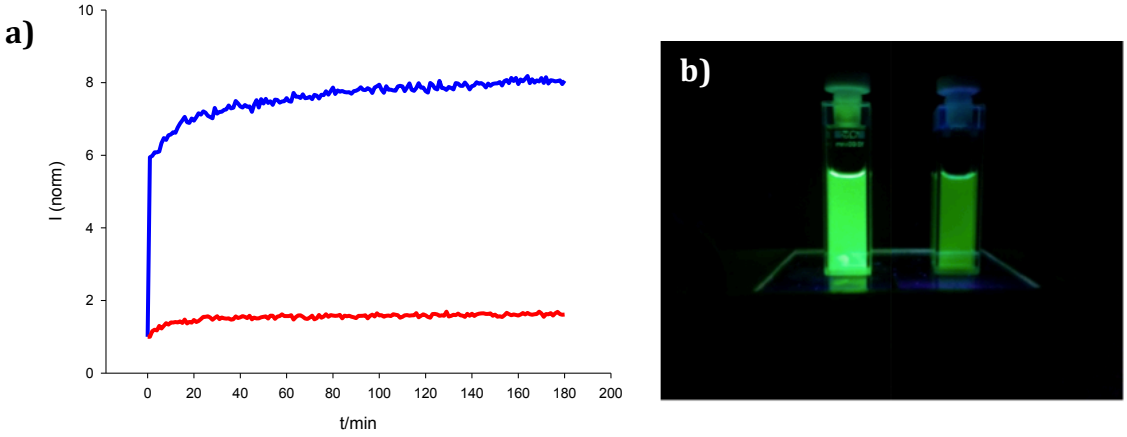

***Figure 4.12*- a) Time-dependent CF^{3-} fluorescence intensity of the irradiated sample (blue) and of that kept in the dark (red). b) Comparison of CF^{3-} emission of an irradiated sample (left) and one kept in the dark ([POPC]= 62 μM, CF 50 mM, pH PBS 7.4).**

In the case of the irradiated sample, a first-order kinetic model does not seem to be adequate in describing the first part of the kinetic curve. In this case, a stretched exponential decay best describes the obtained kinetic curve (*Figure 4.13*) and the associated constants are reported in *Table 4.5*.

This kinetic model describes many different phenomena, such as the kinetic behaviour of fluorophores in micelles, cyclodextrins, polymers, vesicles and membranes.[26] For example, it proved to describe properly the calcein release from POPC liposomes in the presence of PAMAM dendrimers[27] and proteins.[28] Generally, stretched exponentials are observed when leakage of liposomal content is not only due to an increase of vesicle permeability, but also in the presence of aggregation-related processes, even if DLS measurements do not show a significant change of vesicles' hydrodynamic radius after the irradiation.

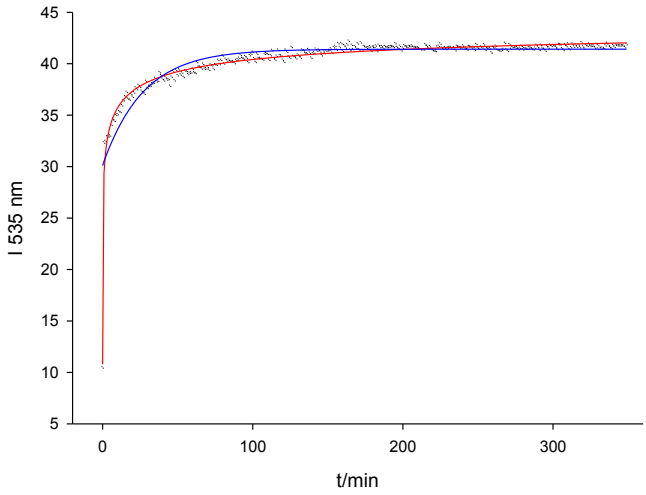

***Figure 4.13*- Kinetic profile of CF^{3-} photoinduced leakage from POPC vesicles containing AZO-4 (3mol%) after irradiation at 365 nm and fitting with a first-order kinetic model (blue) and stretched exponential model (red). ([POPC]=62 μM, CF 50 mM, pH PBS 7.4).**

***Table 4.5*- Kinetic constants for the photoinduced and spontaneous CF^{3-} release in the presence of AZO-4 (3%mol).**

	k (s^{-1})	**β**
AZO-4_cis	$5.22*10^{-1}\pm 5*10^{-3}$	$1.9*10^{-1}\pm 1.5*10^{-2}$
AZO-4_trans	$1.53*10^{-4}\pm 4.8*10^{-5}$	/

These results are more consistentwhen associated to the percentage of CF^{3-} released upon photoisomerization of AZO-4 and compared with that obtained after lysis of vesicles as a consequence of the addition of Trition X-100 (*Figure 4.14*).

This comparison highlightsthe strong impact that photoisomerization exerts on CF^{3-} relelase: in fact, after only 20 minutes of irradiation of POPC liposomes loaded with 3% mol. of AZO-4 there is a 70% release of the entrapped fluorescent dye.

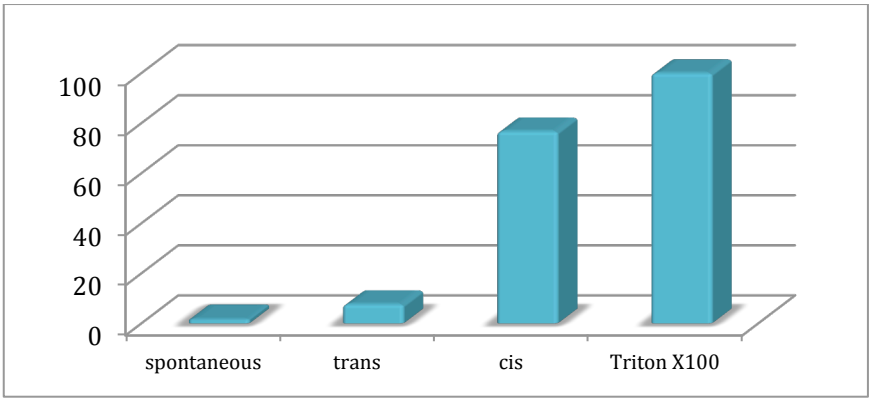

***Figure 4.14*- Percentage of spontaneous and induced CF^{3-} leakage from POPC liposomes (left) containing 3%mol of AZO-4 after 20 min in the dark (middle left), 20 min irradiation at 365 nm (middle right) and after the addition of Triton X-100 (right).**

Another useful parameter in order to get information about membrane permability and to get insights about the organization of liposomal membranes in the presence of an embedded guest is viscosity. The most used approach to determine microviscosity of liposomal membranes is based on the exploitation of the high lipophilicity of pyrene and its ability to form excimers.[29] Excimer formation implies a high mobility of the probe in the bilayer and this accounts for a low viscosity of the medium in which pyrene is dissolved. In general, the ratio of fluorescence intensity referred to the excimer (I_e, 480 nm) and that referred to the monomer (I_m, 395 nm) is used to quantify the translational diffusivity of the probe in the liposomal bilayer, which is inversely proportional to the microviscosity of the system.[30]

This technique assumes that the probe distributes exclusively in the phospholipid bilayer within the mixing time.

Emission spectra of POPC vesicles containing both *trans*-AZO-4 and increasing amounts of pyrene exhibit a gradual increase of the bands at 480 nm and 395 nm, whereas the sample made up by POPC liposomes containing both pyrene and *cis*-AZO-4 shows a slight increase of the band located at 480 nm and a steep increase of the band at 395 nm (*Figure 4.14*) and the corresponding values of the ratio I_e/I_m are listed in *Table 4.6*.

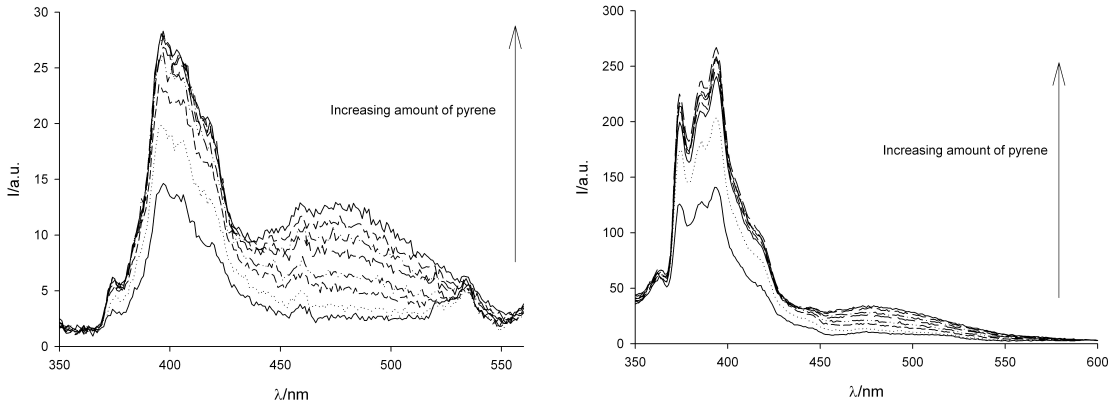

***Figure 4.14*-Emission spectra of POPC liposomes containing *trans*-AZO-4 (left) and *cis*-AZO-4 (right) in the presence of increasing amounts of pyrene.**

***Table 4.6*- I_e/I_m ratio value of liposomal membrane of POPC containing 3%mol of AZO-4 (*cis* and *trans* isomers)**

Liposome composition	I_E/I_M
POPC + *trans*-AZO-4	0.43± 0.01
POPC + *cis*-AZO-4	0.13± 0.01
POPC[31]	0.3

The comparison between microviscosity parameters referring to pure POPC liposomes and those containing both geometric isomers of AZO-4 allows to observe that the presence of both *trans*-AZO-4 and *cis*-AZO-4 influence bilayer viscosity: in particular, in the presence of the latter one, liposomal membrane increases dramatically its viscosity. This result can be explained in terms of a higher "compression" experienced by phospholipids as a consequence of the photoisomerization of the azo unit. This phenomenon reduces pyrene mobility within the phospholipid bilayer, thus making excimers formation more difficult. In this sense, this observation suggests that the bulky structure of *cis*-AZO-4 results in a great disturbance of membrane packing, leading to the creation of many local defects that are responsible for the efficient CF^{3-} leakage observed. In fact, it is well known that photoactive compounds bearing one azobenzene moiety behave as strong substitutional impurities in liposomal bilayers, especially when the are in the *cis* form: this is due to the change of their cross section upon photoisomerization and this is accompanied by a decrease in the phase transition temperature and enthalpy.[32]

The presence of *trans*-AZO-4, indeed, exerts a less pronounced effect on membrane microviscosity, but compared with the value reported in literature for pure POPC it is higher: this can be explained because the amphiphile's length is comparable to the bilayer thickness and, thus, the compound is able to span the bilayer once inserted, favouring the formation of pyrene excimers.

In order to get hints on organization of AZO-4 in POPC bilayers, zeta potential was measured and was compared with the value obtained for pure POPC liposomes (*Table 4.7*). Presence of AZO-4 determines a significant increase in the zeta potential value as a consequence of the increased positive charge on vesicles' surface. This confirms the hypothesis that AZO-4 spans the bilayer of POPC vesicles pointing its terminal ammonium units towards the aqueous external medium.

***Table 4.7*- Zeta potential of pure POPC liposomes and AZO-4 containing 3%mol POPC liposomes**

Liposome composition	ζ(mV)
POPC + *trans*-AZO-4	71.53 ± 2.96
POPC	- 2.74 ± 0.12

4.4 Entrapment of host-guest complexes in POPC vesicles

4.4.1 Introduction

Ion channels and transport proteins are the tool used by cells in order to translocate ions and charged species across their membranes. Mimicry of these natural ways of transmembrane transport consists in the membrane insertion of different species that are able both to interact with hydrophobic tails of phoshpolipids and to bind charged solutes in the aqueous compartment of cells.

Different macrocyclic compounds exhibit this dual behaviour, paving the way for the development of synthetic ion channels. Among them, cholaphanes,[33] calix[4]pyrroles[34] and calix[4]arenes bearing amide groups on their lower rim[35] showed a significant anionophoric activity in Cl^- transport, thus acting as artificial channels. Moreover, it could be interesting to develop artificial systems

whose activity is modulated by the application of external stimuli: for example, the change of substituents located on the lower rim of calix[4]arenes amide derivatives allows the pH-triggered efflux of Cl^- from liposomes.[35b]

Another useful scaffold in the design of artificial ion channels is represented by cyclodextrins and their derivatives. Their employment has two main advantages: first, cyclodextrins themselves[36] enhance membrane permeability towards small molecules and this can be ascribed to POPC inclusion in their cavity.[37]In addition, decoration of liposomal bilayer with these macrocycles allows to exploit their ability to form inclusion complexes with many molecules of biological interest, thus leading to the development of more sophisticated and specific drug delivery systems.

Functionalization of their primary side with pendant amino groups linked to polyether chains allows pH-selective transport of anions and cations,[38] whereas decoration of the same side[39] or of the secondary one[40] with azobenzene allows the photocontrolled vesicles' permeability towards ions and small molecules.

Moreover the transport activity of many different supramolecular systems, such as dendrimers[41] and rotaxanes,[42] has been explored, in order to deal with more complex systems whose molecular design can be adjusted according to the desired effect. The common feature of aforementioned systems is that they are embedded on the phospholipid bilayer or they interact with the external phosphate groups of liposomes: no one of them works being inserted in the internal aqueous compartment of liposomes. Two systems able to achieve faster efflux of small molecules from vesicles' interior exploit the formation of gases after decomposition of molecular species. In the first example, developed Chung *et al.* in 2012,[43] thermal decomposition of NH_4HCO_3led to formation ofCO_2 bubbles that are responsible for liposomal rupture and necrosis of cancer cells. Paret and co-workers followed the same approach, but in this case light was used as the external trigger in order to generate an overpressure of CO_2 and CO as a consequence of the degradation of photolabile 2-oxoacetates profragrances.[44]

In this paragraph, the photochemical activity of a photoactive [2]pseudorotaxane and its ability to change its stoichiometry upon light stimulation is presented.[45]

In particular, the photoactive axle (*Figure 4.15*) is made up by a 1-1'-disubstitutued-4,4'-bipyridinium (viologen) unit and two terminal azobenzene moieties and it is able to interact with cucurbit[7]uril (CB7).[46]

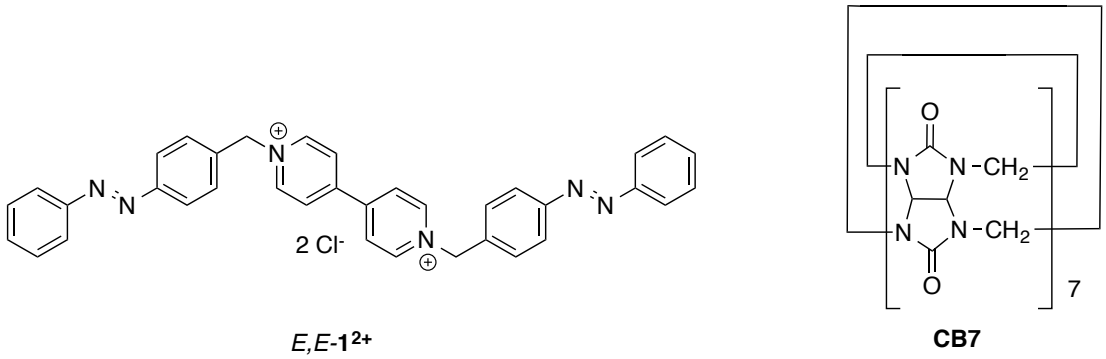

***Figure 4.15*-Structure of pseudorotaxane components.**

More specifically, it is able to switch from a [3]pseudorotaxane to a [2]pseudorotaxane upon photoisomerization of the azobenzene end units.
This supramolecular complex is potentially able to create an osmotic stress if inserted in a compartmentalized environment surrounded by a selective permeable membrane and, thus, it can be used in the development of drug delivery systems based on liposomes as nanocarriers.

4.4.2 Photophysical and photochemical characterization

The absorption spectrum of *E,E*-**1**$^{2+}$ reflects the main characteristics of chromophores present in the compound; an intense band at 332 nm and a weak one, both ascribable to π-π*and n- π*transitions of azobenzene, respectively.[22] In addition, the shoulder at 260 nm refers to the viologen unit.[47] Photoisomerization of azobenzene end units (*Figure 4.16*) yields *Z,Z*-**1**$^{2+}$ and spectral variations observed reflect the behaviour typically observed for azobenzene derivatives. Moreover, the persistence of isosbestic points during the irradiation suggest that the two photoactive units operate independently, allowing to assume that the behaviour of the *EZ* isomer with CB7 is similar to that of the *ZZ* species.

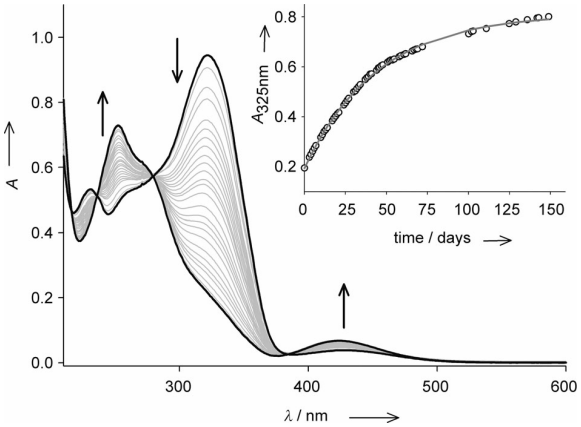

***Figure 4.16*-Absorption spectra of *E,E*-1^{2+} upon irradiation with 365 nm light. Inset: absorption changes at 352 nm associated with the thermal *Z*-*E* thermal reaction and fitting.**

Addition of CB7 to *E,E*-**1**$^{2+}$determines a decrease of the band referring to the viologen unit, coherently to what is usually described for viologen-CB7 complexes[46]; upon addition of an excess of the host, absorption decreases until a plateau is reached (*Figure 4.17*).

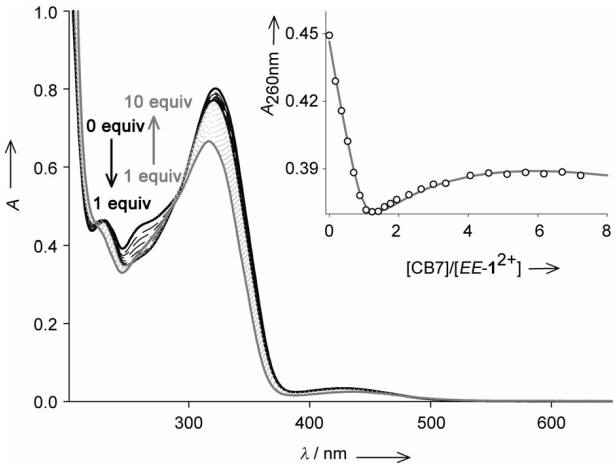

***Figure 4.17*-Absorption spectra of *E,E*-1^{2+} upon addition of CB7. Inset: absorption changes at 260 nm and fitting.**

This suggests the formation of a 1:1 complex, in which the macrocyclic host is located in the viologen unit, and a 1:2 adduct, in which the host moves around the phenylmethylene bridge of the terminal azo unit, pointing its carbonyl moieties toward the viologen unit (*Scheme 1*).

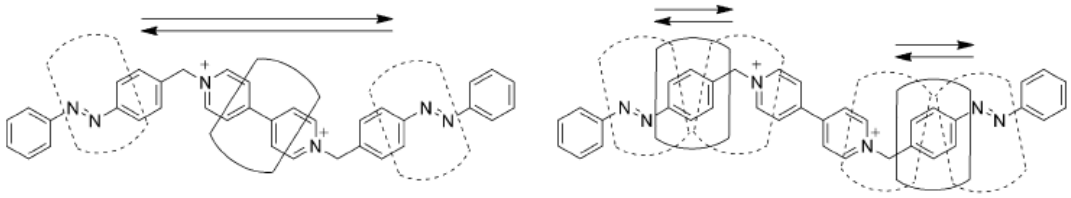

***Scheme 1*- Representation of the CB7 shuttling motion in *E,E*-1^{2+}@CB7 (left) and *E,E*-1^{2+}@2CB7 (right).**

This hypothesis is supported by observing the shift of proton signals referring to viologen and azobenzene moieties in the NMR spectrum of *E,E*-$\mathbf{1}^{2+}$ upon addition of CB7.

In contrast, titration of *Z,Z*-$\mathbf{1}^{2+}$ with CB7 determines a decrease of the absorption band referring to viologen unit (*Figure 4.18*), but in this case the formation of a 1:1 complex occurs.

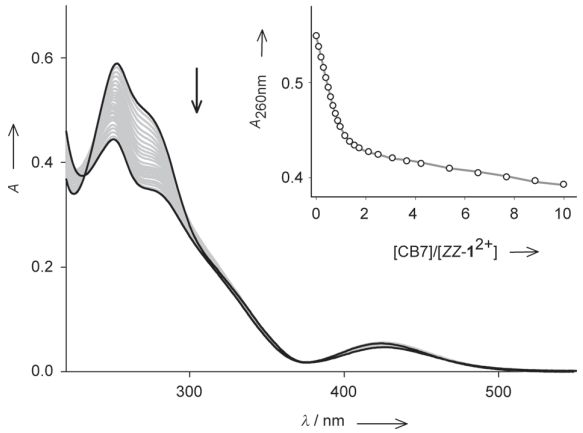

***Figure 4.18*-Absorption spectra of *Z,Z*-1^{2+} upon addition of CB7. Inset: absorption changes at 260 nm and fitting.**

This supramolecular species is the same obtained after irradiation of the 1:2 adduct formed by *E,E*-$\mathbf{1}^{2+}$ and CB7, as confirmed by superimposition of their absorption spectra (*Figure 4.19*).

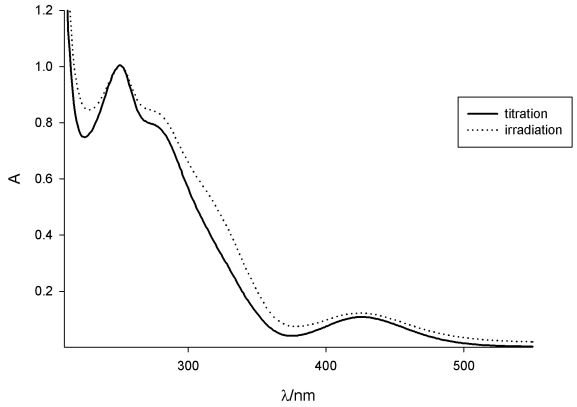

***Figure 4.19*- Comparison between absorption spectrum of *Z,Z*-$\mathbf{1}^{2+}$@2CB7obtained at the end of titration of *Z,Z*-$\mathbf{1}^{2+}$ with CB7 (straight line) and that obtained by irradiating*E,E*-$\mathbf{1}^{2+}$@2CB7 with 365 nm light (dotted line).**

In addition to controlled assembly/disassembly, this system is able to tune the concentration of solutes in solution by means of light inputs. Its insertion in closed system and its disassembly can afford an osmotic stress, [48] if the system is separated from the external medium by a selective permeable membrane.

Liposomes represent the most adequate scaffold, since the phospholipid bilayer acts as selective permeable membrane, allowing to work in aqueous solution.

In this regard, *E,E*-$\mathbf{1}^{2+}$@2CB7 was inserted in the aqueous core of POPC liposomes and irradiated in order to switch to a [2]pseudorotaxane with concomitant release of a CB7 molecule.

Absorption spectrum of the liposomal suspension shows a shoulder located between 300 and 350 nm, which can be assigned to the filamentary component having both azobenzene units with the *E* configuration and irradiation of liposomal suspension leads to spectral variations that are consistent with those observed for the same species in aqueous solution (*Figure 4.20*) without changing their dimension significantly (*Table 4.7*).

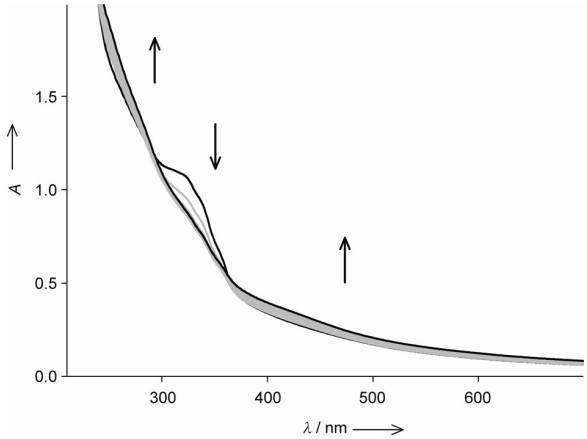

***Figure 4.20*-Absorption spectra of a liposomal suspension containing *E,E*-1^{2+}@2CB7in its aqueous core upon irradiation at 365 nm.**

***Table 4.7*-Hydrodynamic diameter of POPC liposomes containing *E,E*-1^{2+}@2CB7 in thei aqueous interior and kept in the dark and irradiated at 365 nm .**

	0 min.	**165 min.**
POPC + *E,E-**1**$^{2+}$@2CB7*	102.75 ± 0.55	102.63 ± 1.00
POPC + *Z,Z-**1**$^{2+}$@CB7*	97.13 ± 0.38	99.00 ± 0.16

Unfortunately, scattering of liposomal suspension does not allow an accurate estimation of the efficiency of the process and spectroscopic changes suggest that the *E-Z* conversion proceeds to a lower extent.

4.5 Conclusion

Azobenzene photochromism has been extensively exploited in order to design and develop nanoscale objects able to give rise to complex architectures and able to perform different activities using only light as fuel.

Moreover, azobenzene derivatives are largely employed in the development of drug delivery systems based on liposomes as biocompatible nanocarriers: in fact, photoisomerization of pure azobenzene results in a faster efflux of small molecules from vesicles. This suggested the incorporation, in the phospholipid bilayer of liposomes, of photoactive phospholipids, polymers and amphiphiles containing the azobenzene moiety in order to achieve the photocontrolled leakage of their content.

In particular, separation of azobenzene units in polyazobenzene derivatives represents an essential condition for their photoreactivity; in this way, keeping

in mind that the photoisomerization of one azobenzene exerts a destabilizing effect on liposomal membranes, the presence of more photochromic units leads to a fast and efficient leakage of vesicles' contents. Separation of azobenzene units is not the only prerequisite to realize this purpose: in fact, the presence of positively charged end groups helps the self-assembly of the photoactive azobenzene derivative and phospholipids.

In the end, insertion in the liposomal core of photoactive supramolecular systems able to modify the concentration of solutes in solution, allows to explore the possibility to develop biocompatible nanoscale containers that release their contents as a consequence of a photoinduced osmotic stress.

References and notes

The contents of par 4.4 are based on Baroncini, M.; Gao, C.; Carboni, V.; Credi, A.; Previtera, E.; Semeraro, M.; Venturi, M.; Silvi, S., *Chem. Eur. J.*, **2014**, 20, 34, 10737-10744. - Reproduced with permission by John Wiley and Sons.

[1] a) Mills, J.K.; Needham, D., *Biochim. Biophys. Acta,***2005**, 1716, 77-96.
b) Hollmann, A.; Delfederico, l.; Glikmann, G.; De Antoni, G.; Semorile, L.; Disalvo, E.A., *Biochim. Biophys. Acta,***2007**, 1768, 393-400.
c) Bhattacharaya, S.; Haldar, S., *Biochim. Biophys. Acta,***2000**, 1467, 39-53.

[2] Cohen-Kashi, M.; Deutsch, M.; Tirosh, R.; Rachmani, H.; Weinreb, A., *Spectrochim. Acta A*, **1997**, 53, 1655-1661.

[3] Aschi, M.; D'Archivio, A.; Fontana, A.; Formiglio, A., *J. Org. Chem.*, **2008**, 73, 3411-3417.

[4] Chen, R.; Knutson, J.R., *Anal.Biochem.*,**1988**, 172, 61-77.

[5] Weinstein, J.N.; Yoshikami, S.; Henkart, P.; Blumenthal, Hagins, W.A., *Science*, **1977**, 195, 489-491.

[6] Kohlrausch, R., *Annalen der Phys. und Chim.*,**1854**, 91, 56-82, 179-213.

[7] William, G.; Watts, D.C., *Trans. of the Faraday Soc.*, **1970**, 66, 80-85.

[8] Berberan-Santos, M.N.; Bodunov, E.N.; Valeur, B., *Chem. Phys.*, **2005**, 315, 171-182 and references therein.

[9] Koley, D.; Bard, A.J., *Proc. Nat. Ac. Sci.*, **2010**, 107, 39, 16783-16787.

[10] Nojima, Y.; Iwata, K., *J. Phys. Chem. B*, **2014**, 118-8631-8641.

[11] Rau, H.; Lüddeke, E., *J. Am. Chem. Soc.*, **1982**, 104, 1616-1620.

[12] a) Yu. Y.L.; Nakano, M.; Ikeda, T., *Nature*, **2003**, 425, 145-145. b) Harris, K.D.; Cuypers, R.; Scheibe, P.; Van Oosten, C.L.; Bastiaansen, C.W.M.; Lub, J.; Broer, D.J., *J. Mater. Chem.*, **2005**, 15, 5043-5048.

[13] Bléger, D.; Liebig, T.; Thiermann, R.; Maskos, M.; Rube, J.P.; Hecht, S., *Angew. Chem. Int. Ed.*, **2011**, 50, 12559-12563.

[14] Cisnetti, F.; Ballardini, R.; Credi, A.; Gandolfi, M.T.; Masiero, S.; Negri, F.; Pieraccini, S.; Spada, G.P., *Chem.Eur. J.*, **2004**, 10-2011-2021.

[15] a) Venkatamaran, L.; Klare, J.E.; Nuckolls, C.; Hybertsen, M.S.; Steigerwald, M.L., *Nature*, **2006**, 442, 904-907. b) Vonlanthen, D.; Mischenko, A.; Elbing,

M.; Neuburger, M.; Wandlowski, T.; Mayor, M., *Angew. Chem. Int. Ed.*, **2009**, 48, 8886-8890.

[16] Bléger, D.; Dokić, J.; Peters, M.V.; Grubert, L.; Saalfrank, P.; Hecht, S., *J. Phys. Chem. B*, **2011**, 115, 9930-9940.

[17] Kučerka, N.; Nieh, M.-P.; Katsaras, J., *Biochim. Biophys. Acta*, **2011**, 1808, 2761-2771.

[18] a) Liu, X.-M.; Yang, B.; Wang, Y.-L.; Wang, J.-Y., *Biochim. Biophys. Acta*, **2005**, 1720, 28-34. b) Liu, X.-M.; Yang, B.; Wang, Y.-L.; Wang, J.-Y., *Chem. Mater.*, **2005**, 17, 2792-2795.

[19] a) Sebai, S.C.; Cribier, S.; Karimi, A.; Massotte, D.; Tribet, C., *Langmuir*, **2010**, 26, 1435-1441. b) Sebai, S.C.; Milioni, D.; Walrant, A.; Alves, I.D.; Sagan, S.; Huin, C.; Auvray, L.; Massotte, D.; Cribier, S.; Tribet, C., *Angew. Chem. Int. Ed.*, **2012**, 51, 2132-2136.

[20] a) Song, X.; Perlstein, J.; Whitten, D.G., *J. Am. Chem. Soc.*, **1997**, 119, 9144-9159. b) Bisby, R.H.; Mead, C.; Morgan, C.G., *Photochem. Photobiol.*,**2000**, 72, 57-61. c) Bisby, R.H.; Mead, C.; Morgan, C.G., *Biomed. Biophys. Res. Comm.*, **2000**, 276, 169-173.

[21] a) Kano, K.; Tanaka, Y.; Ogawa, T.; Shimomura, M.; Kunitake, T., *Photochem. Photobiol.*,**1981**, 34, 323-329. b) Sakai, H.; Matsumura, A.; Yokoyama, S.; Saji, T.; Abe, M., *J. Phys. Chem. B*, **1999**, 103, 10737-10740.

[22] Dürr, H.; Bousas-Laurent, H, *Photochromism-Molecules and systems*, Elsevier: Amsterdam, **2003**.

[23] a) Yamamoto, S; Nishimura, N.; Hasegawa, S., *Bulletin Chem. Soc. Japan*, **1971**, 44, 2018-2025. b) Gore, P.E.; Wheeler, O.H., *J.Org. Chem.*, **1961**, 26, 3295-3298. c) Gore, P.E.; Wheeler, O.H., *J. Am. Chem. Soc.*, **1956**, 78, 2160-2163.

[24] Bandara, H.M.D.; Burdette, S.C.; *Chem. Soc. Rev.*, **2012**, 41, 1809-1825.

[25] For the determination of the real concentration of guest, see Ref. 7.

[26] Berberan-Santos, M.N.; Bodunov, E.N.; Valeur, B.; *Chem. Phys.*, **2005**, 315, 171-182 and references therein.

[27] a) Evans, K.O.; Laszlo, J.A.; Compton, D.L.; *Biochim. Biophys. Acta*, **2014**, 1838,445-455. b) Karoonuthaishiri, N.; Titiyevskiy, K.; Thomas, J.L.; *Coll. Surf. B*,**2003**, 27, 365-375.

[28] Sepcic, K. *et al.*; *FEBS Letters*, **2004**, 575, 81-85.

[29] a) Pownall, H.J.; Smith, L.C.; *J. Am. Chem. Soc.*, **1973**, 95, 3136. b) Galla, H.-J.; Sackmann, E.; *Biochim.Biophys.Acta*, **1974**, 339, 103-115.

[30] a) Vanderkooi, J.M.; Callis, J.B.; *Biochemistry*, **1974**, 13, 4000-4006. b) Han, S.K.; Lee, Y.-S.; Kim, M.; *Arch. Pharm. Res.*, **1990**, 13, 192-197.

[31] De Maria, P.; Fontana A.; Gasbarri, C.; Velluto, D., *Soft Matter*, **2006**, 2, 595-602.

[32] Kuiper, J.M.; Stuart, M.C.A.; Engberts, J.B.F.N., *Langmuir*, **2008**, 24, 2, 426-432.

[33] Judd, L.W.; Davis, A.P., *Chem. Comm.*, **2010**, 46, 2227-2229.

[34] Tong, C.C.; Quesada, R.; Sessler, J.L.; Gale, P.A., *Chem. Comm.*, **2008**, 6321 6323.

[35] a) Sidorov, V.; Kotch, F.W.; Abdrakhmanova, G.; Mizani, R.; Fettinger, J.C.; Davis, J.T., *J. Am. Chem. Soc.*, **2002**, 124, 2267-2278. b) Okunola, O.A.; Seganish, J.L.; Salimian, K.J.; Zavalij, P.Y.; Davis, J.T., *Tetrahedron*, **2007**, 63, 44, 10743-10750. c) Seganish, J.L.; Santacroce, P.V.; Salimian, K.J.; Fettinger, J.C.; Zavalij, P.Y.; Davis, J.T., *Angew. Chem. Int. Ed.*, **2006**, 45, 20, 3334-3338.

[36] Gasbarri, C.; Guernelli, S.; Boncompagni, S.; Angelini, G.; Siani, G.; De Maria, P.; Fontana A., *J.Lip. Res.*, **2010**, 20, 3, 202-210.

[37] a) Irie, T.; Fukunaga, K.; Pitha, J., *J. Pharma. Sci.*, **1992**, 81, 521-523. b)Puskás, I.; Csempesz, F., *Coll. Surf. B Biointerf.*,**2007**, 58, 518-524.

[38] Madhavan, N.; Robert, E.C.; Gin, M.S., *Angew. Chem. Int. Ed.*, **2005**, 44, 46, 7584-7587.

[39] Jog, P.V.; Gin, M.S., *Org. Lett.*,**2008**, 10, 17, 3693-3696.

[40] Kauscher, U.; Samanta, A.; Ravoo, J.B., *Org. Biomol.Chem.*,**2014**, 12, 600-606.

[41] Suzuki, Y.; Okuro, K.; Takeuchi, T.; Aida, T., *J. Am. Chem. Soc.*, **2012**, 134, 15273-15276.

[42] Dvornikovs, V.; House, B.E.; Kaetzel, M.; Dedman, J.R.; Smithrud, D.B., *J. Am. Chem. Soc.*, **2003**, 125, 8290-8301.

[43] Chung, M.-F.; Chen, K.-J.; Liang, H.-F.; Liao, Z.-X.; Chia, W.-E.; Xia, Y.; Sung, H. W., *Angew. Chem. Int. Ed.*, **2012**, 51, 10089-10093.

[44] Paret, N.; Trachsel, A.; Berthier, D.L.; Herrmann, A., *Agew. Chem. Int. Ed.*, **2015**, 54, 7, 2275-2279.

[45] Baroncini, M.; Gao, C.; Carboni, V.; Credi, A.; Previtera, E.; Semeraro, M.; Venturi, M.; Silvi, S., *Chem.Eur. J.*, **2014**, 20, 34, 10737-10744.

[46] Ong, W.; Gómez-Kaifer, M; Kaifer, A.E., *Org. Lett.*,**2002**, 4,10, 1791-1794.

[47] Monk, P.K., *The viologens: physicochemical properties, synthesis and applications of the salts of 4-4'-bipyridine;* Wiley: New York, **1998**.

[48] Ménager, C.; Cabuil, V., *J. Phys. Chem. B*, **2002**, 106, 32, 7916-7918.

Chapter 5

Photoinduced transport of anions across liposomal membranes

5.1 Introduction

Anions are involved in many processes that are crucial for cell survival: in fact, they are implicated in cellular pH and electrochemical potential regulation, keep osmotic balance and cell volume and they participate in cellular signalling processes. Passive diffusion of charged solutes through biological membranes is not allowed and proceeds through proteins and other compounds that act as transmembrane carriers or channels (*Figure 5.1*).

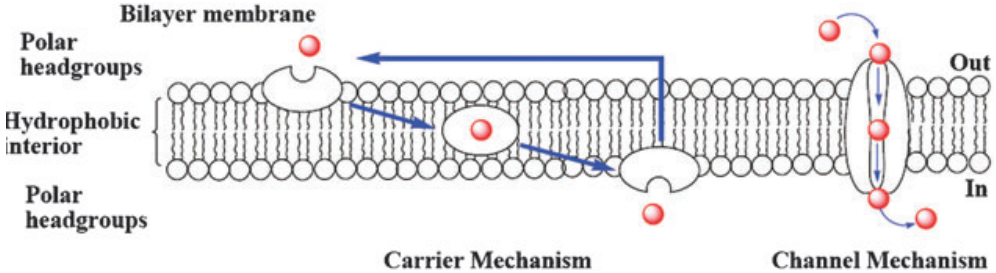

***Figure 5.1*-Mechanisms of ion transport across biological membranes. Reproduced with permission from *Chem. Soc. Rev,* 2010, 39, 3843-3862.© 2010 Royal Society of Chemistry.**

Moreover, it was found that defects in transmembrane transport of anions are involved in the appearance of various diseases [1], such as Dent's disease, osteoporosis and cystic fibrosis.[2]

Therefore, the development of synthetic species able to mimic naturally occurring transport proteins allows to compensate deficiencies in anion transport that are responsible for the onset of aforementioned diseases.

Artificial transmembrane channels and carriers[3] are supramolecular assemblies that enable the passage of ions by exploiting weak interactions, such as hydrogen bond[4], π-anion[5] and π-cation.[6]

Among all supramolecular systems described in literature, it has been found that the imidazolium cation motif is able to induce anion transport across a biomembrane[7] in a highly efficient manner and this has lead to the development of selective and valuable antimicrobial agents.[8]

Moreover, the biocompatibility of the imidazole moiety makes it a useful structural motif for biomimetic applications,[9] since it undergoes self-organized and ordered supramolecular structures by means of hydrogen bonding. Imidazolium salts constitute a versatile class of anion transporters since it is possible to modulate their anionophoric activity by means of formation of inclusion complexes with different macrocycles, such as CB7 and α-cyclodextrin.[10] Moreover, the mechanism of anion efflux from vesicles is strictly related to molecular structure of ionophores: the presence of 4-ethynylbenzyl substituents on imidazolium cation infers structural rigidity, resulting in the formation of transmembrane channels as a consequence of π–π interactions[7a] and transport of anions is ensured by π-anion interactions. On the other hand, the presence of less rigid structures due to other substituents, such as adamantyl units,[11] avoids self-aggregation and formation of transmembrane channels, thus yielding a more flexible structure that is able to move within the biomembrane, acting as a mobile anion transporter.

In this Chapter, the synthesis of a photoactive anion transporter and preliminary results referring to photoinduced chloride transport from EYPC liposomes are presented. This work has been performed during a resaerch stay in the laboratory of Prof. A. Schmitzer, Université de Montréal, Montréal, Quebéc,

(Canada).

5.2 Retrosynthetic analysis

With the aim join the known anionophoric activity of imidazolium salts and the ability of azobenzene in the translocation of small molecules across biomembranes and Cl^- anions exhibited by anion transporters bearing an azobenzene spacer unit in their molecular structure,[12] the photoactive compound **8** (*Figure 5.1*) was synthesized.

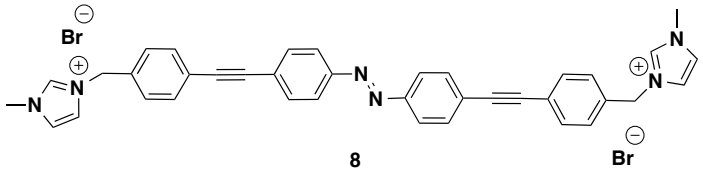

***Figure 5.1*-Structure of photoactive anion transporter.**

The retrosynthetic analysis of **8** provides two different synthetic approaches in order to get the target compound (*Figure 5.2*).

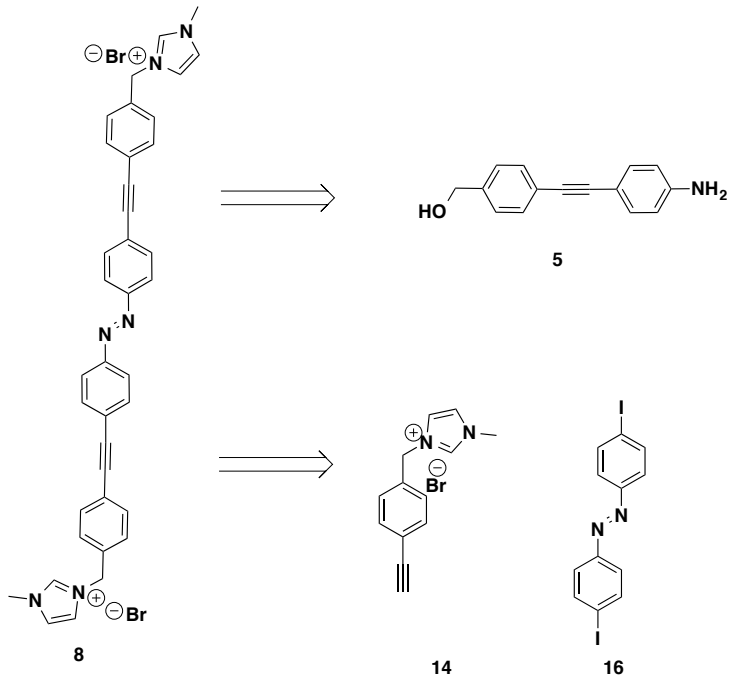

***Figure 5.2*-Retrosynthetic analysis and identified synthons.**

For the retrosynthetic analysis of the final compound, it is possible to identify three different synthons:

a) 4-((4-(hydroxymethyl)phenyl)ethynyl)aniline (**5**), resulting from cleavage of the double bond of the azobenzene core;
b) 3-(4-ethynylbenzyl)-1-methyl-1H-imidazol-3-ium bromide (**14**) and *p*-diiodoazobenzene (**16**), by disconnecting the 4-ethynylbenzyl moiety.

The first synthetic strategy envisages the synthesis of 4-((4-(hydroxymethyl)phenyl)ethynyl)aniline (**5**) and its dimerization to get the corresponding azobenzene derivative (**6**). Synthesis[10] of **5** starts from reduction of 4-iodobenzoic acid to afford the corresponding alcohol (**2**). Then, Sonogashira coupling between **2** and Boc-protected 4-ethynylanyline[13] (**3**) yields **4**. The choice of *tert*-butoxycarbonyl protecting group for the amine was not trivial, since other amine protecting groups, such as acetyl group, proved to require too harsh conditions for their cleavage, affecting yield and purity of the resulting compound. Deprotection[14] of **4** and dimerization[15] afforded the corresponding azobenzene derivative **6**, which reacted with PBr_3 to give dibromide **7**. Reaction with 1-methylimidazole afforded the target compound (*Figure 5.3*).

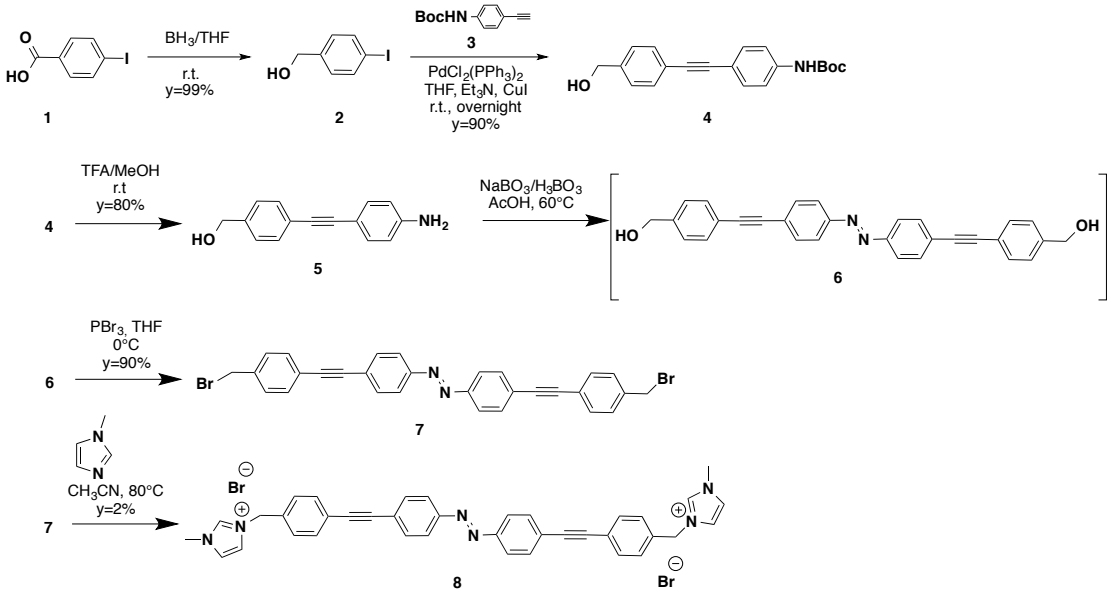

***Figure 5.3*-Proposed synthetic strategy.**

Another possibility (*Figure 5.4*) lies on a Sonogashira coupling between 3-(4-ethynylbenzyl)-1-methyl-1H-imidazol-3-ium bromide (**14**) and *p*-diiodoazobenzene (**16**). The synthesis[16] for **14** starts from Sonogashira

coupling between 4-iodotoluene (**9**) and trimethylsilylacetylene (**10**). Then, selective bromination of the benzylic position of **11** affords **12** and deprotection[17] yields the corresponding phenylacetylene (**13**). In parallel, oxidative dimerization of 4-iodoaniline (**15**) allows to isolate 4-diiodoazobenzene **16**.[18]

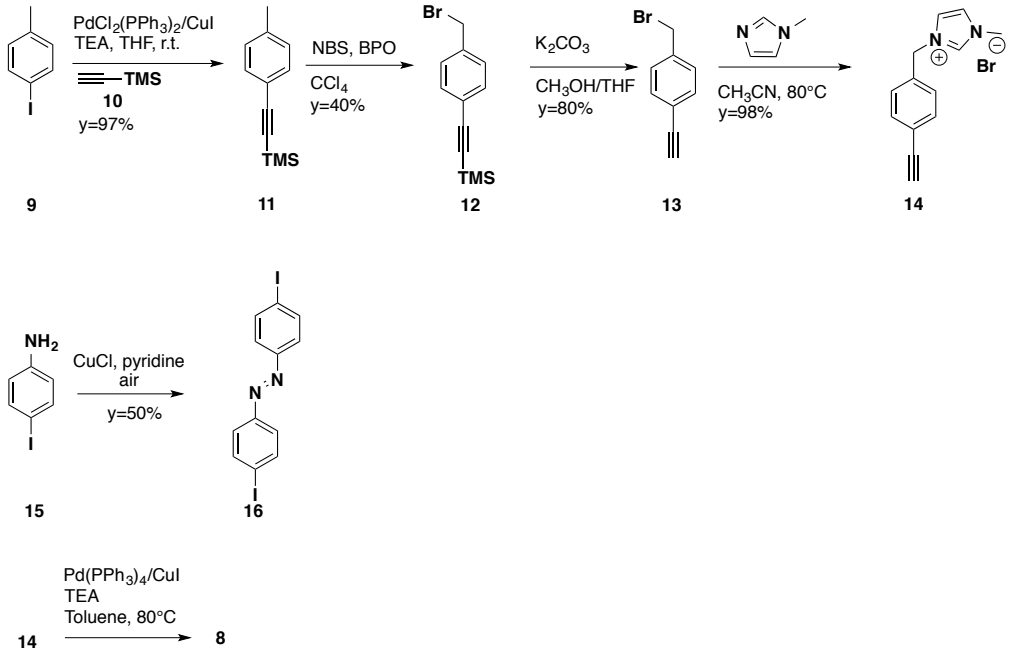

***Figure 5.4*- Proposed synthetic strategy.**

Sonogashira coupling between **16** and **14** did not afford the target compound and another possibility to get **8** could be to perform the Pd-catalyzed coupling on brominated compound **13** and then convert the obtained product to the corresponding imidazolium bromide at the end, but also in this case the product resulting from Sonogashira coupling could not be isolated.

5.3 Photoinduced chloride efflux from EYPC liposomes

The absorption spectrum of **8** (*Figure 5.5*) shows absorption maximum located at 372 nm and this band is assigned to π-π* electronic transitions of the azobenzene moiety. Meanwhile, characteristic azobenzene bands are no longer distinguishable and are overlapped by π-π* bands.

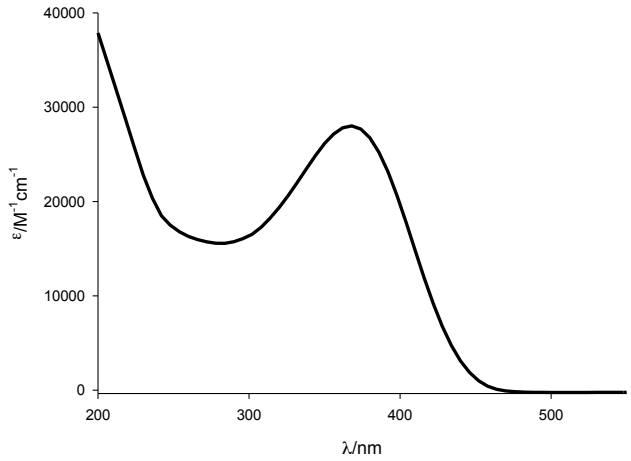

***Figure 5.5*- Absorption spectrum of an air equilibrated solution of 8 in CH_3OH.**

For this compound, no emission was detected and irradiation at 365 nm resulted in absorption changes that are consistent with *trans-cis* photoisomerization that occurs for this class of compounds,[19] as depicted in *Figure 5.6*.

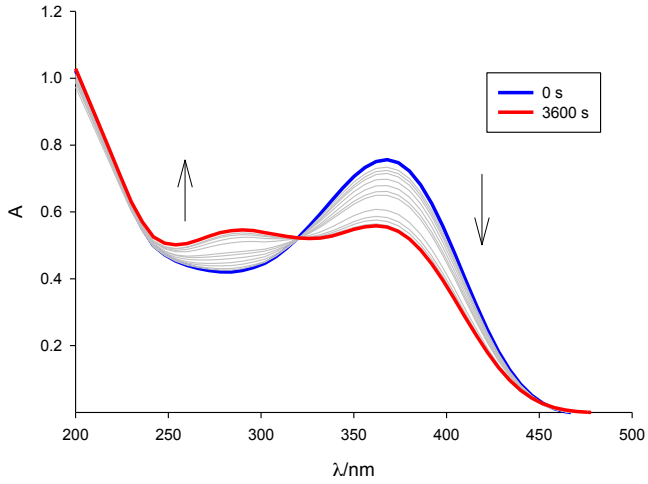

***Figure 5.6*- Time dependent changes in the absorption spectrum of 8 upon irradiation at 365 nm.**

By observing spectral variations recorded during the irradiation, it is possible to observe a decrease of the band at 372 nm and an increase of the one located at 290 nm. Moreover, the presence of isosbestic points at 320 and 450 nm can be observed.

Lucigenin assays allow to test the anionophoric activity of **8**. In fact, lucigenin experiences a quenching of its fluorescence in the presence of halides as a consequence of the formation of a charge-transfer complex.[20]

Addition of 10% mol. of **8** to lucigenin/Cl^-loaded EYPC liposomes results in a slight increase of lucigenin fluorescence. Irradiation at 365 nm affords to an almost total Cl^- leakage from vesicles (*Figure 5.7*), as a consequence of azobenzene photoisomerization. In order to state that photoisomerization of the azobenzene core is essential for fast and efficient Cl^- transport, the same kinetic was recorder on lucigenin/Cl^- loaded EYPC liposomes without adding **8**.

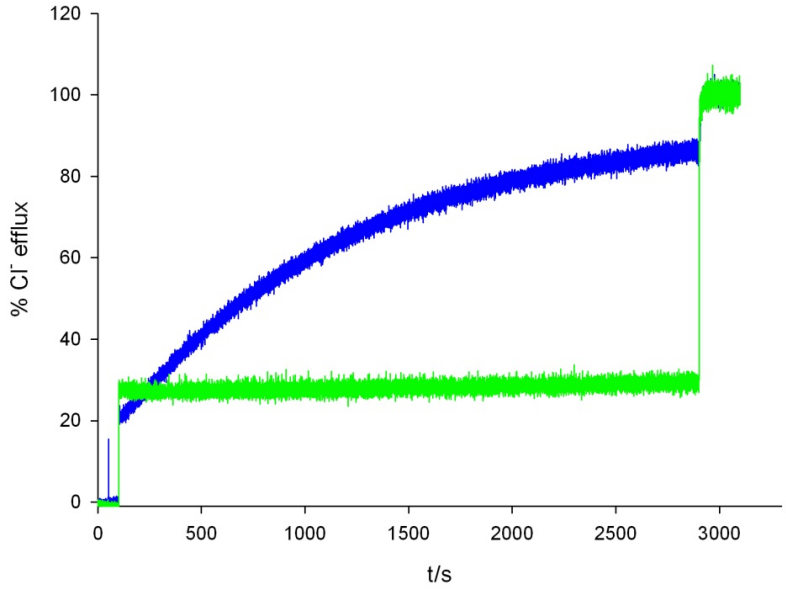

***Figure 5.7*-Comparison of chloride transport activity in lucigenin/Cl^- loaded EYPC liposomes in the presence of 8 (blue) and without 8 (green). Injection of 8, irradiation at 365 nm and Triton X100 addition were performed at 50, 100 and 2900 s, respectively. Intravesicular: lucigenin 2mM, 10 mM phosphate buffer (pH=6.2), NaCl 100 mM. Extravesicular: 100 mM $NaNO_3$, 10 mM phosphate buffer (pH=6.4).**

In the absence of **8**, no spontaneous leakage of Cl^- nor massive increase in percentage of Cl^- efflux occurred in the absence of **8**, upon addition of this ionophore in its *trans* form, confirming the essential role exerted by photoisomerization of the azobenzene moiety in anion transport.

5.4 Conclusion and Perspectives

Multifunctional systems are molecular architectures composed of different units able to perform different operations by joining the ability of their single constituting units, leading to the development of complex and sophisticated systems.

In this Chapter, the design, synthesis and anionophoric activity of a photoactive anion carrier are presented. This molecular specie joins the known anionophoric activity of imidazolium cations and the photoreactivity of the azobenzene photochromic unit for the transport of anions across biomembranes. Moreover, it could be potentially able to transport small molecules from the aqueous interior of vesicles to the external medium in which they are dispersed.

In this direction, the mechanism of transport has to be elucidated and its ability in the transport of small molecules has to be tested. Moreover, it could be interesting to compare the activity of both geometric isomers in the transport of ions and small molecules from liposomes.

References

[1] a) Jentsch, T.J.; Hubner, C.A.; Fuhrmann, J.C., *Nature Cell Biol.*, **2004**, 6, 1039-1047. b) Cordat, E.; Casey, J.R., *Biochem. J.,***2009**, 417, 423-439.

[2] a) Eggermont, J.,*Proc. Am. Thorac. Soc.*, **2004**, 1, 22–27. b) Gadsby, D.C.; Vergani, P.; Csanádi, L., *Nature*, **2006**, 440, 477-483.

[3] a) Davis, J.T. *et al*., *Chem.Soc.Rev*, **2010**, 3843-3862. b) Gale, P.A. *et al.*, *Angew. Chem. Int. Ed.*, **2013**, 52, 1374-1382.

[4] a) Jentzsch, A. V.; Emery, D.; Mareda, J.; Nayak, S. K.; Metrangolo, P.; Resnati, G.;Sakai, N.; Matile,S.,*Nat. Commun.*,**2012**, 3, 905–913.b)Gale, P. A.; Busschaert,N.; Haynes,C. J. E.; Karagiannidis, L. E.; Kirby, I. L.,*Chem. Soc. Rev.*, **2014**, 43, 205–241. c) Haynes, C. J. E.; Busschaert, N.; Kirby, I. L.; Herniman,J.; Light,M. E.; Wells, N. J.; Marques, I.; Felix, V.; Gale,P. A., *Org. Biomol. Chem.*, **2014**, 12, 62–72.

[5] a) Dawson, R. E.; Hennig, A.; Weimann, D. P.; Emery, D.; Ravikumar, V.; Montenegro, J.; Takeuchi, T.; Gabutti, S.; Mayor, M.; Mareda, J.; Schalley, C. A.; Matile, S., *Nat. Chem.*, **2010**, 2, 533–538. b) Frontera, A.; Gamez, P.; Mascal, M.; Mooibroek, T. J.; Reedjik, J., *Angew. Chem. Int. Ed.*, **2011**, 50, 9564–9583. c) Salonen, L. M.; Ellermann, M.; Diederich, F., *Angew. Chem. Int. Ed.*, **2011**, 50, 4808–4842. d) Chifotides, H. T.; Dunbar, K.R., *Acc. Chem. Res.*, **2013**, 46, 894–906.

[6] Mareda, J.; Matile, S., *Chemistry*, **2009**, 15, 28–37.

[7] a) Elie, C-R.; Charbonneau, M.; Schmitzer, A.R., *Med. Chem. Comm.*, **2012**, 3, 1231-1234.b) Elie, C.-R.; Hébert, A.; Charbonneau, M.; Haiun, A.;Schmitzer, A.R., *Org. Biomol. Chem.*, **2013**, 11, 923-928.

[8] Vidal, M.; Elie, C-R.; Campbell, S.; Claing, A.; Schmitzer, A.R., *Med. Chem. Comm.*, **2014**, 5, 436-440.

[9] Anderson, E.B.; Long, T.E., *Polymer*, **2010**, 51, 2447-2454.

[10] Elie, C-R.; Noujeim, N.; Pardin, C.; Schmitzer, A.R., *Med.Chem. Comm.*, **2011**, 47,1788-1790.

[11] Gravel, J.; Schmitzer, A.R., *Supramol. Chem.*, **2014**, 26, 1-9. (DOI: 10.1080/10610278.2014.969265)

[12] Choi, Y.R.; Kim, G.C.; Jeon, H.-G.; Park, J.; Namkung, W.; Jeon, K.-S., *Chem.*

Comm., **2014**, 50, 15305-15308.

[13] Godínez Sánchez, J.; Fomina, L.; Rumsh, L., *Polym. Bull.*,**2010**, 64, 8, 761-770.

[14] Shendage, D.M.; Frölich, R.; Haufe, G., *Org. Lett.*,**2004**, 6, 21, 3675-3678.

[15] Santurri, P.; Robbins, F.; Stubbings, R., *Org. Synth.*,**1960**, 40, 18-20.

[16] Kawamura, H.; Takeyama, Y.; Yamamoto, M.; Kurihara, H.; Morino, K.; Yashima, E., *Chirality*, **2011**, 23, E35-E42.

[17] Zdobinsky, T.; Maiti, S.P.; Klajn, R., *J. Am. Chem. Soc.*,**2014**, 136, 7, 2711 2714.

[18] Strueben, J.; Gates, P.J.; Staubitz, A., *J. Org. Chem.*, **2014**, 79, 1719-1728.

[19] Liu, R.; Xiao, Q.; Li, H.; Chen, H.; Yan, Z.; Zhu, H., Zhu, H., *Dyes and Pigm.*, **2011**, 92, 626-632.

[20] Legg, K.D., Hercules, D.M.; *J. Phys. Chem.,* **1970**, 74, 2114.

Chapter 6

Conjugated oligoazobenzenes in the development of organic solar cells

6.1 Introduction

Artificial channels consist in rigid structures involved in the active transport of charged species that are usually repelled by phospholipid bilayer of cell membrane. Mimicry of these proteins involves the synthesis of compounds bearing rigid cores, such as biphenyl[1], triphenylbenzymidazole[2], naphtalenediimide[3] and perylenediimide[4] cores, that resulted in efficient transport of anions across liposomal membranes, by means of π-anion interactions. In theory, organic compounds bearing conjugated azobenzene moieties possess a rigid structure and could be embedded in liposomal membranes: in this sense, transport of ions or small molecules could occur as a consequence of light interaction, avoiding the use of chemical fuels in order to supply the stimulus required for their transport.

Moreover, since polyazobenzene derivatives having electronically separated azobenzene units resulted in an efficient leakage of liposomal contents (see

chapter 4), it would be interesting to compare their activity with the one of their *p*-conjugated counterparts. Unfortunately, this was not possible, since direct *p*-conjugation of azobenzene units results in a suppression of the photochemical activity.[5]Linking of azobenzene moieties through meta connections reduces electronic coupling, allowing the partial recovery of photoreactivity at the expense of structure linearity, which represents the main prerequisite in artificial channel development.

As noted in Chapter 4, separation of photochromic units allows the total recovery of photoreactivity, leading to molecular architectures composed by many azobenzene units that operate independently.[6]

The molecular structure of *p*-conjugated oligoazobenzene derivatives resembles the one of oligo(*p*-phenylenevinylene) (PPV) derivatives, so that oligoazobenzene can be considered the azo-analogue of this latter family of organic compounds.[7]

The electron-rich nature of PPV derivatives has been exploited in optoelectronics as hole conducing materials in organic solar cells. Its most popular architecture is the bulk heterojunction, schematically represented in *Figure 6.1*.[8]

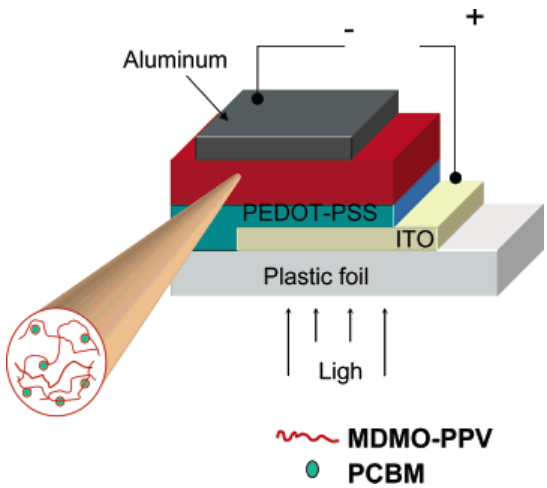

***Figure 6.1*-Bulk heterojunction configuration in organic solar cell. Reproduced with permission from *Chem. Rev,* 2007, 107, 1324-1338. © 2007 American Chemical Society.**

The main components of the cell are:

- *donor*: it is a *p*-type hole conducting polymer (usually PPV derivatives);
- *acceptor*: it is a *n*-type electron conducting compound (usually fullerene derivatives);
- *hole transport layer*: it is composed of poly(3,4-ethylendioxythiohene)-polystyrene-para-sulphonic acid, *i.e* PEDOT-PSS);

- *electrodes.*

The main steps referring to conversion of light into electrical energy can be summarized as follows[9]:

- light absorption and exciton formation;
- exciton migration;
- exciton dissociation at donor/acceptor interface;
- charge transport.

It is obvious that photophysical and electrochemical properties of both donor and acceptor materials are essential in order to achieve high efficiencies: in particular, the donor material must possess high absorption coefficients and the interfacial area between donor and acceptor has to be large, since these parameters affect the performance of the resulting device. For example, in bulk heterojunction[10] devices donor and acceptor are blended, so that the distance between donor-acceptor interfaces is less than exciton diffusion length from the absorption site and this improves the solar cell performance. In this regard, control over the morphology of phase separation of the resulting interpenetrating network is essential and leads to increasing power conversion of solar cells.[11]

By virtue of the aforementioned considerations about electrochemical properties of acceptor materials, it is possible to conclude that the ideal acceptor must be an electron-poor material and, of course, its band gap has to be superimposable with that of the acceptor.

In this Chapter, the photophysical, photochemical and electrochemical properties of two conjugated azobenzene oligomers and their monomer model (*Figure 6.2*) are presented.

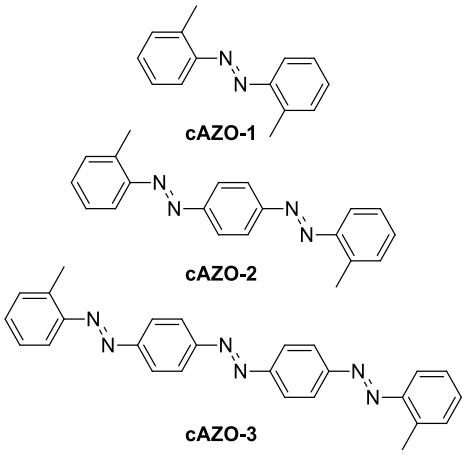

***Figure 6.1*-Structure of conjugated oligoazobenzenes.**

For this family of compounds it was observed that a relationship between the number of azobenzene units and electrochemical properties exists: in fact, they exhibit a shift of their reduction potential towards more positive values upon increasing azobenzene units, allowing to test their application as electron acceptors in photovoltaic cells.

This work was performed in collaboration with Prof. S. Masiero, University of Bologna, Bologna (Italy) who provided support for the synthesis of the studied compounds; Dr. N. Camaioni, ISOF-CNR, Bologna (Italy) who tested their feasibility as electron acceptor materials for photovoltaic applications; Prof. F. Negri, University of Bologna (Italy), who performed quantum mechanical calculations.

6.2 Conjugated oligoazobenzenes

6.2.1 Photophysical and photochemical characterization

The absorption spectra of the studied compounds (*Figure 6.3*) show an auxochromic effect in a linear fashion upon increasing azobenzene units, in line with spectra computed with TD-CAM-B3LYP. Moreover, increasing conjugation in the system results in a bathochromic effect for the absorption band referring to $\pi-\pi^*$ transitions and in cAZO-3 the bands referring to $\pi-\pi^*$ and $n-\pi^*$ transitions are superimposed.

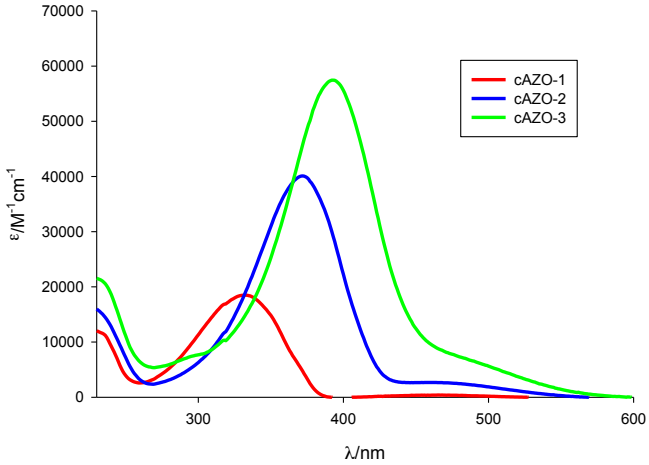

***Figure 6.3*-Absorption spectra of conjugated oligoazobenzenes in CH_2Cl_2 at r.t.**

The photoreactivity of the three conjugated azobenzene oligomers decreases upon increasing the number of azobenzene units. [5]In fact, cAZO-1 shows the typical spectral variations of azobenzene upon irradiation at 365 nm (*Figure 6.4*): in particular, a decrease of the band located at 332 nm and an increase of the one at 468 nm is observed, with the presence of isosbestic points at 280 and 290 that remain fixed for the whole irradiation time.

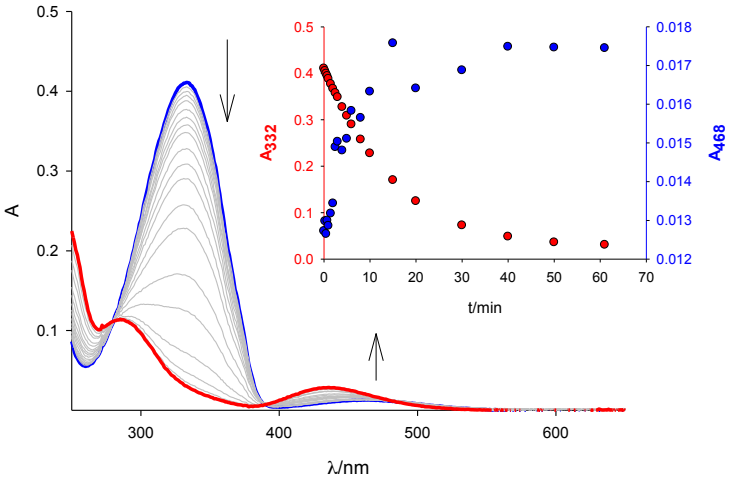

***Figure 6.4* - Changes in the absorption spectra of cAZO-1 upon irradiation at 365 nm. Inset: time dependent absorption changes in the $\pi-\pi^*$ and $n-\pi^*$ bands upon irradiation.**

The photostationary state is composed by 96% of the *Z*-isomer and the same isosbestic points are found for the thermal *Z-E* isomerization, highlighting the reversibility of the isomerization process.

Moreover, the presence O_2 does not exert any effect on the photoreaction.

The same compound was irradiated with visible light (436 nm): in this case the conversion is lower (*Figure 6.5*), due to reabsorption of light by the product and the photostationary state contains 20% of *Z*-cAZO-1.

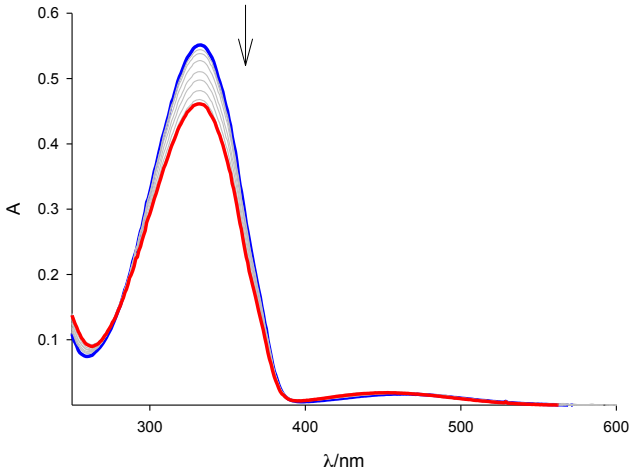

***Figure 6.5* - Changes in the absorption spectrum of cAZO-1 upon irradiation at 436 nm.**

The addition of a second azobenzene moiety decreases the photoreactivity (*Figure 5.6*) and, consequently, the *E*→*Z* photochemical quantum yield (*Table 6.1*); moreover, no thermal *Z*→*E* isomerization was observed for cAZO-2. Also in this case, the compound was irradiated in a deoxygenated solution and no variations in the reaction were observed. Irradiation in correspondence of the band referring to n–π^* transition leads to the same spectral variations (*Figure 6.6*) but to a modest conversion.

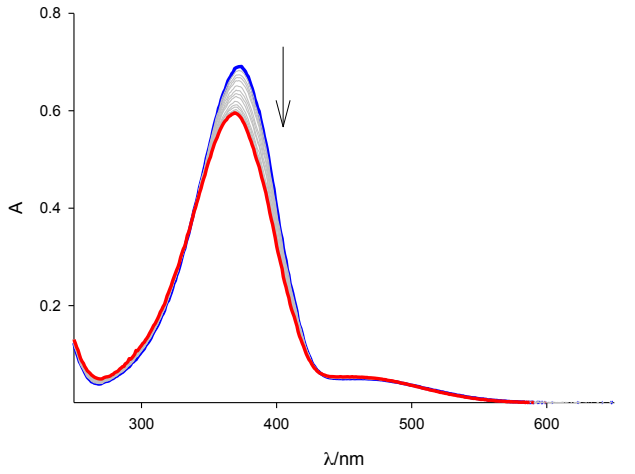

***Figure 6.6* - Changes in the absorption spectra of cAZO-2 upon irradiation at 365 nm.**

For cAZO-3 no significant changes in its absorption spectrum were observed upon UV irradiation (*Figure 6.7*), neither in the presence nor in the absence of O_2, confirming that conjugation of azobenzene units is responsible for suppression of photoreactivity. This behaviour is markedly different with respect to the one found for decoupled oligo- and polyazobenzene derivatives, in which the azobenzene units are separated and operate independently. [6]

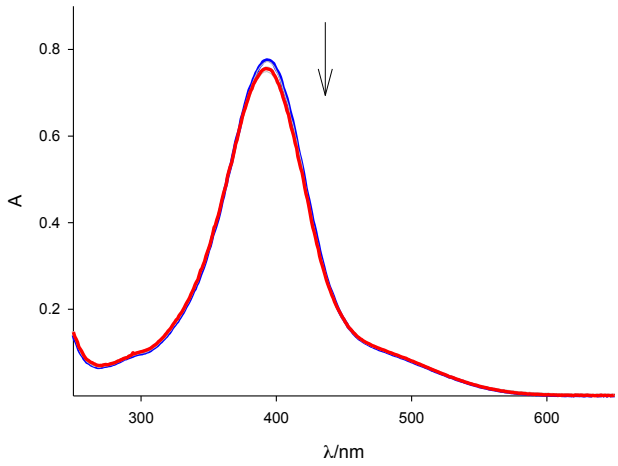

***Figure 6.7* - Changes in the absorption spectra of cAZO-3upon irradiation at 365 nm.**

***Table 6.1* - Photophysical and photochemical parameters for conjugated oligoazobenzenes.**

		cAZO-1	cAZO-2	cAZO-3
ε /M^{-1}cm^{-1}		18500	40100	57500
E:Z	π–π* irradiation	4:96	80:20	/
	n–π* irradiation	80:20	88:12	
Φ	π–π* irradiation	0.1	0.06	/
	n–π* irradiation	0.19	0.19	
$k_{Z->E}$ (s^{-1})		3.03x10^{-6}	/	/

6.2.2 Electrochemical characterization

Cyclic voltammetries (*Figure 6.8*) of cAZO-1, cAZO-2 and cAZO-3 show both oxidation and reduction processes.

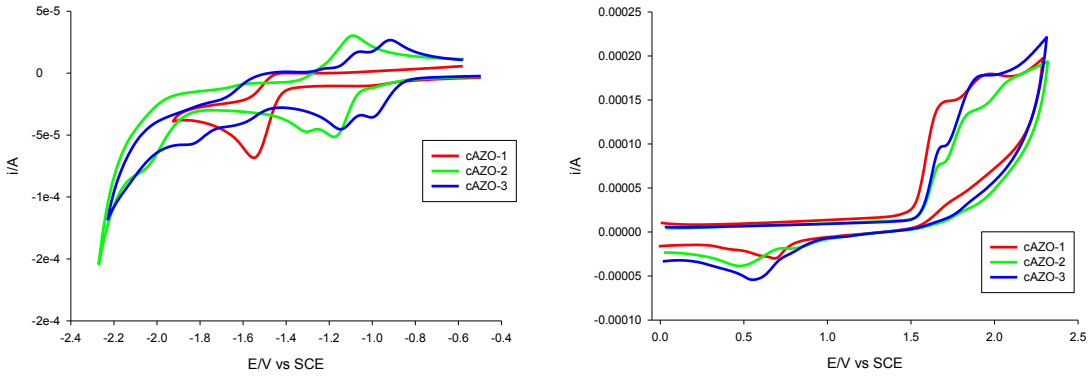

***Figure 6.8* - Cyclic voltammograms of deoxygenated solutions (1 mM) of the conjugated oligoazobenzene derivatives in CH_2Cl_2. Supporting electrolyte: $TBAPF_6$; internal reference: decamethylferrocene; scan rate: 200 mV/s; working electrode: glassy carbon.**

All compounds exhibit two irreversible oxidation processes, but the most interesting part of voltammograms is that referring to reduction processes, in order to state if they can be used as electron conducing materials for photovoltaic applications.

In all cases, the reduction processes, referring to the formation of the corresponding radical anion, become more reversible and occur at less negative potentials by increasing the number of azobenzene units. (*Figure 6.9* and *Table 6.2*).

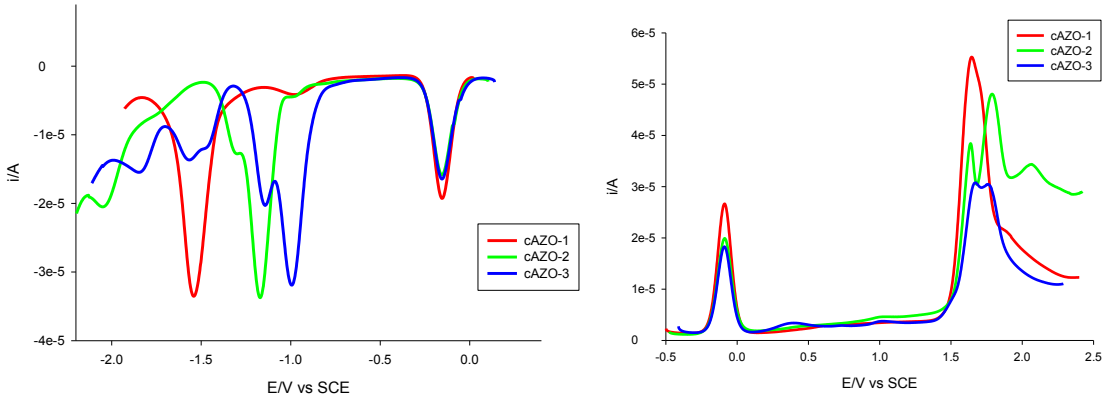

Figure 6.9 **- DPV of deoxygenated solutions (1 mM) of conjugated oligoazobenzene derivatives in CH_2Cl_2. Supporting electrolyte: $TBAPF_6$; internal reference: decamethylferrocene; modulation time: 40 ms; modulation amplitude: 75 mV; scan rate 20 mV/s; working electrode: glassy carbon.**

Table 6.2 **- Electrochemical parameters for conjugated oligoazobenzenes.**

	E_{OX}(V)	E_{RED}(V)	N° e^-_{RED}
cAZO-1	1.65	-1.54	/
cAZO-2	1.66 1.77	-1.16	0.6
cAZO-3	1.65 1.78	-0.99	0.7

The observed trend for reduction potential can be explained by looking at the energy of their frontier orbitals. Calculations show that the energy of the LUMO lowers considerably moving from cAZO-1 to cAZO-3 (*Figure 6.10*), supporting what emerged from experimental data.

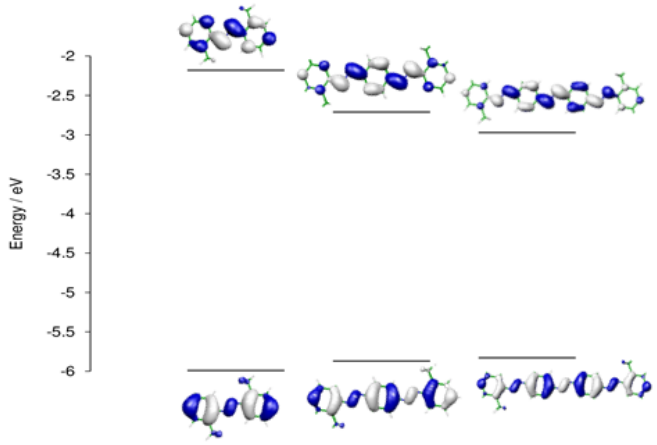

Figure 6.10 **- Frontier molecular orbitals and B3LYP/6-31G* computed orbital energies of conjugated oligoazobenzenes.**

This trend reflects a concomitant increase of the electron affinity of these compounds and Koopmans' theorem[12] allows to correlate the first redox potential of these conjugated systems with their LUMO energies (*Figure 6.11*): in this case, a linear relationship is observed between redox potential and computed LUMO energy, suggesting that the addition of more azo units will lower further LUMO energy and the reduction potential will move towards more positive values.

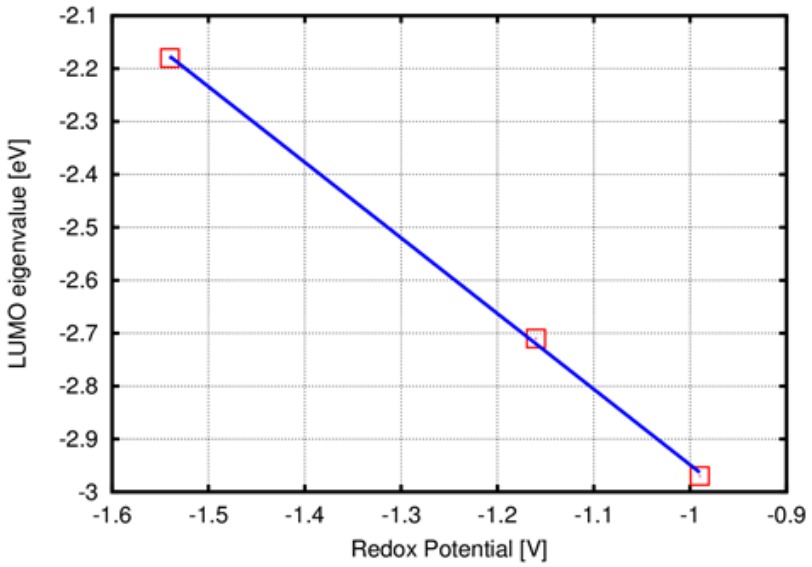

Figure 6.11 **- Plot of B3LYP/6-31G* computed LUMO energies vs first reduction potential of conjugated oligoazobenzenes.**

6.2.3 Oligoazobenzenes as electron acceptor materials

Since cAZO-3 exhibits energetic levels that are comparable with those found for PCBM (1-[3-methoxycarbonyl)propyl]-1-phenyl-[6,6]C_{61})[10a, 13], its use as an electron acceptor material was tested. The results presented in the following section were obtained in Dr. N. Camaioni's laboratory (ISOF-CNR, Bologna, Italy). Commercially available electron-donating polymers were used as electron-donors counterparts: P3HT (poly-3-hexylthiophene), PTB7 (poly{4,8-bis[(2-ethylhexyl)oxy]benzo[1,2-b:4,5-b']dithiophene-2,6-diyl-alt-3-fluoro-2-[(2-ethylhexyl) carbonyl]thieno[3,4-b]thiophene-4,6-diyl}) and MDMO-PPV (poly[2-methoxy-5-(3′,7′-dimethyloctyloxy)-1,4-phenylenevinylene]) (*Figure 6.12*).

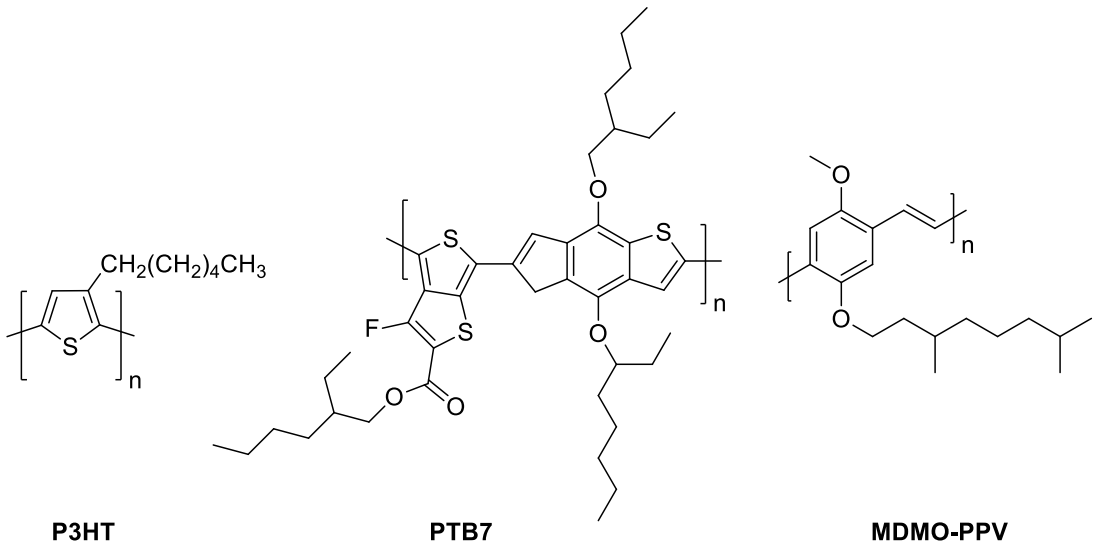

Figure 6.12 **- Structure of donor polymers.**

The energy levels of the materials used are reported in *Figure 6.13*: HOMO/LUMO levels for cAZO-3 were obtained from its reduction and oxidation potentials in solution.

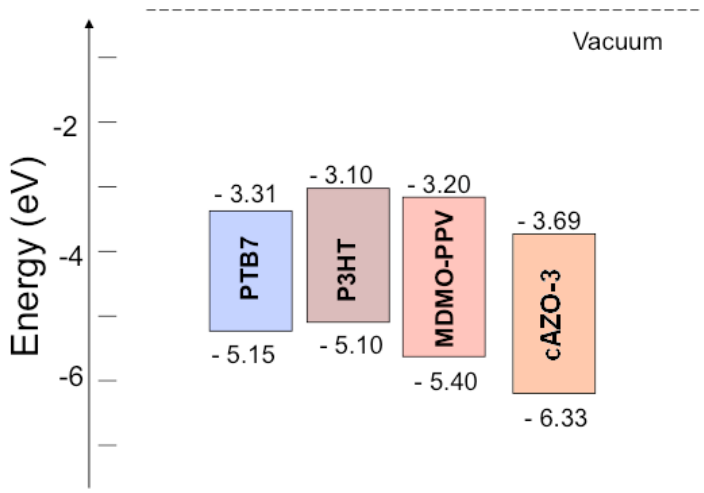

Figure 6.13 **- Energy levels for donor polymers and cAZO-3.**

It emerges that the energy offset for LUMO orbitals for acceptor and donors is between 0.4 and 0.6 eV; since the binding energy (that corresponds to the difference between optical and electrochemical band gaps) for the generated exciton for the donors materials used does not exceeds 0.5 eV, the found energy offset could be sufficient for the photoinduced electron transfer from donors to cAZO-3.

By observing optical microscopy images of composite films of PTB7/cAZO-3, P3HT/cAZO-3 and MDMO-PPV/cAZO-3 (*Figure 6.14*), it is possible to observe high phase segregation between donor and acceptor, ascribable to cAZO-3 aggregation.

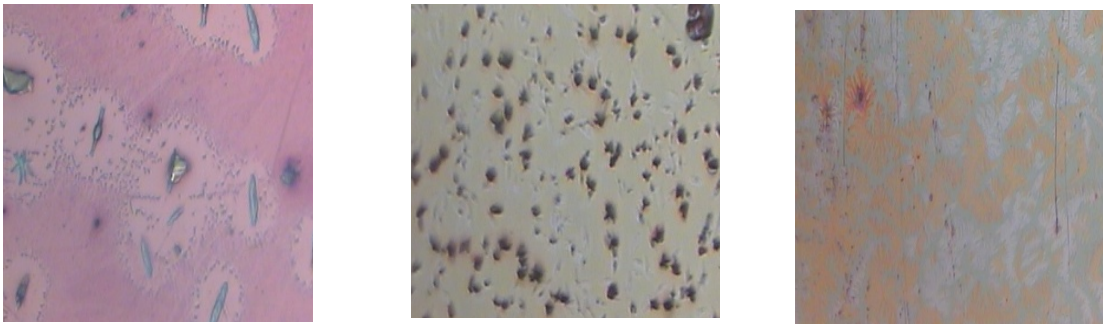

***Figure 6.14* - Optical microscopy images of composite films of PTB7/cAZO-3 (left), P3HT/cAZO-3 (middle) and MDMO-PPV/cAZO-3 (right) deposited on quartz (561x457 µm).**

Moreover, the blends were deposed on quartz and their absorption and emission spectra were compared with those obtained for pure acceptor polymers (*Figure 6.15*).

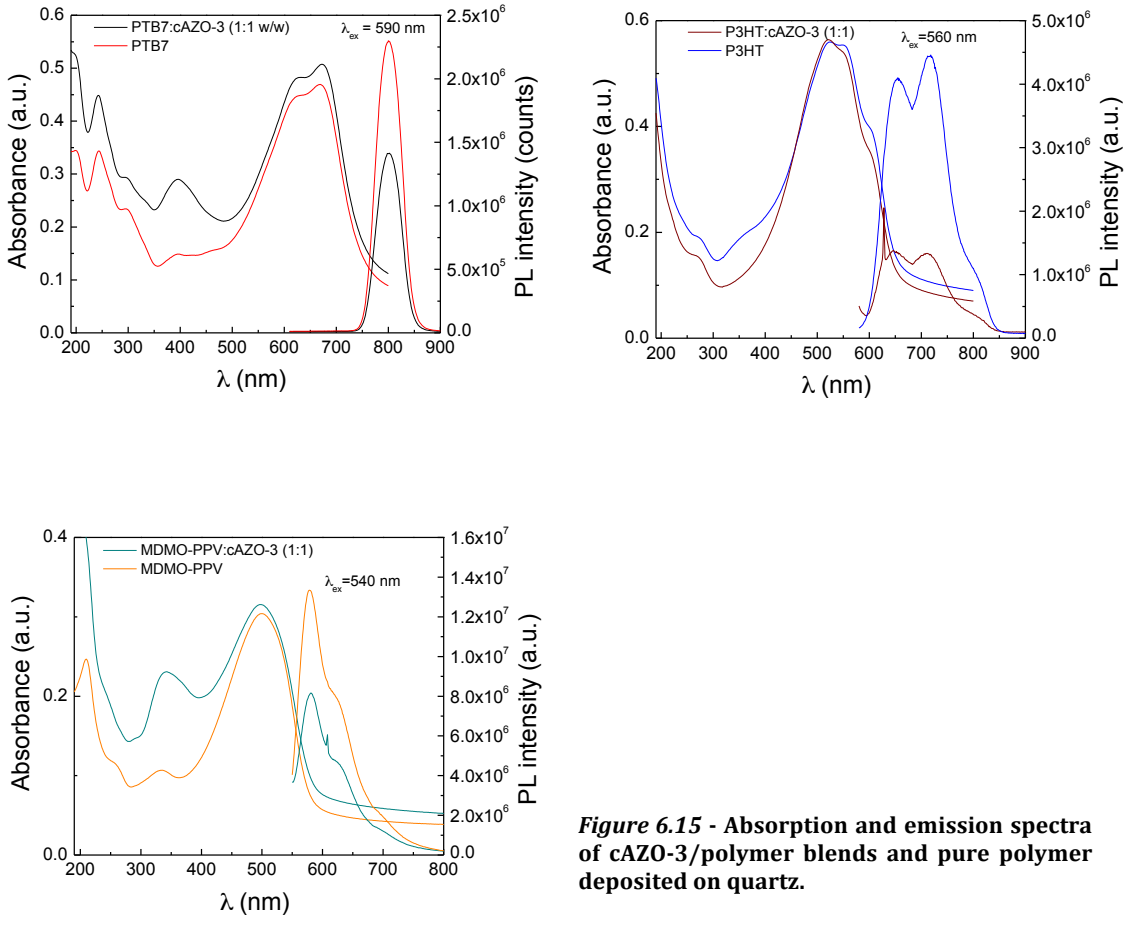

***Figure 6.15* - Absorption and emission spectra of cAZO-3/polymer blends and pure polymer deposited on quartz.**

In all cases, a negligible quenching of the donor emission is observed, indicating an insufficient accepting activity for cAZO-3 (*Table 6.3*). This observation suggests that the microstructure of the obtained blend is an important parameter to take into account in order to increase the overall efficiency of solar cells. [14]

***Table 6.3* - Photoluminescence quenching of polymer/cAZO-3 blends.**

Blend	PL quenching
PTB7:cAZO-3	1.6
P3HT:cAZO-3	2.8
MDMO-PPV:cAZO-3	1.6

To better understand if the modest quenching of photoluminescence can be attributed to the high phase segregation in the polymeric blend or to apoorly efficient for the photoinduced charge transfer at the polymer/cAZO-3 interface, the charge transfer efficiency has been evaluated by comparing the photoluminescence quenching obtained in acceptor/donor double-layered structures, in which thin films of pure acceptors and donors are overlaid. In addition to polymeric species P3HT and PTB7, N,N'-Bis(3-methylphenyl)-N,N'-diphenylbenzidine (TPD, *Figure 6.16*) was employed as donor material.

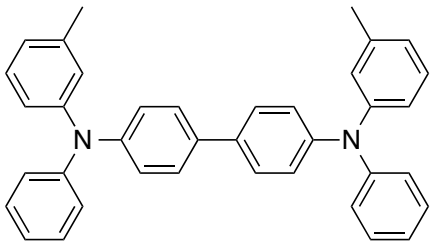

***Figure 6.16*- Structure of TPD.**

For the TPD donor compound the HOMO/LUMO energy levels are highly separated (*Figure 6.17*), thus providing a high driving force for the photoinduced charge transfer at the TPD/cAZO-3 interface.

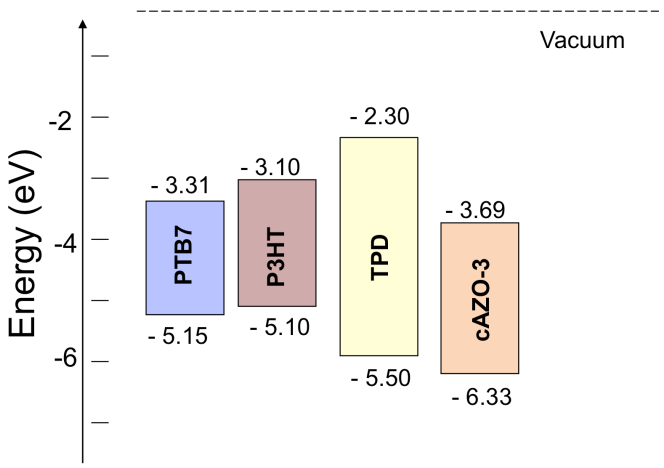

Figure 6.17 **- Energy levels for donor polymers and cAZO-3.**

In contrast to what observed for P3HT and PTB7, a significant quenching has been observed for TPD/cAZO-3 (*Figure 6.18*), that is comparable to that found for TPD/C_{60} bilayer.

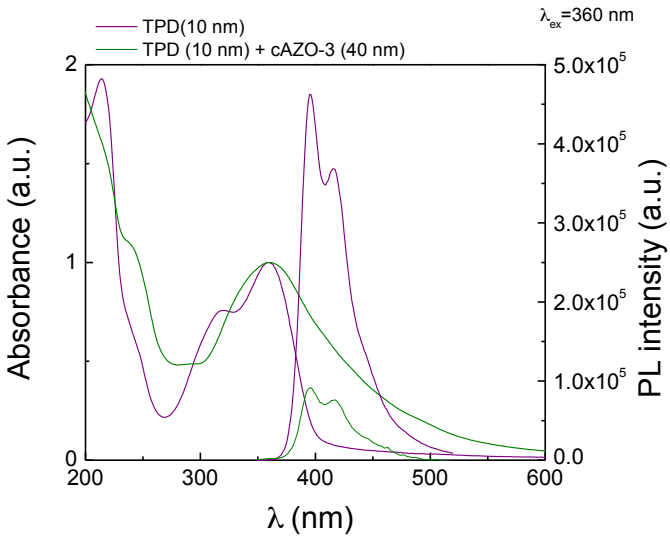

Figure 6.18 **- Absorption and emission spectra of cAZO-3/TPD bilayer and pure TPD deposited on quartz.**

The small photoluminescence quenching found for polymer/cAZO-3 double layers suggests that the driving force for the efficient photoinduced charge transfer at polymer/cAZO-3 interface is not sufficient. Moreover, the low miscibility of azobenzene-based acceptor materials and polymeric donors has to be addressed: in this direction, other conjugated derivatives have been synthesized and preliminarily characterized.

6.2.4 Future perspectives

In order to overcome the above-mentioned solubility issues, photochemical and electrochemical properties of another conjugated oligoazobenzene derivative have been investigated. The present compound (*Figure 6.19*) bears *tert-butyl* terminal groups that can increase its miscibility in the final polymeric blend.

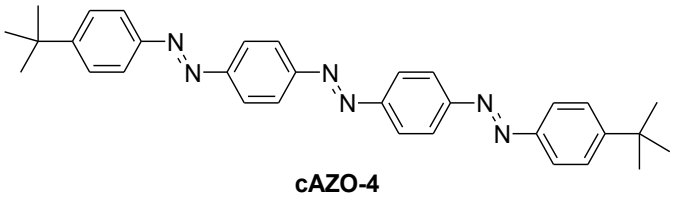

***Figure 6.19*- Structure of cAZO-4.**

As found for other conjugated oligoazobenzene derivatives, cAZO-4 experiences an almost total suppression of its photoreactivity (*Figure 6.20*), thus confirming that its photophysical and photochemical properties are comparable with those found for cAZO-3 (*Table 6.4*).

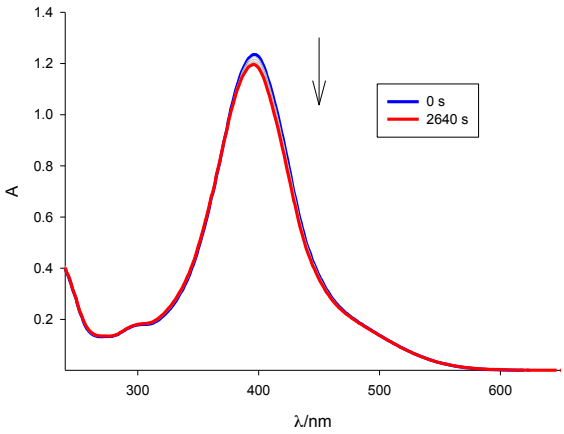

***Table 6.4* - Photophysical and photochemical parameters for cAZO-3 and cAZO-4.**

	$\varepsilon / M^{-1}cm^{-1}$	Φ
cAZO-3	57500	/
cAZO-4	53500	/

***Figure 6.20* - Changes in the absorption spectra of cAZO-4upon irradiation at 365 nm.**

Moreover, its electrochemical behaviour resembles the one found for cAZO-3: in fact, two irreversible oxidation processes and quasi- reversible reduction processes are seen for the present compound (*Figure 6.21*) and the value of the first reduction process is comparable with that of cAZO-3 (*Table 6.5*).

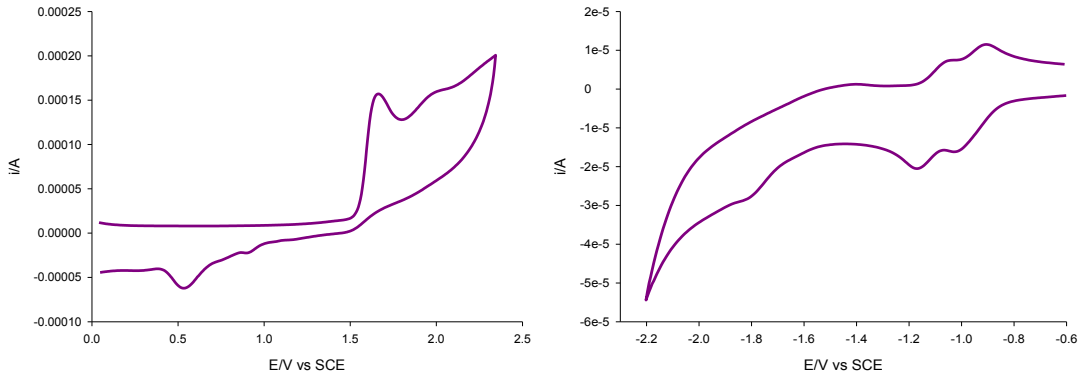

Figure 6.21 **- Cyclic voltammograms of a deoxygenated solution (0.5 mM) of cAZO-4 in CH_2Cl_2. Supporting electrolyte: $TBAPF_6$; internal reference: decamethylferrocene; scan rate: 200 mV/s; working electrode: glassy carbon.**

Table 6.5 **- Electrochemical parameters for cAZO-3 and cAZO-4.**

	E_{OX} (V)	E_{RED} (V)
cAZO-3	1.65 1.78	-0.99
cAZO-4	1.74 2.00	-1.00

By comparing the potential values for oxidation, it can be observed that electron-donor substituents shift the two processes towards higher potential values, whereas no effect is exerted on the value of reduction potential. Since the value referring to the first reduction process is comparable with that found for cAZO-3 and PCBM, the next step will be to test this compound as an electron acceptor material when blended with a donor species.

6.3 Conclusion

Conjugation of azobenzene photochromic units leads to the development of rigid molecular structures and it has been found that structural rigidity is an important prerequisite for the design of artificial transmembrane channels.

On the other hand, conjugation of azobenzene units leads to almost total suppression of photoreactivity, thus making these derivatives less appealing for the design of photoactive transmembrane channels.

Nevertheless, the structure of these organic compounds resembles that of oligo(*p*-phenylenevinylene) (PPV) derivatives and, under a structural point of view, they can be considered their electron poor counterparts. In fact, their reduction potential shifts to less negative values upon increasing the number of azo units and the linear trend found for the redox potential and computed LUMO energy levels suggests that the addition of more azo units would lower further LUMO energy, thus moving the reduction potential towards less negative values. This makes possible their potential application as electron acceptor materials in the development of organic solar cells. Preliminary tests, performed on donor/acceptor blended films, did not a show a significant reduction of donor materials' photoluminescence and this can be ascribable to high phase segregation between donor and acceptor, due to aggregation of acceptor material. The obtained results suggest that an improvement in the design of conjugated oligoazobenzene has to be made in order to avoid phase segregation and to tune their electrochemical properties, in order to obtain more efficient electron poor organic materials.

References

[1] Sakai, N.; Brennan, K.C.; Weiss, L.A.; Matile, S., *J. Am. Chem. Soc.*, **1997**, 119, 8726-8727.

[2] Kempf, J.; Noujeim, N.; Schmitzer, A.R., *RSC Adv.*, **2014**, 4, 42293-42298.

[3] a) Gorteau, V.; Bollot, G.; Mareda, J.; Perez-Velasco, A.; Matile, S., *J. Am. Chem. Soc.*, **2006**, 128, 46,14788–14789. b) Gorteau, V.; Bollot, G.; Mareda, J.; Matile, S., *Org. Biomolec. Chem.*, **2007**, 5, 3000-3012.

[4] a) Mareda, J.; Matile, S., *Chem. Eur. J.,***2009**, 15, 1, 28-37. b) Perez-Velasco, A.; Gorteau, V.; Matile, S., *Angew.Chem. Int. Ed.*, **2008**, 47, 921-923.

[5] Cisnetti, F.; Ballardini, R.; Credi, A.; Gandolfi, M.T.; Masiero, S.; Negri, F.; Pieraccini, S.; Spada, G.P., *Chem.Eur. J.*, **2004**, 10-2011-2021.

[6] Bléger, D.; Dokić, J.; Peters, M.V.; Grubert, L.; Saalfrank, P.; Hecht, S., *J. Phys. Chem. B*, **2011**, 115, 9930-9940.

[7] Moneo, A.; Justino, G.C.; Carvalho, M.F.N.N.; Oliveira, M.C.; Antunes, A.M.M.; Bléger, D.; Hecht, S.; Telo, J.P., *J. Phys. Chem. A*, **2013**, 117, 51, 14056-14064.

[8] a) Günes, S.; Neugebauer, H.; Sariciftci, N.S., *Chem. Rev*, **2007**, 107, 1324-1338. b) Hoppe, H.; Sariciftci, N.S., *J. Mater. Res.*, **2004**, 19, 7, 1924-1945.

[9] Brédas, J.-L.; Norton, J.E.; Cornil, J.; Coropceanu, V., *Acc. Chem. Res.*, **2009**, 42, 11, 1691-1699.

[10] a) Yu, G.; Gao, J.; Hummelen, J.C.; Wudl, F.; Heeger, A.J., *Science*, **1995**, 270, 5243,1789-1791. b) Roncali, J., *Acc. Chem. Res.*, **2009**, 42, 11, 1719-1730.

[11] a) Van Duren, J.K.J; Yang, X.; Loos, J.; Bulle-Lieuwma, W.T.; Sieval, A.B.; Hummelen, J.C.; Janssen, R.A.J., *Adv. Funct. Mat.,***2004**, 14, 5, 425-434. b) Benanti, T.L.; Venkatamaran, D., *Photosynth. Res.*, **2006**, 87, 73-81.

[12] Koopmans, T., *Physica*, **1934**, 1, 104-113.

[13] Hummelen, J.C.; Knight, B.W.; LePeq, F.; Wudl, F., *J. Org. Chem.*, **1995**, 60, 3, 532-538.

[14] Treat, N.D.; Varotto, A.; Takacs, C.J.; Batara, N.; Al-Hashimi, M.; Heeney, M.J.; Heeger, A.J.; Wudl, F.; Hawker, C.J.; Chabinyc, M.L., *J. Am. Chem. Soc.*, **2012**, 134,15869-15879.

Chapter 7

Conclusion

The results presented in this work concern the study and development of photoactive nanodevices for potential application in bioimaging and drug delivery.

In the first part, we investigated the photophysical, photochemical and electrochemical properties of a family of tunable blue emitting organic salts, bearing the triazolopyridinium and triazoloquinolinium unit.

These compounds exhibited tunable blue light emission with "mega" Stokes shift both in solution and in the solid state. Moreover, they exhibited phosphorescence by performing 77 K measurements and it was found that lifetime of triplet states is quite long compared to that found for other blue emitting organic compounds.

Since their molecular structure resembles the one found in several classes of known DNA molecular intercalator and groove binders, we studied their possible interaction with DNA, but unfortunately the obtained results did not show groove binding or intercalation.

In the second part, we investigated the light-driven efflux of ions and small molecules from liposomes for the development of photoactive drug delivery systems based on liposomes as biocompatible platforms. We found that photoisomerization of azobenzene is essential to achieve a fast and efficient

efflux of ions and small molecules entrapped in the aqueous compartment of liposomes, by means of induced defects in their membrane as a consequence of photoisomerization process experienced by photoactive guests inserted in the phospholipid bilayer. Moreover, we demonstrated that the presence of more azobenzene units leads to a fast and efficient leakage of vesicles' contents and the presence of positively charged end groups helps the self-assembly of the photoactive azobenzene derivative and phospholipids. In addition, we found that separation of azobenzene units in oligoazobenzene derivatives is an essential prerogative for photoreactivity, since we found that conjugated counterparts do not exhibit an appreciable photoreactivity and this make these molecular species not suitable for their insertion in the phospholipid bilayer. Alternatively, we inserted in the liposomal aqueous core photoactive supramolecular systems able to modify the concentration of solutes in solution, allowing to explore the possibility to develop biocompatible nanoscale containers able to release their contents as a consequence of the photoinduced osmotic stress.

We also synthesized a new photoactive anion transporter for the photoinduced efflux of chloride anions from liposomes. This new compound joins the known anionophoric activity exhibited by imidazolium salts and the ability of azobenzene in the translocation of small molecules across biomembranes, thus being potentially able to transport small molecules from the aqueous interior of vesicles to the external medium in which they are dispersed. We performed lucigenin assays performed on liposomes and obtained results highlighted the relationship between photoisomerization of the azobenzene unit and efficiency of chloride efflux from liposomes.

In addition, we evaluated the possibility of inserting conjugated oligoazobenzene derivatives in the phospholipid bilayer of liposomes, since their molecular structure accounts for the structural rigidity found in many transmembrane channels. Photochemical experiments showed that these compounds exhibit poor photoreactivity, but their electrochemical properties make them valuable electron-poor materials in the development of organic solar cells. Moreover, this hypothesis is supported by obtained electrochemical data and computed LUMO energy levels, since in both cases we found that the addition of more azo units lowers LUMO energy, thus moving the reduction potential towards more positive

values. Polymeric blends of plain donor polymers and a conjugated oligoazobenzene derivative were prepared, but preliminary test did not a show a significant reduction of donor materials' photoluminescence. This can be ascribable to high phase segregation between donor and acceptor, since we observed the formation of aggregates of acceptor material within the polymeric blend. The obtained results suggest that an improvement in the design of conjugated oligoazobenzene have to be made in order to avoid phase segregation and to tune electrochemical properties, in order to obtain more efficient electron poor organic materials.

Scientific contributions

Papers

Massimo Baroncini, Chao Gao, Valentina Carboni, Alberto Credi, Elia Previtera, Monica Semeraro, Margherita Venturi and Serena Silvi
"Light Control of Stoichiometry and Motion in Pseudorotaxane Comprising a Cucurbit[7]uril Wheel and an Azobenzene-Bipyridinium Axle".
Chemistry - A European Journal **2014**, 20, 34, 10737-10744.

Presentations

1. Valentina Carboni, Monica Semeraro, Serena Silvi, Massimo Baroncini and Alberto Credi
"Photocontrolled Assembly/Disassembly of a Pseudorotaxane System in a Compartmentalized Solution Environment". (flash presentation and poster)
European Winter School on Physical Organic Chemistry, **2013**.
2. Valentina Carboni, Monica Semeraro, Serena Silvi and Alberto Credi
"Azobenzene-based nanoscale containers" (oral communication)
Italian Photochemistry Meeting, **2013**.
3. Valentina Carboni, David Bléger, Stefan Hecht, Andreea Schmitzer and Alberto Credi
"Azobenzene for the transport of small molecules and ions across liposomal membranes." (oral communication)
Italian Photochemistry Meeting, **2014**.

Acknowledgments

Prof. Alberto Credi, Prof. Andreea Schmitzer, Prof. Stefano Masiero, Monica Semeraro, Serena Silvi, My wonderful Family, Tommaso Avellini, Massimo Sgarzi, Giulia Casulli, Francesca Colò, Eleonora Ussano, Andrea Fermi, Lucia Marcantoni, Giulio Cingolani, Simone Monaco, Chiara Canducci, Susanna Sampaolesi, Francesca Panfoli, Michele Ambrosini, Chiara Paolucci, Denis Didu, Marco Cammarata, Luca Petrizza, Mirko Locritani, Enrico Marchi, Marianna Marchini, Giulio Ragazzon, Julien Gravel, Vanessa Kairouz, Julie Kempf, Giulia Battistelli, Raffaello Mazzaro, Vincent Gauchot, Marc Vidal, Mathieu Charbonneau, Luca Ravotto, Prunelle Rios, Andrea Cantelli, Jeannette Manzi, Francesca De Giorgio, Benoit Colasson, Giacomo Bergamini, Marcello La Rosa, Dat Tien Do, Thierry Havard, Audrey Hébert, Francesco Palomba, Gloria Guidetti, Marie-Pier Dinel, Minh Nguyễn, Claude Rosnie-Elie, Solène Fortun.